

**Localized Tolerance and Development of an Alternative Transplant Site to Treat Type 1
Diabetes**

By

Michael J. Skoumal

A dissertation submitted in partial fulfillment
of the requirement for the degree of
Doctor of Philosophy
(Chemical Engineering)
In the University of Michigan
2017

Doctoral Committee:

Professor Lonnie D. Shea, Chair
Assistant Professor Timothy Scott
Professor Jan P. Stegemann
Assistant Professor Greg M. Thurber

Michael Skoumal

mskoumal@umich.edu

ORCID ID: 0000-0001-6993-7369

© Michael J. Skoumal 2017

DEDICATION

This dissertation is dedicated to my family, lab members, and friends.

ACKNOWLEDGMENTS

Thank you everybody who has supported me on this journey. And not just the PhD journey, but all the steps that led me here. It is certain that without your support, I would never have been able to have the opportunity to get where I am. Thank you, Lonnie, for your guidance, insight, and dedication. Thank you Professors Scott, Stegemann, and Thurber for your time and excellent input. And thank you, Pat, for your wizardry.

Thank you to Stephanie and Ryan (Pearson) for enduring my constant questions about biochemistry. I feel like most of the conversations usually ended with, “It’s thermodynamics, that’s just how it is,” but I appreciated that you humored me and my long chain of questions. Hannah, Ryan (Boehler), and Jackie – thank you for getting me acquainted with the lab and setting the culture in our awesome L.A.B. I’m sure you’d be surprised how much the lab has changed since you graduated, and you might be not be surprised how much certain aspects have stayed the same. At least we have larger lab coats now. Thank you to Daniel and Jeff for meaningful collaborations. And thank you to Richard, who has the task of continuing this work.

Thank you to my friends outside the lab, particularly my roommates Emily, Yamil, Teresa, and Erik. Without your support, I would have surely lost my mind. Thank you to my friends back in Iowa, particularly Ravi and Eric, who always set an example in excellence that I hope to follow. Finally, I would like to thank my family, particularly my parents. I know you would have liked me to be a real doctor, but Mike Rea was too persuasive. Engineering really is the best.

TABLE OF CONTENTS

DEDICATION	ii
ACKNOWLEDGMENTS	iii
LIST OF TABLES	vii
LIST OF FIGURES	viii
ABSTRACT	xiv
CHAPTER 1. Introduction	1
1.1 Motivation and objective	1
1.2 Overview of this dissertation	2
CHAPTER 2. Background	4
2.1 Introduction	4
2.2 Alternative transplant sites	6
2.3 Biomaterial scaffolds	10
2.4 Viral delivery of soluble factors	12
2.5 Immunoregulation	14
CHAPTER 3. Evaluation of Encapsulating and Microporous Hydrogel Scaffold Designs on Islet Engraftment in Rodent Models of Diabetes	17
3.1 Introduction	17
3.2 Materials and methods	19
3.2.1 Encapsulated and microporous hydrogel fabrication	19
3.2.2 Islet isolation and transplantation	21
3.2.3 Intraperitoneal glucose tolerance test	22
3.2.4 Immunohistochemistry	22
3.3 Results	23
3.3.1 Encapsulating and Microporous Hydrogel Fabrication	23
3.3.2 Syngeneic islet transplants in encapsulating and microporous hydrogels	26
3.3.3 Histological Analysis of Hydrogel Explants from Syngeneic Transplants	29
3.3.4 Allogeneic Islet Transplants in Encapsulating and Microporous Hydrogels	31
3.3.5 PEG hydrogels create a microenvironment conducive to islet survival	34

3.4 Discussion	36
CHAPTER 4. Localized Lentivirus Delivery via Affinity Peptides	41
4.1 Introduction	41
4.2 Materials and methods	42
4.2.1 Virus production	42
4.2.2 PLL functionalization with cysteine	43
4.2.3 Macrophage differentiation	44
4.2.4 Peptide synthesis	44
4.2.5 Biotinylated VSV-G	44
4.2.6 Solution phase phage display	45
4.2.7 ELISA	46
4.2.8 Hydrogel preparation	46
4.2.9 Transgene expression	47
4.2.10 Statistics	47
4.3. Results	48
4.3.1 PLL length	48
4.3.2 Binding dynamics, release, and stability	50
4.3.3 VSV-G protein solution-phase panning	52
4.4 Discussion	59
CHAPTER 5. Localized Immune Tolerance from FasL-Functionalized PLGA Scaffolds	64
5.1 Introduction	64
5.2 Materials and methods	66
5.2.1 Biotinylation of PLGA and characterization	67
5.2.2 Particle and scaffold fabrication	67
5.2.3 Particle characterization	68
5.2.4 Scanning electron microscopy	68
5.2.5 Protein loading and quantification	68
5.2.6 Apoptosis assay	69
5.2.7 Mice and recombinant proteins	69
5.2.8 Islet isolation and engineering with SA-FasL protein	70
5.2.9 Islet transplantation	70

5.2.10 Intraperitoneal Glucose Tolerance Test	71
5.2.11 Immune monitoring	71
5.2.12 Statistical analysis	72
5.3 Results	72
5.3.1 Transplantation of SA-FasL modified islets onto microporous scaffolds	72
5.3.2 Synthesis and characterization of biotin-poly(lactide-co-glycolide) conjugates and particle formation	74
5.3.3 FasL loading on biotin-PLGA scaffolds	79
5.3.4 FasL scaffolds support allogeneic graft function without sustained immunosuppression	81
5.4 Discussion	84
CHAPTER 6. Conclusions and Future Directions	89
6.1 Conclusions	89
6.2 Future directions	91
6.2.1 Scaffold improvement	91
6.2.2 Localized protein delivery from biomaterial scaffolds	92
BIBLIOGRAPHY	94

LIST OF TABLES

Table 3-1. Particle size of gelatin and salt particles used as a porogen for microporous hydrogels. Mean is reported with standard error mean. Gelatin (n = 52), salt (n=41).	25
Table 4-1. Equal masses of the different poly-L-lysines were added to provide an identical net charge for each condition.	49
Table 4-2. Phage display clones that appeared multiple times were selected for further analysis.	60

LIST OF FIGURES

Figure 3-1. Fabrication of PEG-maleimide hydrogels. **(A)** Encapsulated hydrogels are formed by mixing the peptide cross linker GCYKNRGCYKNRRCG with a PEG/islet solution in a PDMS mold. Cross linking is induced via Michael-type reaction between the thiols in the peptide and the maleimide groups on the PEG. **(B)** Microporous hydrogels are formed by packing gelatin particles into a PDMS mold and adding PEG. After initiating free-radical polymerization via UV light and the photoinitiator I-2959, the gelatin particles are leached out at 37 °C, leaving a porous hydrogel that can be seeded with islets. **(C)** Microporous hydrogels with salt pores are formed in a manner similar to the gelatin microspheres, but require the PEG precursor solution to be saturated with salt prior to being added to the salt-packed PDMS mold. After polymerization, the salt is quickly leached out and the scaffold can be seeded with islets. 24

Figure 3-2. Encapsulating and microporous hydrogels for islet transplantation. (A) 10% (wt/vol) bulk PEG hydrogels were fabricated to encapsulate islets. (B) Gelatin particles (size = 107 ± 4 μm , n = 41) were fabricated, incorporated into 20% PEG (wt/vol), and subsequently leached to form a (C-D) resultant hydrogel with a microporous architecture for islet seeding. Similarly, (E) salt particles (size = 274 ± 12 μm , n = 41) were incorporated into 20% PEG (wt/vol) to form a (F-G) microporous gel for islet seeding. Scale bar: 1 mm (A, C, F), 100 μm (B), 200 μm (D,E,G). Gels were stained with sirius red for visualization. 25

Figure 3-3. Blood glucose monitoring post-transplant with hydrogel materials in fat pad transplantation site of diabetic mice. **(A)** Bulk, non-degradable encapsulating hydrogels with 700 IEQ reversed diabetes in recipient mice, and approached normoglycemic levels by Day 12 (<200 mg/dL), with consistent normoglycemia achieved after Day 17 (n=3, \pm SEM). **(B)** A gelatin-leached, microporous hydrogel seeded with 700 IEQ (400 islets) reversed diabetes in a recipient mouse by Day 10 and displayed long-term function until graft removal at Day 106 (n=1, \pm SEM). **(C)** Gelatin-leached, microporous hydrogels seeded with 200 islets reversed diabetes in recipient mice by Day 9 (n=4, \pm SEM). Mice receiving a PLGA scaffold, used an internal control due to success in previous studies, reversed a few days earlier, by Day 7 (n=1). **(D)** Salt-leached, microporous hydrogels seeded with 700 IEQ displayed normoglycemic levels as early as Day 1 post-transplant, and consistently maintained normoglycemia after Day 15 (n=5 pre-graft removal, n=4 post-graft removal, \pm SEM). Recipient mice in all groups reverted to a diabetic state within 2-4 days following hydrogel removal (indicated with a black arrow). 28

Figure 3-4. Glucose responsiveness of microporous hydrogels. **(A)** Encapsulated hydrogels with 700 IEQ (n=5, \pm SEM) achieved normoglycemia (<200 mg/dL) 120 minutes post-glucose injection. In contrast, **(B)** mice receiving gelatin-leached, microporous hydrogels with 200 islets (n=4, \pm SEM), a PLGA scaffold with 200 islets (n=1), or **(C)** salt-leached, microporous scaffolds

with 700 IEQ (n=5, ± SEM) achieved normoglycemia 60 minutes post-glucose injection, similarly to control mice with native pancreata. IPGTT performed at Day 32 (A), and Day 30 (B) post-transplant. 30

Figure 3-5. Insulin-positive islets confirmed in microporous hydrogels (A-B) Insulin-positive islets were identified in gelatin-leached, microporous scaffolds removed at Day 32 and (C) salt-leached, microporous scaffolds removed at Day 30 (Scale bar: 100 µm). (D) Explanted salt-leached microporous hydrogel 1 month post-transplant. Histology for encapsulated hydrogels will be completed in the near-future. 32

Figure 3-6. Allogeneic transplants failed to engraft before rejection. (A) Encapsulating hydrogels with 500 (n=4, ± SEM) or 1,000 islets (n = 2, ± SEM) are unable to maintain normal blood glucose levels more than 2 weeks post-transplant, indicating encapsulation alone is not sufficient to prevent graft rejection. (B) With the exception of one mouse (blue line), salt-leached microporous hydrogels with an IEQ of 1300 failed to achieve normoglycemia. 33

Figure 3-7. Transforming growth factor-β1 (TGF-β1) *in vitro* release from PLGA scaffolds and incorporation into hydrogel materials. (A) A cumulative release of 0.66 µg was determined from PLGA disc loaded with 2 µg of TGF-β1. (B) More than 80 % of total protein was released by Day 3 (n = 5, ± SEM). (C) For encapsulating hydrogel transplants, a PLGA disc containing 2 µg of was placed on top of the hydrogel and wrapped in the fat pad. (D) For microporous hydrogels, the PLGA disc containing 2 µg was incorporated into the middle of the hydrogel. (E) Cross-section view of PLGA scaffold in microporous hydrogel. (F) Islets seeded on a microporous scaffold. A representative islet is indicated with a white arrow. 35

Figure 3-8. Allogeneic graft function of scaffolds with TGF-β1 (A) Encapsulating hydrogels combined with TGF-β1 delivery delays rejection until Day 24 compared to rejection at Day 12 without TGF-β1 (n = 2 per group, ± SEM). Rejection is denoted as two consecutive days of blood glucose >250 mg/dL. (B) Graft Function 7-days post-transplant in salt-leached microporous hydrogels. - TGF-β1 condition (n=2, ± SEM), + TGF-β1 condition (n=4, ± SEM). At day 7, the microporous hydrogels were removed for flow cytometry. 37

Figure 4-1. Influence of PLL molecular weight on virus localization. PEG hydrogels containing 2.5 mM RGD were functionalized with 0.45 mg/mL of 1 kDa (n=3) (A), 10 kDa (n=3) (B), and 30-70 kDa (n=5). (C) PLL and incubated with GFP-encoding lentivirus. Hydrogels were washed to remove non-binding virus then seeded with HT1080 cells for 72 hours. (D) Significantly more cells were transduced with 30-70 kDa PLL than the shorter PLL's. (*p≤0.05; ***p≤0.001) 49

Figure 4-2. PLL functionalized hydrogels promote transduction of macrophages. PEG hydrogels were functionalized with 2.5 mM RGD (A) and 2.5 mM RGD + 1.35 mg/mL of 30-70 kDa PLL (B). Conditions without PLL (A) had no GFP expression while PLL functionalized hydrogels demonstrated significant GFP expression (B). 49

Figure 4-3. PLL enhances virus localization on PEG hydrogels. PEG hydrogels containing 2.5 mM RGD were functionalized with either 30-70 kDa PLL (0.45 mg/mL) or additional RGD (2.5 mM)

(n=3). Designated wells were blocked with BSA (5 mg/mL) prior to forming the hydrogels. The “No virus” condition contains PLL but was incubated with PBS instead of lentivirus. Lentivirus encoding for GLuc was incubated with the hydrogels then washed with PBS to remove non-binding virus. HT1080 cells were incubated with the hydrogels for three days and then luciferase activity was assayed. Significant difference compared to No virus and RGD (****p≤0.0001). 51

Figure 4-4. Transgene expression can be modulated via virus-hydrogel incubation time and PLL concentration. **(A)** PEG hydrogels functionalized with 2.5 mM RGD and 0.45 mg/mL of PLL were incubated with virus for varying times (n=3). Fold increase in GLuc expression relative to RGD control. Significant difference compared to RGD control (**p≤0.01; ***p≤0.001). **(B)** Hydrogels were functionalized with varied concentrations of PLL and incubated with virus for 3 hours (n=3). Significant difference compared to RGD control (****p≤0.0001). 51

Figure 4-5. Retention of lentivirus on PLL-functionalized PEG hydrogels. **(A)** PEG hydrogels containing 2.5 mM RGD were functionalized with either 30-70 kDa PLL or additional RGD (0.45 mg/mL) (n=4). Virus was incubated with the hydrogels for three hours at 37 °C then washed with PBS to remove non-binding virus. Unbound virus in the supernatant was collected and assayed via qPCR at different time points. Following the two washes, no detectable level of virus was found in the PLL-functionalized hydrogels. **(B)** The fraction of lentivirus released from the hydrogel was calculated by dividing the eluted virus particles by the initial virus loading. Significant differences between corresponding RGD and PLL conditions are denoted by an asterisk (**p≤0.01; ****p≤0.0001). 53

Figure 4-6. Increased viral stability in PLL-functionalized hydrogels at 37°C. PEG hydrogels with 2.5 mM RGD and either 30-70 kDa PLL or additional RGD (0.45 mg/mL) were incubated with virus at 37 °C for three hours (n=3). All hydrogels were washed and incubated with PBS. At each time point, the PBS was replaced with HT1080 cells and subsequent luciferase expression was assayed 72 hours later. (**p≤0.01; ***p≤0.001) 54

Figure 4-7. Analysis of lentivirus purification methods using SDS-PAGE protein gel. (Lane 1, 3 = VSV-G, 0.5 µg; lane 4, 5 = VSV-G, 2.0 µg; lane 6, 7 = Lentivirus, Lenti-X purification; lane 8, 9 = Lentivirus, PEG-it purification; lane 10 = ladder; Lane 2 intentionally left blank). The Lenti-X affinity column removed almost all detectable amounts of contaminating protein, except for a faintly detectable band at approximated 65 kDa whereas the PEG-it precipitation failed to remove significant amounts of undesired protein. 54

Figure 4-8. Solution phase phage display. Biotinylated VSV-G and the phage library are mixed (1) and allowed to incubate (2). (3) Phage/VSV-G complexes are captured on a streptavidin-coated plate and non-binding phages are washed away (4). VSV-G bound phages are eluted from the plate using a low pH buffer (5) and the phages are collected for additional rounds of panning. 56

Figure 4-9. After three rounds of panning, phages demonstrate binding affinity to VSV-G. A fourth round of panning was completed with (+) and without (-) VSV-G immobilized on the

plate surface. After washing to remove non-binding phages, 10^5 PFU/ μ L were eluted from the plate surface coated with VSV-G whereas only 10 PFU/ μ L. 56

Figure 4-10. Relative variability analysis of the sequences derived from phage display shows a decreased variability at position 1 and 4-7. Position 12 is closest to the phage body and position 1 has the most freedom of movement. This analysis removed any repeat sequences. 58

Figure 4-11. ELISA results of the STQ phage shows increased binding compared to the naïve phage library. As the titer of phages added to VSV-G coated plates was increased, phages displaying the STQ sequence demonstrated increased binding whereas the non-specific naïve library did not demonstrate a noticeable change in binding. 58

Figure 4-12. Phage display identified peptides specific to the VSV-G protein on the lentivirus. Specific binding of lentivirus to phage display peptides. PEG hydrogels were functionalized with 2.5 mM RGD and 2.5 mM of the synthesized phage display peptides conjugated with a 5 kDa PEG linker (n=4). HLKHTHNTYKTCG (“HLK”), HWKPHSNLHLSRCG (“HWK”), STQHHSKQSRG (“STQ”), and WPGHHNSMKHKCG (“WPG”). RGD and 30-70 kDa PLL (0.45 mg/mL) were also functionalized to the PEG linker to serve as negative and positive controls, respectively. Lentivirus was incubated with the hydrogels for 3 hours followed by washing to remove non-binding virus. HT1080 cells were seeded on the hydrogels and luciferase activity was assayed 72 hours later. Fold increase in GLuc expression relative to RGD control. Significant differences between RGD and PLL are denoted by an asterisk ($p < 0.05$). 60

Figure 5-1. SA-FasL engineered islets establish allogeneic tolerance when transplanted on PLGA scaffolds. **(A)** Schematic showing biotinylated allogeneic islets functionalized with SA-FasL are loaded on microporous PLGA scaffolds and planted in the epididymal fat pad of mice. **(B)** Kaplan Meier analysis of allogeneic BALB/c islets transplanted under the short cover of rapamycin on unmodified PLGA scaffolds in C57BL/6 recipients. Conditions include SA-FasL-engineered islets (n = 5, MST >200 days, $P = 0.0018$ vs. rapamycin alone, $P = 0.0308$), naïve islets (n = 5, MST = 23 ± 2.19 days), and unmodified syngeneic islets (n = 3, MST > 100 days). **(C)** Intraperitoneal glucose tolerance test of long-term islet grafts compared to naïve C57BL/6 mice after fasting for 6 hours, followed by i.p. glucose injection. Blood glucose of mice was taken starting just before injection and at the indicated time points. **(D)** T cell proliferative response from recipients of long-term (> 200 days) BALB/c SA-FasL-engineered islets mounted on unmodified PLGA scaffolds plus rapamycin (n = 3) and naïve C57BL/6 as controls (n = 3). Responders were labeled with CFSE and used against BALB/c donor and third party C3H stimulators in a standard ex vivo mixed lymphocyte reaction. After 4 days of culture, cells were stained with antibodies against CD4 and CD8 molecules and incubated with 7AAD to gate out dead cells before flow cytometry analysis. Bars represent mean and SEM. Asterisks represent level of significance ($*p < 0.05$, $**p < 0.01$) found by using a two-tailed Welch’s t-test. 74

Figure 5-2. Characterization of biotin-PLGA microparticles. **(A)** Conjugation of NH_2 -PEG₂-biotin to PLGA resulting in biotin-PLGA. **(B)** ¹H-NMR of PLGA (top), biotin linker (middle), and biotin-PLGA (bottom). **(C)** Size (860 ± 40 nm) and charge (-15.8 ± 4.98 eV) of biotin-PLGA particles was

measured using dynamic light scattering (DLS). **(D)** Scanning electron microscope (SEM) image of biotin-PLGA particles. 77

Figure 5-3. Blending unmodified PLGA with biotin-PLGA is necessary to consistently form spherical particles. **(A)** SEM image of particles formed only with biotin-PLGA formed unstable particles. **(B)** Two ratios of biotin-PLGA : PLGA (50:50 and 75:25) were analyzed. There was no significant difference in SA binding between the two blends. 78

Figure 5-4. Biotin-PLGA particles can be efficiently conjugated with SA-FasL and induce apoptosis in mouse B lymphoma cell line. **(A)** Schematic of biotin-PLGA particles being functionalized with SA-FasL. **(B)** The amount of fluorescently tagged SA bound to the particles was investigated by varying the protein concentration (0, 100, 200, 400, 800, and 40,000 ng SA/mL in 1 mL) incubated with 1 mg of biotin-PLGA particles (“biotin particles”). As a control, 1 mg of unmodified PLGA particles was incubated with the same SA concentrations (“blank particles”). After two spins and washes, particles were dissolved in DMSO and fluorescence was measured, n=3. **(C)** The loading efficiency was calculated by dividing the bound SA by the incubated SA, n=3. **(D)** Biotin-PLGA particles functionalized with SA-FasL induce cell death in A20 cells. Particles were incubated with 400 ng / mL of SA-FasL in 1 mL with 1 mg of particles. After washing to remove unbound SA-FasL, particles were incubated with 1.5×10^5 A20 cells for 18 hours and cell death was analyzed via propidium iodide stain and flow cytometry (n=3). For comparison, soluble FasL was added to cells (0 and 10 ng) and demonstrated the ability to induce cell death at low concentrations (n=3). 80

Figure 5-5. Biotin-PLGA scaffolds can be efficiently conjugated with SA-FasL. **(A)** Schematic of biotin-PLGA particles functionalization with SA-FasL. **(B)** The amount of fluorescently tagged SA bound to scaffolds was investigated by varying the protein concentration (0, 100, 200, 400, and 800 ng SA/20 μ L) incubated with 2.5 mg biotin-PLGA scaffolds (“biotin”). As a control, unmodified PLGA scaffolds were incubated with the same SA concentrations (“blank”). After two washes, scaffolds were dissolved in DMSO and fluorescence was measured, n=3. **(C)** The loading efficiency was calculated by dividing the bound SA by the incubated SA, n=3. 82

Figure 5-6. FasL-decorated scaffolds induce apoptosis in mouse lymphoma cell line. **(A)** Scaffolds were incubated with SA-FasL (0, 40, 200, and 400 ng / 20 μ L). After washing to remove unbound SA-FasL, scaffolds were incubated with 1.5×10^5 A20 cells for 18 hours. Apoptotic and dead cells were analyzed via propidium iodide and annexin V staining and flow cytometry (n=3). **(B)** Scaffolds required a minimum loading of 200 ng FasL / mg scaffold to induce apoptosis in the majority of A20 cells. 83

Figure 5-7: Islets on scaffolds conjugated with SA-FasL demonstrate robust long-term tolerance. **(A)** Survival of allogeneic BALB/c islets mounted on PLGA scaffolds and transplanted in the epididymal fat pad of chemically diabetic C57BL/6 recipients. Groups included naïve islets mounted on SA-FasL-engineered PLGA scaffolds plus rapamycin (n = 6, MST > 200 days, P=0.0007 vs rapamycin alone), SA-FasL-engineered islets mounted on SA-FasL-engineered PLGA scaffolds (n = 6, MST = 46 days, P = 0.0007 vs rapamycin alone), and naïve islets transplanted

under a short cover of rapamycin ($n = 5$, $MST = 23 \pm 2.19$ days). All mice received islets loaded on 2 PLGA scaffolds. PLGA scaffolds were engineered with $2.5 \mu\text{g}/\text{scaffold}$, except 3 mice in the islet-FasL+PLGA-SA-FasL that were transplanted with PLGA scaffolds engineered with $0.5 \mu\text{g}/\text{scaffold}$ and all 3 animals rejected their grafts. Rapamycin was given to the indicated groups through i.p. injection at $0.2 \text{ mg}/\text{kg}$ daily for 15 days starting on the day of transplantation. Mice were monitored twice weekly for blood glucose levels. Those with $> 250 \text{ mg}/\text{dL}$ for two consecutive readings 24 hours apart were considered diabetic and rejecting the graft. Analysis done using log-rank test, $**P < 0.01$, $***P < 0.001$. **(B)** Blood glucose readings of two groups of mice from (A). **(C)** Intraperitoneal glucose tolerance test (IPGTT) of long-term islet grafts compared to naïve C57BL/6 mice after fasting for 6 hours, followed by i.p. glucose injection. Blood glucose of mice was taken starting just before injection and at the indicated time points.

85

ABSTRACT

Islet transplantation is an attractive treatment for type 1 diabetes (T1D) to restore the body's ability to endogenously produce insulin and rapidly respond to changes in blood glucose levels. Current clinical strategies where donor islets were intrahepatically transplanted have demonstrated success in a small number of patients. However, the widespread use of this approach is limited due to the generation of allo- and autoimmune responses, which contributes to significant islet loss and eventual graft failure. This dissertation presents the development of an extrahepatic biomaterial scaffold that creates an alternative transplant site for the localized delivery of soluble factors and immunoregulatory proteins to enhance long-term transplant function. Two scaffold designs were employed to improve islet cell transplantation and explore the effects of different scaffold architectures on islet engraftment in the form of encapsulating and microporous polyethylene glycol (PEG)-based hydrogels to support islet function in the fat pad transplantation site of mice using syngeneic and allogeneic models. This allowed for the unique comparison of encapsulation and microporous techniques with the same material. Microporous hydrogels demonstrated rapid response to glucose challenge and were quickly infiltrated by host tissue. In contrast, islet-encapsulating PEG hydrogels both engraft and respond to fluctuations in blood glucose slower than microporous scaffolds. To modulate the local inflammatory environment, transforming growth factor β 1 (TGF- β 1) was delivered from the PEG hydrogels and delayed rejection of allogeneic islets. Methods for sustained delivery of soluble factors were further explored by utilizing affinity peptides to localize lentiviral vectors for viral

gene delivery. Poly-L-lysine (PLL), a cationic polypeptide, was covalently attached to PEG hydrogels and demonstrated the ability to modulate the extent of virus adsorption and increase the half-life of the adsorbed virus by 20%. An alternative to PLL was discovered through phage display technology, with peptide sequences specific for the glycoprotein of the vesicular stomatitis virus (VSV-G) ectodomain, an envelope protein pseudotyped on the virus. These short, 12 amino acid affinity peptides were easily incorporated into the hydrogel, and reporter protein expression was increased 20-fold relative to control peptide, comparable to levels observed with the high molecular weight PLL. Finally, the modification of biomaterials scaffolds with Fas ligand (FasL) was explored to create an immunoprivileged microenvironment that is translatable to the clinic. Poly(lactide-co-glycolide) (PLGA) was conjugated with biotin and fabricated into particles and microporous scaffolds to allow for rapid and efficient conjugation with the chimera protein streptavidin-FasL (SA-FasL). PLGA particles and microporous scaffolds coated with FasL demonstrated the ability to induce apoptosis in a mouse B lymphoma cell line. Scaffolds were functionalized with FasL, seeded with islets from BALB/c donors, and implanted in epididymal fat pad C57BL/6 recipients. Scaffolds with FasL and a short course treatment of rapamycin restored euglycemia and showed robust tolerance indefinitely without the sustained use of immunosuppressive drugs. Together, this dissertation presents work that will further our understanding of allogeneic transplants and create tools that can be applied to treat T1D.

CHAPTER 1. Introduction

1.1 Motivation and objective

Type 1 diabetes (T1D) is a disorder that affects up to 3 million people in the United States and results from destruction of β -cells in the pancreas by autoreactive immune cells [1]. The disease requires constant management of the patient's diet and activity in addition to frequent monitoring of the blood glucose level. Although insulin can be produced through exogenous sources and administered via intramuscular injections or subdermal pumps, these treatments do not entirely prevent serious symptoms such as kidney failure, blindness, and tissue necrosis [2-5]. The highly dynamic nature of blood glucose levels makes regulating it with injections challenging and still leaves patients prone to complications [6].

An attractive alternative to insulin therapy is cell replacement therapy due to its ability to endogenously produce insulin and rapidly respond to changes in blood glucose levels. Due to these properties, islet transplants have been associated with reducing progression of diabetic microvascular diseases [7]. In order to provide long-term function, therapies must be developed that address immune system challenges and improve transplantation efficiency. The goal of this dissertation is to develop novel tools that modify the microenvironment and provide signals to resident cells that encourage tissue regeneration. By developing hydrogel scaffolds, which control cell-material interactions, an improved and translatable microenvironment was created that serves as a platform for future studies. These scaffolds were modified to locally deliver viral vectors which serve as a method to induce expression of therapeutically relevant proteins.

Additionally, scaffolds were modified with immunoregulatory proteins that locally modulate the immune system in order to prolong survival of transplanted cells.

1.2 Overview of this dissertation

Following the introductory chapter, Chapter 2 provides background information for topics relevant to the experimental work. After Chapter 2.1 provides an overview on current clinical treatments for T1D, Chapter 2.2 describes alternatives to portal vein transplantation. Chapter 2.3 covers biomaterials and their relation to treating T1D. Chapter 2.4 considers gene delivery and their importance in delivering soluble factors. Chapter 2.5 reviews techniques utilized to regulate the immune system in allogeneic transplants.

The experimental work in this dissertation was focused on modulating the islet microenvironment to promote transplantation survival. Chapter 3 developed PEG hydrogel scaffolds as alternative transplant site and explored how hydrogel architecture affects islet engraftment and survival. In addition to encapsulating and microporous designs, short-term localized protein delivery was demonstrated.

Chapter 4 discovered affinity peptides that bind lentivirus to enhance gene delivery from hydrogels. Although viral gene delivery is a potent tool for converting cells into bioreactors to produce therapeutic proteins, options for localizing the viral particles to PEG scaffolds are limited. Cationic peptides were investigated and phage display was utilized to identify lentivirus-specific peptides.

Chapter 5 addressed challenges presented by the immune system by employing PLGA scaffolds decorated with FasL, an immunoregulatory protein, to create an immunoprivileged

microenvironment that protects allogeneic cell transplants. Together, these methods will control the scaffold microenvironment to create conditions conducive to the survival of insulin-producing cells and subsequently provide a path towards a viable treatment of type 1 diabetes.

CHAPTER 2. Background

2.1 Introduction

Type 1 diabetes is a metabolic disease characterized by insufficient insulin production and subsequently high blood glucose concentrations (hyperglycemia). Insulin functions as a peptide hormone that is secreted from β cells in the pancreas and stimulates the uptake of glucose from the bloodstream into muscle, liver, and fat cells. Although the cause of disease onset is not known, it is suspected that a combination of genetic and environmental factors play a role in initiating the T-cell mediated autoimmune response to β cells. This theory is supported by the frequency of patients with the disease and specific HLA haplotypes that are associated with autoimmune regulation [8].

Although exogenous administration of insulin has vastly improved the prognosis for patients suffering from diabetes, it has become apparent that proper glycemic control is essential to prevent secondary microvascular complications (diabetic nephropathy, retinopathy, and neuropathy) and macrovascular complications (coronary artery disease, peripheral artery disease, and strokes) [9, 10]. Insulin pumps and continuous glucose monitors were a significant step forward in modulating glucose control and have made considerable advancements in recent years in approximating the pancreas. Despite advances in these technologies, maintaining proper glucose levels remains a challenge for many patients [11]. Long term imperfections in glycemic control lead to complications. Islet transplants reduces severe fluctuations. Furthermore, production of C-peptide, a byproduct of endogenous insulin

production, plays a role in minimizing nephropathy and improves peripheral nerve function [12].

A cell-based solution is preferable, as it can provide improved feedback regulation and endogenously produce insulin. Whole organ pancreas transplants have been performed since 1966 and have seen considerable success, but the process is considered invasive, technically challenging, and requires management of the pancreatic exocrine secretions. Islet transplants offer more flexibility and, similar to whole pancreas transplants, can reverse many of the secondary complications. Notably, the technique known as the Edmonton Protocol has shown promising results in which islets from several donors are implanted into the hepatic portal vein and administered a life-long regimen of immunosuppressants. Following the procedure, 44% of the patients were insulin independent with adequate glycemic control three years after the final transplantation [13]. However, this approach faces serious short and long-term challenges as intraportally transplanted islets are directly exposed to blood that triggers an instant blood-mediated inflammatory reaction (IBMIR), a pathological nonspecific inflammatory response that results in severe islet damage and significant graft loss. Islets introduced into the portal vein must also remodel and vascularize their microenvironment as the low oxygen tension in the liver results in ischemia-induced cell loss [14]. Together, the inflammatory response can account for more than 60-80% of islet loss days post-transplant within a matter of hours to days [15].

Furthermore, IBMIR promotes a pro-inflammatory environment which then leads to activation of the adaptive immune system in the form of activated T- and B-cells that causes additional injury to islets [16]. The combined effects of the auto- and alloimmune response require the administration of a lifelong regimen of immunosuppressants that leaves the patient

vulnerable to infection and cancer [17]. Despite refinements in specific immunosuppressive drugs and dosage used in islet transplantation [18, 19], these challenges have resulted in only 15% of cases still euglycemic after nine years [20]. Furthermore, the number of islets required for the procedure is unsustainable for widespread use, as the harmful effects of IBMIR necessitate the need for multiple transfusions from two to four donors into a single recipient [21, 22].

2.2 Alternative transplant sites

Although the liver has historically been a favored islet infusion site due to its ease of access, the inflammatory effects from IBMIR and hepatic tissue ischemia make it a suboptimal location [23]. Furthermore, the liver cannot be extensively modified since it carries out important functions such as blood detoxification and aids in digestion. In order to avoid many of these complications, an alternative transplant site must be established in which the environment around the islets can be carefully modulated. Qualities that are considered desirable for islet transplants include sufficient vascularization for the high oxygen requirement of the islets, creation of a microenvironment that prevents early islet loss, minimally invasive procedure, and easily retrievable transplants for follow-up studies. Of particular note, revascularization is essential not only for the high oxygen requirements of the islets, but also to allow for rapid response to fluctuations in the blood glucose concentration [24]. Furthermore, the islet isolation process puts stress on the islets, thus highlighting the importance of rapid revascularization in the post-transplant environment. Otherwise, poor vascularization leads to islet dysfunction and impairs metabolic function [25].

Besides the intravascular portal vein, extravascular sites (pancreas [26], omentum [27], kidney capsule [28], and gastric submucosa [29]) and immunoprivileged sites (anterior chamber of the eye [30] and testis [31]) have been considered. The pancreas is the native tissue site of islets and is expected to be an ideal environment for islet transplantation. Indeed, in studies utilizing mouse models that compared intraportal to intrapancreatic transplants, the pancreas demonstrated better insulin production and control, improved glucose oxidation, and higher (pro)insulin biosynthesis [25]. These results also highlighted the challenges faced with intraportal transplants in which islets are chronically exposed to high glucose levels produced by the surrounding hepatocytes in addition to functioning in environment that is the site of blood detoxification. Islets still experience physiological changes when transplanted back into the pancreas, as suggested by evidence showing they are slightly hypoglycemic and undergo some gene expression changes [25, 32]. Even though intrapancreatic transplants have provide a viable microenvironment that requires fewer islets to reverse hyperglycemia than other sites like the portal vein or the kidney capsule and provide efficient glycemic control [33], many of these studies have been performed in syngeneic models that do not take into account the immune response. Furthermore, the surgery site is technically challenging as it risks acute complications from digestive enzyme leakage and it is theorized that the autoimmune response from T cells will respond quicker [34]. As such, it is not considered a viable option for clinical applications.

The omentum is a layer of peritoneum that surrounds abdominal organs and provides several attractive properties, including its good vascularization, portal drainage, and has been shown to safely handle large transplant volumes in large animals models [35]. Previous studies in rats and dogs that utilized an omental pouch successfully restored euglycemia but required an

increased graft volume when compared to intraportally transplanted islets. [36, 37]. The omentum in mice differs significantly from humans in that it is considerably smaller and poorly vascularized. Therefore, studies with mice wishing to translate to the human omentum often utilize the epididymal fat pad which is well vascularized and is similarly easily accessible and removed from the animal without disrupting any vital bodily functions [38]. This site has also been the site of numerous studies implanting biomaterial scaffolds to further modify the microenvironment [39-41]. However, the epididymal fat pad differs from the human omentum in that it lacks portal drainage. Overall, the omentum offers sustained insulin control due to its high vasculature and pro-angiogenesis cytokines [42], but the requirement for large islet number necessitates the need for additional long-term data.

A widely used option is the renal subcapsular site (also known as the kidney capsule) which is frequently applied in murine models. Compared to the native tissue in the pancreas, the renal capsule has relatively poor blood supply (15 mmHg O₂) and does not provide an oxygen-rich environment required for maximal islet viability (40 mmHg O₂) [43]. However, the capsule in mice is readily accessible and has been demonstrated to reverse chemically-induced diabetes within a few days after transplants [44]. It is also considered an attractive site as it requires less islet volume when compared to intraportal transplants (250 islets in the subcapsular site versus 700 islets in the portal site [45, 46]) and the ease of retrieval via a simple nephrectomy [47]. Unfortunately, the surgery in humans is more difficult and access is much more invasive. Finally, the space available for transplanting islets severely limits its use beyond a tool in murine models.

The gastric submucosa is an appealing option as it is a natural entry site for glucose into the body which makes it a strong candidate for islet transplants as it allows for rapid response to

glucose stimuli. It consists of a dense network of vasculature, lymphatics, and connective tissue that makes it a suitable environment for islets and is available via endoscopy [48]. Because of its relative ease of access, follow-up analysis is straightforward. Although it has shown efficacy in rat, hamster, and pig models with better glycemic control than the kidney capsule, there has not been any head to head study with portal vein transplants [29, 49, 50]. As such, it has not yet been translated into the clinical studies and further studies must be completed before it can be considered a viable alternative to portal vein transfusion.

In regards to immunoprivileged transplant sites, the anterior chamber of the eye and the testis are commonly studied sites due to their ability to promote engraftment while not requiring the use of immunosuppressants. The ocular microenvironment's immune privileged status is well-characterized and is maintained by a blood barrier along with immunoregulatory and immunosuppressive molecules [51]. *In vivo* characterization of the anterior eye chamber using laser-scanning microscopy has shown allogeneic islet transplants engraft into the iris, became vascularized, responded to glucose stimuli, and reversed chemically-induced diabetes in all mice within two weeks [52]. In this study, mice were euglycemic for over 200 days until transplant removal. More long-term studies have demonstrated survival of α , β , and δ -cells after 1.5 years, although function was not assessed [53], and the procedure has been proven safe in non-human primates without causing vision problems or other adverse effects [30].

The testes have a developed immune privileged mechanisms similar to the eye, but with its own unique features. The Sertoli cells provide a physical blood barrier to isolate germ cells from the immune system along with a host of immunoregulatory compounds that suppress pro-inflammatory responses from the immune cells to maintain the immunoprotective environment.

Allografts [54] and even xenografts [55] into the testes have been proven successful in delaying rejection and it has been shown that grafts generate much less CD8(+) T cells while inducing increased numbers of CD4(+)CD25(+) regulatory T cells when compared to subrenal transplants [56]. Interestingly, Sertoli cells have been transplanted under the renal capsule with allogeneic islets and slightly delayed rejection by 15 days even when no immunosuppression was used [57]. Despite the success that these immunoprivileged sites have seen in animal models, these sites are generally not considered clinically relevant due to the small size of their organs.

2.3 Biomaterial scaffolds

As no transplant site is clearly superior and meets all the requirements for islet transplantation, an alternative site can be engineered. Scaffolds are biomaterial devices that provide chemical and physical cues to control the microenvironment and subsequently alter cellular behavior. Cells sense and respond to physical cues on the scaffold surface via integrins and other cell adhesion molecules which integrate these signals into cellular processes and gene expression [58]. Scaffolds also serve as a platform for controlled release of chemical cues such as anti-inflammatory drugs, growth factors, or inhibitors [59-61]. Three dimensional scaffolds can even be engineered to spatially regulate drug release in the microenvironment to fulfill specific functions [62, 63]. In addition to providing signals, the scaffold is space filling and provides an environment that resists compression and tension to create an environment in a part of the body that would normally not be possible [64]. The porous nature of scaffolds is essential to promote cellular infiltration, nutrient transfer, and vascularization to increase cell survival. In the context

of transplanting β cells, vascularization is required for sensing and release of insulin in addition to efficient nutrient and oxygen transfer.

Material selection plays a central role in scaffold creation. Scaffolds are formed from natural materials (e.g. collagen, fibrin, or alginate) or synthetic polymers (e.g. poly(lactic-co-glycolic acid) (PLGA), polycaprolactone (PCL), or polyethylene glycol (PEG)). Natural scaffolds possess intrinsic signals such as cell binding domains and cell-triggered degradation [65, 66]. However, these materials may elicit immunogenic responses due to purification concerns [67]. Synthetic materials offer greater control as they consist of well-defined polymers and their mechanical properties can be engineered for specific applications.

Alternatively, materials can be classified based on their mechanical properties, with hydrogels being of especial interest for tissue engineering. Hydrogels are a promising platform for therapeutic applications due to their tissue-like mechanical properties and ease of cell encapsulation. Hydrogels are typically categorized as either natural (e.g. fibrin, alginate, and collagen) or synthetic (e.g. PEG and poly(hydroxyethyl methacrylate) (pHEMA)). Whereas natural hydrogels have established interactions with cells, synthetic hydrogels allow for more precise interactions and can be modified with proteolytically degradable linkers to target specific cell populations [68]. To provide dynamic control of cell integration and release of encapsulated factors, both natural and synthetic hydrogels have been engineered to degrade in response to pH or temperature [69, 70]. Of particular interest are PEG hydrogels, which is a versatile material that can be easily functionalized with peptides and proteins for localized delivery, or chemical cues can be encapsulated and released via diffusion. Degradation can be controlled by incorporating proteolytically degradable peptide linkers. Furthermore, PEG is a

biologically inert material and known to have a low immunogenic response [71]. By reducing the response of the innate immune system to the scaffold, activation of the adaptive immune system can be minimized, thus reducing the risk of transplant rejection [72].

2.4 Viral delivery of soluble factors

Delivery of soluble factors to the local environment of the transplanted islets can promote survival, vascularization, and growth. Systemic delivery frequently results in off-target effects and requires higher doses. The localized delivery of gene therapy vectors represents a versatile method to promote the sustained expression of inductive factors in numerous applications of regenerative medicine. The delivery of gene therapy vectors is considered versatile as the nucleotide sequence can readily be exchanged to express one or more factors using a single delivery system [73, 74]. Both non-viral and viral vectors can promote prolonged transgene expression, with non-viral vectors generally considered to be safer as they generally do not integrate into the host chromosome, yet have significantly lower levels of transgene expression than viral vectors. Viral vectors have evolved mechanisms for effectively transducing target cells and thus provide the greatest levels of expression.

Of particular interest, lentiviral vectors are well-suited for clinical gene delivery applications due to their capacity for stable, long-term integration by inserting its genes into the host genome [75], and have recently received approval in a Phase 2/3 clinical trial [76]. Lentiviral tropism has been greatly expanded by pseudotyping its envelope with the glycoprotein of the vesicular stomatitis virus (VSV-G) which not only allows for the virus to infect a wide range of cell types, but also deliver genes to both dividing and non-dividing cells [77-80]. Additionally, their

ease of production, relatively low immunogenic profile [81], and large genetic payload make them excellent candidates as gene delivery vectors. Advances in lentiviral vector design have yielded improvements in their safety and efficiency over early generation viruses, and have been effectively used in clinical research to treat a variety of diseases including immune disorders [82], brain disease [83], and retinal dystrophy [84, 85].

Current methods to localize lentivirus to scaffolds have applied a variety of methods that take advantage of properties of the virus and scaffold material. A simple approach is the direct adsorption of the virus to a charged polymer's surface like poly(1,8-octanediol citrate) (POC) and poly(glycerol-sebacate) (PGS) which utilize electrostatic interactions between the viral particle and negatively charged carboxyl groups on the materials' surface [86]. Similarly, positively charged hydroxyapatite nanoparticles have been incorporated into poly(lactide-co-glycolic acid) (PLGA) scaffolds and demonstrated a 10-fold increase in transgene expression and increased the half-life of the virus by 17% [87, 88]. However, these approaches rely on electrostatic interactions, which are subject to non-specific adsorption by unwanted proteins, and are material-specific. Alternatively, methods that utilize specific interactions avoid these off-target effects. Phosphatidylserine (PS), a phospholipid, has been implicated in lentiviral binding to cell membranes and has been incorporated into PLGA microspheres to enhance localized lentiviral delivery [89]. Not only did the PS prolong the expression of the reporter gene, but its specific binding capability was demonstrated by lack of non-specific adenovirus binding. Another approach is the modification of the lentiviral coat proteins to enable covalent crosslinking with fibrin hydrogels, which allows for release of lentiviral particles as the hydrogel degrades [90]. However, these specific-binding approaches still face significant challenges. The incorporation

of PS into other scaffold materials is difficult and its role in signaling apoptosis may make it undesirable for further *in vivo* applications. Although the modification of the lentiviral coat protein provides excellent specificity for localization to the fibrin hydrogel, the virus is covalently cross linked to the material. Due to the half-life of the lentivirus being only 8-9 hours at 37°C, most of the virus will deactivate before coming in contact with cells.

2.5 Immunoregulation

Although considerable progress has been made with transplanting islets in biomaterial scaffolds, much of the success has occurred in syngeneic transplants with chemically-induced diabetes. A critical challenge that needs to be addressed is the immune system's role in the destruction of insulin-producing cells. T1D is mediated by CD4 positive T cells that react to antigens specific to β cells [91]. In addition to recurrence of the original autoimmune disease, the allogeneic response to transplanted tissue represents a significant hurdle. Tissue transplants are rejected via the adaptive immune system which senses mismatched MHC's and induces a subsequent inflammatory cascade. The Edmonton protocol's principle innovation was the special combination of immunosuppressants to limit immune-mediated islet destruction, but the lifelong systemic administration results in undesirable side effects. Complications such as lymphopenia and expansion of autoreactive CD8 positive T cells motivate the need for a targeted approach that locally modulates the immune system [92].

In an effort to isolate islets from the immune system, groups have tried to encapsulate islets in a semi-permeable membrane that physically shields insulin producing cells from the immune system while still allowing for oxygen, nutrients, and protein transport [93, 94].

However, mass transport limitations, insufficient immunoprotection, and the inability to reproduce results in large animal models have limited use of micro- or macro-encapsulating technologies. Encapsulated islets inherently limit vascularization and subsequently delays the response of β cells to fluctuations in blood glucose concentrations. Many encapsulating systems suffer graft failure as a result of fibrosis around capsules [95]. Finally, these membranes do not limit the transport of inflammatory cytokines and other immunoreactive molecules [96, 97].

An alternative approach to achieve localized immunosuppression is the controlled release of immunoregulatory proteins from biomaterial scaffolds. Due to the central role of T-cells in allogeneic rejection, FasL is a viable option due to its role as a major regulator of T cell homeostasis. After antigen clearance by CD 8 positive T cells, deletion of effector cells by FasL-mediated apoptosis occurs [98]. FasL works by binding the Fas receptor (FasR) which forms the death-inducing signaling complex (DISC) which is composed of Fas-associated protein with death domain (FADD) and caspase 8 which subsequently transduces a downstream signal cascade that leads to cell death. The challenge with protein or drug delivery is that rejection is only delayed and will fail as soon as the compounds are depleted from the local environment unless tolerance is induced.

Early studies in inducing tolerance demonstrated that development of autoimmune diabetes in NOD mice can be prevented and reversed with bone marrow (BM) transplants from non-autoimmune allogeneic sources and subsequently inducing donor-specific tolerance [99, 100]. However, this approach suffers from graft vs host disease (GvHD) in which T cells transplanted with the BM attack the host. This approach has been refined to use hematopoietic stem cells (HSC's) [101]. Tolerance can also be induced by treating donor splenocytes with 1-

ethyl-3-(3-dimethylaminopropyl)carbodiimide (EDC) which target recipient antigen presenting cells (APC's) and induce expression of co-inhibitory molecules [102].

CHAPTER 3. Evaluation of Encapsulating and Microporous Hydrogel Scaffold Designs on Islet Engraftment in Rodent Models of Diabetes

3.1 Introduction

Islet transplantation is therapy which can mimic normal pancreas physiology and aid in maintenance of normoglycemia [9]. However, this procedure is not widely employed in the clinic due to graft failure post-transplant, largely mediated by inflammatory factors and the host immune response. Upon injection into the hepatic portal vein, transplanted islets are subject to IBMIR, which can account for significant islet death within hours to days after the transplant [15]. Furthermore, IBMIR promotes a pro-inflammatory environment, which then leads to activation of adaptive immunity and additional islets loss [16]. Scaffold-based strategies have been successfully employed to create alternative transplant sites [103-105]. Previous work in our lab has made extensive use of PLGA scaffolds, but its material properties are dissimilar to tissue and the mechanical disparity can promote inflammation [106]. In contrast, PEG hydrogels are a versatile material ideally suited for tissue engineering due to its tissue-like mechanical properties, ease of functionalization, and controlled rate of degradation [107]. Furthermore, its macrostructure can be further modified to contain pores and channels to enhance cell infiltration and promote entrapment of viral or non-vectors [108].

PEG-maleimide hydrogels were adapted into an encapsulating and microporous scaffold architecture using polydimethylsiloxane (PDMS) molds to easily and reproducibly fabricate the gels with matching dimensions. PEG functionalized with maleimide offers a fast and efficient

reactive group for functionalization [109]. PEG-acrylate, which is commonly used to form photopolymerized hydrogels, is prone to hydrolysis of conjugated peptides [110], whereas maleimide groups can form covalent bonds that are resistant to uncontrolled degradation [111]. Pores for cellular infiltration can be created by casting the PEG precursor around sacrificial particles followed by photocrosslinking of hydrogel. Photocrosslinked hydrogels are favorable because they quickly form at ambient conditions while providing spatial and temporal control, thus allowing for geometrically complex hydrogels to be formed with relative ease [112]. The particles are leached from the scaffold in an aqueous buffer, leaving behind a porous structure. This particle leaching process is advantageous compared to other porogen approaches such as freeze drying or gas foaming due to the ease of which pore size and porosity can be controlled [113]. Encapsulating hydrogels were formed utilizing Michael-type addition reactions to eliminate any concerns associated with free-radical polymerization affecting the viability of the cells. Initial studies employed a syngeneic transplant model in an extrahepatic site (i.e. epididymal fat pad) of diabetic mice to evaluate islet survival and function, and to characterize the innate immune response to the transplantation and surgical process. Subsequent studies employed allogeneic islet transplantation, with similar characterization of the islet function, and characterization of both the innate and adaptive response to the transplanted cells.

Finally a method to locally deliver proteins from the PEG scaffolds was developed. In addition to mechanical cues provided by the scaffold, another method of modulating the microenvironment is controlled release of soluble compounds from the scaffold. There are a variety of delivery mechanisms such protein entrapment in the nanoporous PEG network [114], peptide affinity binding [115], or viral gene delivery [116]. Previous work in our lab has indicated

that proteins entrapped in the PEG rapidly diffuse out of the scaffold during the leaching step which results in insufficient protein delivery. Additionally, the high salt concentration used in the fabrication of the scaffold may damage any protein that is retained. We demonstrated that a PLGA disc loaded with protein and inserted inside of the porous PEG scaffolds was able to deliver therapeutically relevant amounts of protein. Herein, we used TGF- β due to its ease of detection in *in vitro* and *in vivo*, in addition to its release being well characterized in PLGA scaffolds [117].

3.2 Materials and methods

3.2.1 Encapsulated and microporous hydrogel fabrication

Encapsulated hydrogels were formed by mixing PEG-maleimide (4-arm, 20kDa MW, JenKem Technology USA) and CGRGDS (CelTek Peptides) in HEPES Buffer (pH 7.2) to yield a final PEG concentration of 10% (wt/vol) and RGD concentration of 5 mM. The PEG-CGRDS solution was allowed to react via Michael-Type addition for 5 minutes at room temperature and then stored on ice. Next, the functionalized PEG precursor was added to sedimented islets in an Eppendorf tube (in approximately 6 μ L of HBSS 1X media (Corning) supplemented with 10% FBS). The bottom of a disc-shaped PDMS mold (diameter = 5 mm, height = 1 mm) was covered with 3 μ L of a non-degradable peptide crosslinker solution (G_CY_DKN_DRG_CY_DKN_DRC_G, custom synthesis and purification by CelTek Peptides). The peptide contained tyrosine (Y) and asparagine (N) amino acids in the D-configuration to prevent cleavage from plasmin, which inhibits hydrogel degradation. The PEG precursor containing islets was added to the mold containing the YKNR solution and an additional 3 μ L of YKNR was added on top for a final YKNR concentration of 9.6

mM. The hydrogel was incubated at 37°C for 30 minutes to allow the crosslinking reaction to reach completion. Final gel volume was approximately 25 μ L.

Gelatin microspheres were formed by dissolving type A gelatin, bloom strength 300 (Sigma), into ultrapure water heated to 80 °C for a final concentration of 10% (w/w). The gelatin solution was added dropwise into mineral oil heated to 80 °C and stirred at 500 rpm. The water-oil emulsion was cooled using an ice jacket while maintaining a stir speed of 500 rpm for 1 hour. The ice jacket was removed and acetone was added while the stirring speed was maintained. Next, the stirring was stopped and the mineral oil and acetone were allowed to separate, followed by removal of the mineral oil. The acetone wash and mineral oil removal was repeated for a total of three times before all liquid was removed and the remaining gelatin microspheres were mixed by hand until all acetone evaporated. Particles were stored under dry inert gas until use.

Microporous PEG hydrogels were fabricated by dissolving 20 kDa 4-arm PEG-maleimide (JenKem Technology USA) in HEPES buffer for a final concentration of 20% (wt/vol). The photoinitiator, Irgacure 2959 (BASF) was dissolved in N-vinylpyrrolidone at a concentration of 600 mg/mL and added to the PEG precursor solution for a final concentration of 1 wt%. For hydrogels utilizing NaCl as a porogen, NaCl was added to the PEG precursor to make a saturated solution. Forty milligrams of NaCl particles (average diameter = 250 μ m) or gelatin microspheres were then added to a polydimethylsiloxane (PDMS) mold (diameter = 5 mm, height = 1 mm) and 10 μ L the saturated PEG solution was added. After irradiation with UV light, the porogen was leached from the scaffolds by incubating in ultrapure water overnight. Final gel volume was approximately 25 μ L.

Non-porous PLGA discs containing TGF- β 1 were fabricated as described in Liu, et al [117]. Briefly, 2 mg of PLGA microparticles and 2 μ g of TGF- β 1 were reconstituted in 100 μ L of an aqueous 10 mg/mL D-mannitol solution and lyophilized. The PLGA-protein-mannitol powder was pressed in a 3 mm KBr pellet hand press (Pike Technologies) and gas-foamed at 800 psi under CO₂ gas for eight hours using a previously described technique [118]. These discs were either placed on top of the encapsulated hydrogels or the microporous scaffold was formed around the disc.

3.2.2 Islet isolation and transplantation

For syngeneic studies, islets were isolated from healthy 10-12 week old male and female C57BL/6J mice (Jackson Laboratories) following standard islet isolation procedures. Male C57BL/6J recipient mice were between 14-18 weeks of age. For allogeneic transplants, female BALB/c (Jackson labs) islet donors and male C57BL/6J transplant recipients between 10-12 weeks were used. Four days prior to islet transplantation, recipient mice were injected with 220mg/kg of streptozotocin (Sigma) to chemically induce irreversible diabetes. Nonfasting blood glucose levels were taken using a OneTouch Basic Glucose Monitor (Aviva) and only those mice with a measurement of 300 mg/dL or greater on consecutive days (day before and day of transplant) were used as recipients. Normoglycemia was denoted as <200 mg/dL in syngeneic studies. All hydrogel scaffolds in syngeneic studies were loaded with 700 islet equivalents (IEQ). To load microporous hydrogels, islets were concentrated in 30 μ L and applied to the top of a dehydrated hydrogel. Each mouse received one gel into the fat pad transplantation site. For allogeneic studies, 10-12 week old female BALB/c mice (Harlan Laboratories) were used as donors.

Normoglycemia was denoted as <250 mg/dL and mice received 1,300 IEQ for allogeneic transplant studies. Each mouse received one hydrogel implant into the fat pad. All studies were approved by the Northwestern University Animal Care and Use Committee.

3.2.3 Intraperitoneal glucose tolerance test

Intraperitoneal glucose tolerance tests (IPGTTs) were performed at 4 weeks post-transplantation to assess the ability of the hydrogel materials to respond to glucose challenges. A D-glucose solution (250 mg/mL sterile PBS (-/-)) was created for injection. After a 3 hour fast period, 2 g/kg of D-glucose was injected intraperitoneally. Blood glucose levels were measured at baseline (before injection), 15, 30, 60, 90, 120, and 150 minutes after the glucose injection.

3.2.4 Immunohistochemistry

Snap-frozen histological sections were stained with primary antibodies guinea pig polyclonal anti-swine insulin (Jackson Labs) and Hoechst (Invitrogen) at dilutions 1:250 and 1:2000, respectively. Secondary antibodies included Dylight donkey anti-guinea pig 488 (Jackson Labs) at a dilution of 1:400.

*3.2.5 TGF- β 1 *in vitro* release studies*

Scaffolds were leached in 10 mL of water containing 1% BSA (Millipore), sterile filtered, for two 10 minute washes. Leached scaffolds were placed in a 24 well plate with 1 mL of media (DMEM supplemented with 10% FBS, 1% penicillin and streptomycin) and incubated at 37 °C. At days 1, 3, 7, 14, and 21 the supernatant was replaced with fresh media and the old media was frozen. TGF- β 1 in the media was quantified with a TGF- β 1 ELISA kit (R&D Systems).

3.3 Results

3.3.1 Encapsulating and Microporous Hydrogel Fabrication

Encapsulated hydrogels were formed by functionalizing 4-arm PEG maleimide with 5 mM CGRGDS and crosslinked in a PDMS mold, using a non-degradable, three-cysteine-containing crosslinking peptide (GCYKNRGCYKNRCG) (Fig. 3-1A). After 5 minutes at 37°C, gels were fully crosslinked and intact with no residual macromer (Fig. 3-2A). Resultant gels were 25 μ L and 10% (wt/vol). Dimensions of the encapsulating gel were 5 mm in diameter and approximately 1 mm in height, adequate for implantation into the fat pad. Islet viability with these gelation conditions was confirmed in a previous study [41].

To fabricate microporous hydrogels, 20 (w/v)% 4-arm PEG-maleimide (20,000 kDa) was dissolved in HEPES buffer and the cell adhesion peptide NH₂-CGRGDS-Ac was conjugated to the PEG via Michael-type addition between the maleimide and the cysteine's thiol group. Salt (NaCl) and gelatin were selected as porogens due to their nontoxic properties and their ability to be rapidly leached from the scaffold in mild conditions (Fig. 3-1B, C) [119, 120]. To prevent the salt porogen particles from dissolving in the aqueous environment prior to gelation, salt was added to the PEG precursor to make a saturated solution. Gelatin microspheres (size: 107 \pm 4 μ m, n = 41, \pm SEM) or salt crystals (size: 274 \pm 12 μ m, n = 41, \pm SEM) were added to a polydimethylsiloxane (PDMS) mold followed by the PEG solution (Table 3-1, Fig. 3-2B, E). Hydrogels were cross linked with UV light and Irgacure-2959, a commercially available photoinitiator commonly used due to its relatively cytocompatible properties [121]. The scaffolds were incubated in ultrapure water at 37°C for overnight to rapidly dissolve the porogen and leave a highly porous PEG scaffold (Fig. 3-2C, D, F, G). The PEG wt% (wt/vol) of the microporous hydrogel was 20%, as lower concentrations

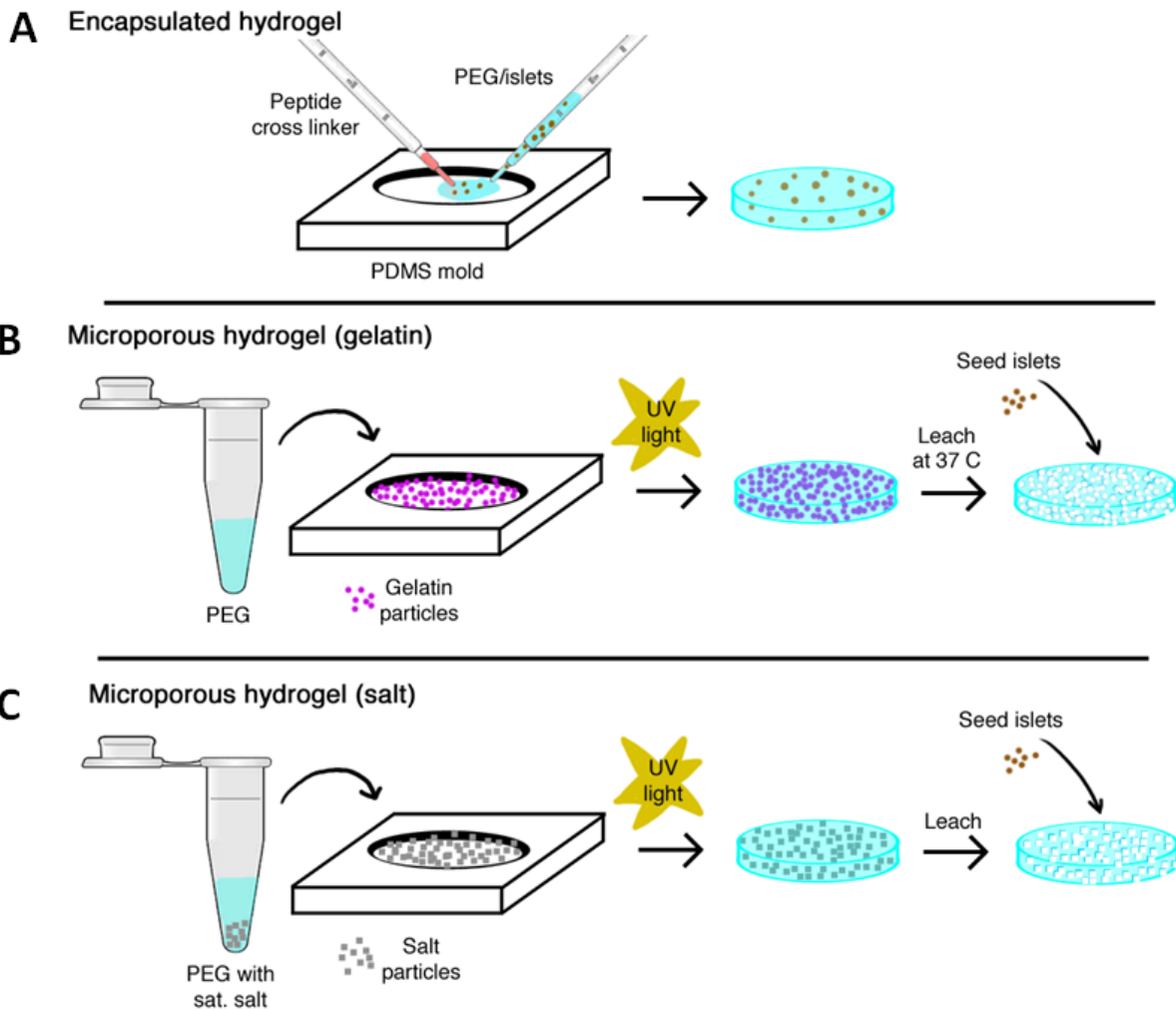


Figure 3-1. Fabrication of PEG-maleimide hydrogels. **(A)** Encapsulated hydrogels are formed by mixing the peptide cross linker $\text{G}\underline{\text{C}}\text{YKNR}\text{G}\underline{\text{C}}\text{YKNR}\underline{\text{C}}\text{G}$ with a PEG/islet solution in a PDMS mold. Cross linking is induced via Michael-type reaction between the thiols in the peptide and the maleimide groups on the PEG. **(B)** Microporous hydrogels are formed by packing gelatin particles into a PDMS mold and adding PEG. After initiating free-radical polymerization via UV light and the photoinitiator I-2959, the gelatin particles are leached out at 37 °C, leaving a porous hydrogel that can be seeded with islets. **(C)** Microporous hydrogels with salt pores are formed in a manner similar to the gelatin microspheres, but require the PEG precursor solution to be saturated with salt prior to being added to the salt-packed PDMS mold. After polymerization, the salt is quickly leached out and the scaffold can be seeded with islets.

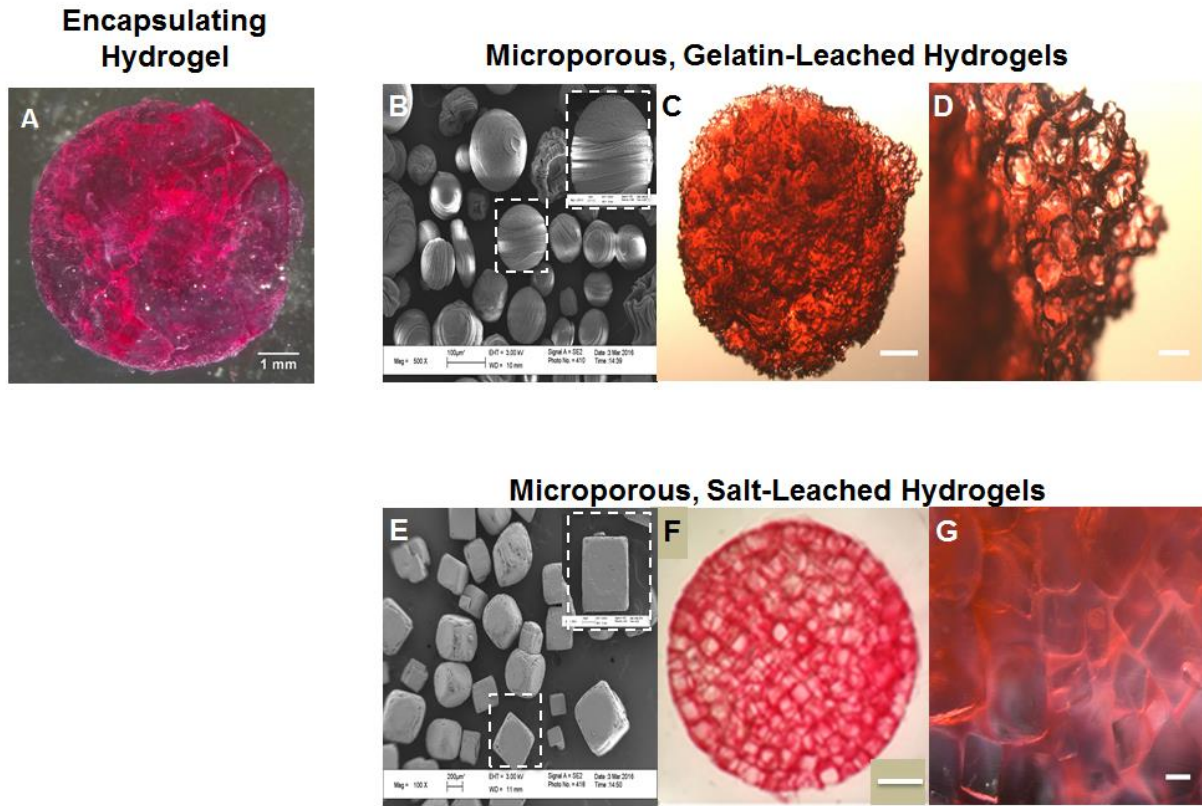


Figure 3-2. Encapsulating and microporous hydrogels for islet transplantation. (A) 10% (wt/vol) bulk PEG hydrogels were fabricated to encapsulate islets. (B) Gelatin particles (size = $107 \pm 4 \mu\text{m}$, $n=41$) were fabricated, incorporated into 20% PEG (wt/vol), and subsequently leached to form a (C-D) resultant hydrogel with a microporous architecture for islet seeding. Similarly, (E) salt particles (size = $274 \pm 12 \mu\text{m}$, $n = 41$) were incorporated into 20% PEG (wt/vol) to form a (F-G) microporous gel for islet seeding. Scale bar: 1 mm (A, C, F), 100 μm (B), 200 μm (D,E,G). Gels were stained with sirius red for visualization.

Particle	Mean (μm)	95% CI (μm)
Gelatin	107 ± 4	99-114
Salt	274 ± 12	114-299

Table 3-1. Particle size of gelatin and salt particles used as a porogen for microporous hydrogels. Mean is reported with standard error mean. Gelatin ($n = 52$), salt ($n=41$).

resulted in collapsible gels with insufficient integrity for islet seeding. The volume and dimensions of the microporous hydrogel were the same as the encapsulating hydrogels. Following swelling, encapsulating and microporous hydrogels were approximately 6.5 mm in diameter and 1.5 mm in height, a size still suitable for transplantation.

3.3.2 Syngeneic islet transplants in encapsulating and microporous hydrogels

The engraftment and function of encapsulated islets and islets seeded on microporous hydrogels were investigated by transplantation into the fat pad site of streptozotocin-induced diabetic mice. Initial studies were performed in a syngeneic model to confirm the hydrogel materials can support islet function in the absence of an immune response. Bulk, non-degradable encapsulating hydrogels with 700 islet equivalents (IEQ) reversed diabetes in recipient mice, and an average normoglycemic (<200 mg/dL) blood glucose level of 175 ± 31 mg/dL ($n=3$, \pm SEM) was achieved by day 17 (Fig. 3-3A). Normoglycemic readings were recorded for all recipient mice at day 21 (140 ± 6 mg/dL) and mice remained normoglycemic until the end of the 2-month study. Encapsulating hydrogels were removed (indicated with a black arrow) at day 62 and recipient mice reverted to hyperglycemic state within 2-4 days post-removal, which confirmed glycemic control is due to the hydrogel graft and not any remaining endogenous islets post-streptozotocin injection.

A pilot study of the gelatin-leached microporous hydrogels were seeded with 700 IEQ demonstrated the ability to reverse diabetes by day 10. Interestingly the blood glucose levels spiked between days 87 and 100 for unknown reasons. Following removal of the hydrogel at day 108, mice immediately reverted to hyperglycemia. Gelatin-leached hydrogels were more

extensively explored in Fig. 3-3C in which the microporous hydrogels were seeded with 200 islets, similar to previous studies in PLGA scaffolds [104, 122]. The average normoglycemic blood glucose level was 173 ± 10 mg/dL ($n=4$, \pm SEM) and all mice reversed diabetes by day 9. For comparison, a microporous PLGA scaffold was also seeded with 200 islets and restored euglycemia by day 7, two days earlier than the microporous hydrogel. Both scaffolds reverted to hyperglycemia within 2-4 days after graft removal.

Salt-leached, microporous hydrogels seeded with 700 IEQ displayed an average normoglycemic blood glucose level of 190 ± 20 mg/dL ($n=5$ pre-graft removal, $n=4$ post-graft removal, \pm SEM) by day 15 post-transplant (Fig. 3-3D). Normal blood glucose levels were recorded for all recipient mice at day 20 (139 ± 15 mg/dL). Upon removal of the transplanted microporous hydrogel at day 30, mice reverted to a hyperglycemic state within 2-4 days. Engraftment rates did not differ between encapsulating and microporous hydrogels containing 700 IEQ, as consistent normoglycemia was achieved approximately at 3 weeks post-transplant in both experimental groups. Collectively, these syngeneic transplant studies confirm the feasibility of non-degradable, encapsulating and microporous PEG hydrogels to support islet function post-transplant in the fat pad transplant site.

An intraperitoneal glucose tolerance test (IPGTT) was performed on mice that received hydrogels to investigate glucose responsiveness. The blood glucose levels of diabetic recipient mice with encapsulating hydrogels peaked at 30 minutes post-injection of glucose, versus control mice which peaked at 15 minutes post-injection (Fig. 3-4A). At 60 minute time points, blood glucose levels mice decreased toward normoglycemia in both groups. Normoglycemic levels (<200 mg/dL) were achieved at 120 minutes and 90 minutes for the encapsulating gel (175 ± 9

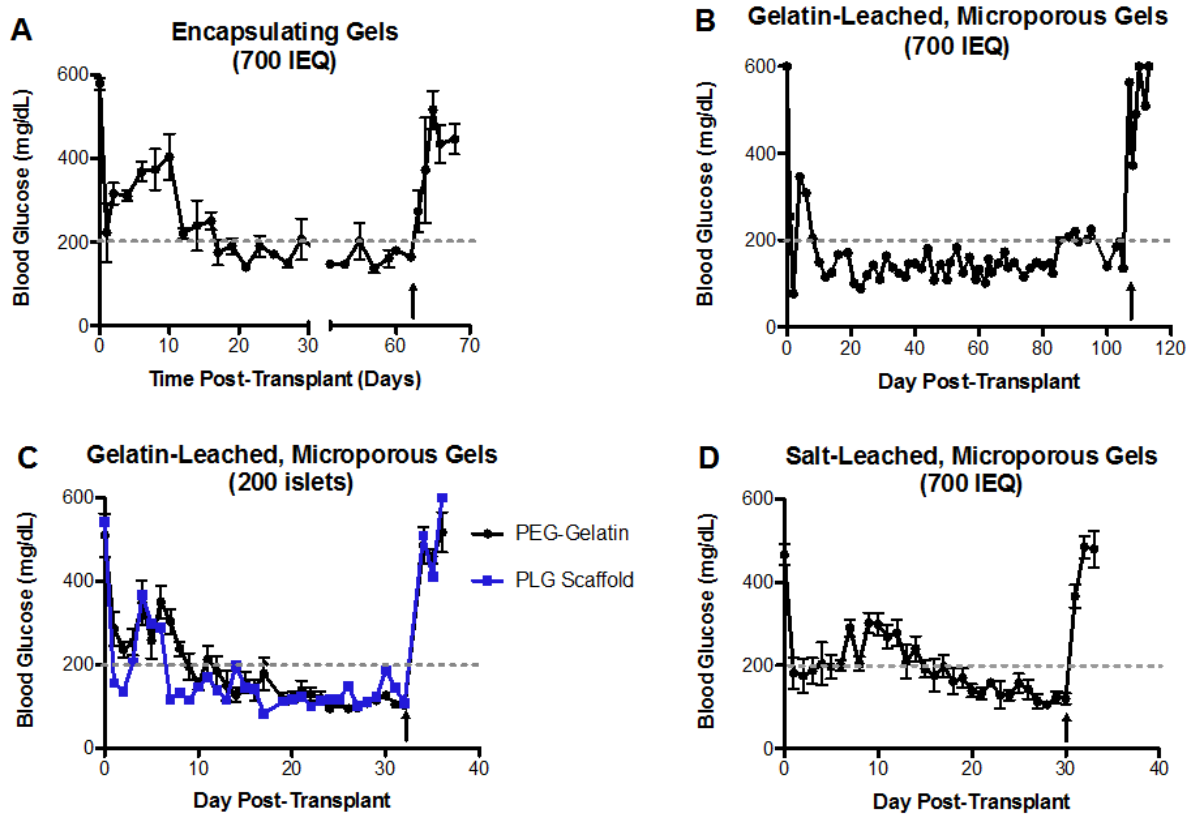


Figure 3-3. Blood glucose monitoring post-transplant with hydrogel materials in fat pad transplantation site of diabetic mice. **(A)** Bulk, non-degradable encapsulating hydrogels with 700 IEQ reversed diabetes in recipient mice, and approached normoglycemic levels by Day 12 (<200 mg/dL), with consistent normoglycemia achieved after Day 17 (n=3, \pm SEM). **(B)** A gelatin-leached, microporous hydrogel seeded with 700 IEQ (400 islets) reversed diabetes in a recipient mouse by Day 10 and displayed long-term function until graft removal at Day 106 (n=1, \pm SEM). **(C)** Gelatin-leached, microporous hydrogels seeded with 200 islets reversed diabetes in recipient mice by Day 9 (n=4, \pm SEM). Mice receiving a PLGA scaffold, used an internal control due to success in previous studies, reversed a few days earlier, by Day 7 (n=1). **(D)** Salt-leached, microporous hydrogels seeded with 700 IEQ displayed normoglycemic levels as early as Day 1 post-transplant, and consistently maintained normoglycemia after Day 15 (n=5 pre-graft removal, n=4 post-graft removal, \pm SEM). Recipient mice in all groups reverted to a diabetic state within 2-4 days following hydrogel removal (indicated with a black arrow).

mg/dL) ($n=5$, \pm SEM) and control group (187 ± 4 mg/dL) ($n=4$, \pm SEM), respectively. Blood glucose levels remained stabilized for the remainder of time points. Area under the curve indicated statistical significance at 30 minute ($p=0.0061$), 60 minute ($p=0.0007$), and 90 minute time points ($p=0.0005$) between the encapsulating and control group. Glucose tolerance tests were also performed on diabetic mice which received microporous hydrogels (gelatin leached $n=4 \pm$ SEM, salt leached $n=5 \pm$ SEM) (Fig. 3-4B, C). In both of the hydrogel groups and the control group ($n=5\pm$ SEM), the blood glucose levels peaked at 15 minutes post-injection of glucose. At 30 minutes, blood glucose levels in mice decreased toward normoglycemia in all groups. At 60 minutes, the microporous gel (153 ± 14 mg/dL) and control group (150 ± 18 mg/dL) both achieved normoglycemic levels and their blood glucose remained normoglycemic for the remainder of time points. For comparison, glucose tolerance of a PLGA microporous scaffold was also included, which followed identical trends to the hydrogels. Area under the curve indicated no statistical significance at any time point between the microporous hydrogels and controls. The glucose challenge results demonstrate recipient mice with microporous hydrogels containing transplanted islets can respond to a glucose load in a similar manner to mice with native pancreata. However, a slight delay in achieving normal blood glucose levels is observed in recipient mice with encapsulating hydrogels. Similar findings for this delay have been reported for hydrogels containing encapsulated islets in a recent study [41].

3.3.3 Histological Analysis of Hydrogel Explants from Syngeneic Transplants

Hydrogel materials remained intact and well-secured in the highly vascular fat pad transplant site upon removal (Fig. 3-5D). Hydrogels were sectioned and stained with insulin

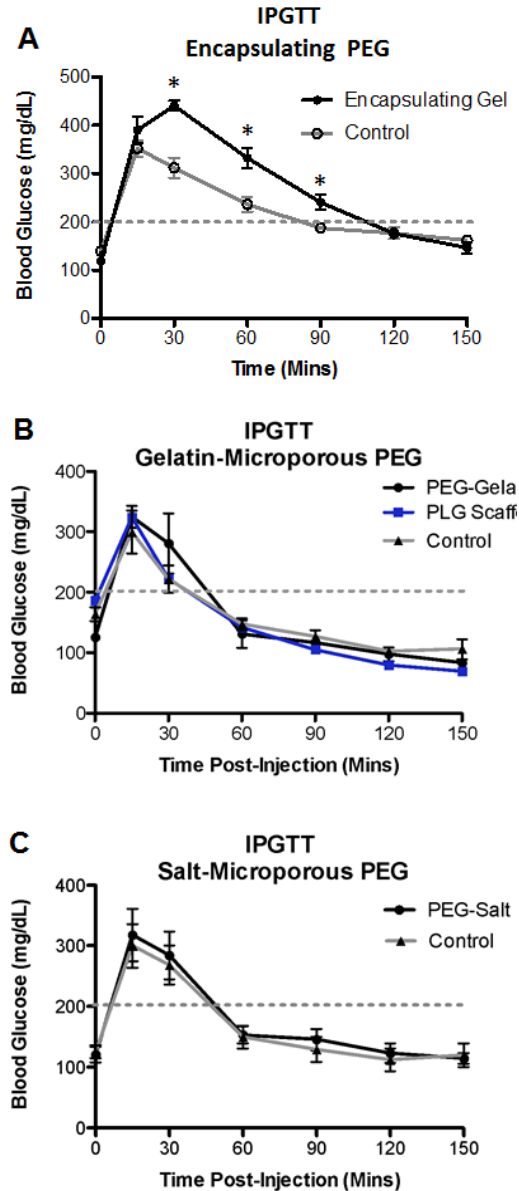


Figure 3-4. Glucose responsiveness of microporous hydrogels. **(A)** Encapsulated hydrogels with 700 IEQ (n=5, \pm SEM) achieved normoglycemia (<200 mg/dL) 120 minutes post-glucose injection. In contrast, **(B)** mice receiving gelatin-leached, microporous hydrogels with 200 islets (n=4, \pm SEM), a PLGA scaffold with 200 islets (n=1), or **(C)** salt-leached, microporous scaffolds with 700 IEQ (n=5, \pm SEM) achieved normoglycemia 60 minutes post-glucose injection, similarly to control mice with native pancreata. IPGTT performed at Day 32 (A), and Day 30 (B) post-transplant.

and a Hoechst nuclear counterstain to confirm their functionality post-encapsulation *in vivo*. Insulin-positive islets were retained in and identified in implanted both gelatin leached and salt leached microporous hydrogels at day 32 and 30 post-transplant, respectively (Fig. 3-5A-C). Histological analysis of encapsulated hydrogels will be completed in the near future. These results indicate islets seeded on PEG hydrogels were able to maintain their morphology, function, and engraft in the fat pad transplant site.

3.3.4 Allogeneic Islet Transplants in Encapsulating and Microporous Hydrogels

Encapsulating hydrogels containing 1500 IEQ islets from BALB/c donors were transplanted into C57/BL6 diabetic recipient mice (n=4) to evaluate graft function (Fig. 3-6A). For the first 1-2 days post-transplantation, blood glucose levels decreased to normoglycemic levels, typically indicative of some transplanted islet loss. After day 3, the mice returned to hyperglycemia. An additional study was performed and the islet loading was increased to 3000 IEQ (n=2) which lead to extended graft function of up to two weeks, but still failed to provide protection from the immune response (Fig. 3-6A). This indicates that encapsulation is not sufficient to prevent graft rejection. Allogeneic studies involving microporous hydrogels focused on utilizing salt as a porogen, as the syngeneic data did not indicate any significant difference between gelatin and salt porogens, and salt was considered more easily translated into the clinical setting. Although microporous hydrogels, which offer no inherent protection against an immune response, failed to achieve normoglycemia (Fig. 3-6B), one mouse did maintain normoglycemia until day 8 (blue line).

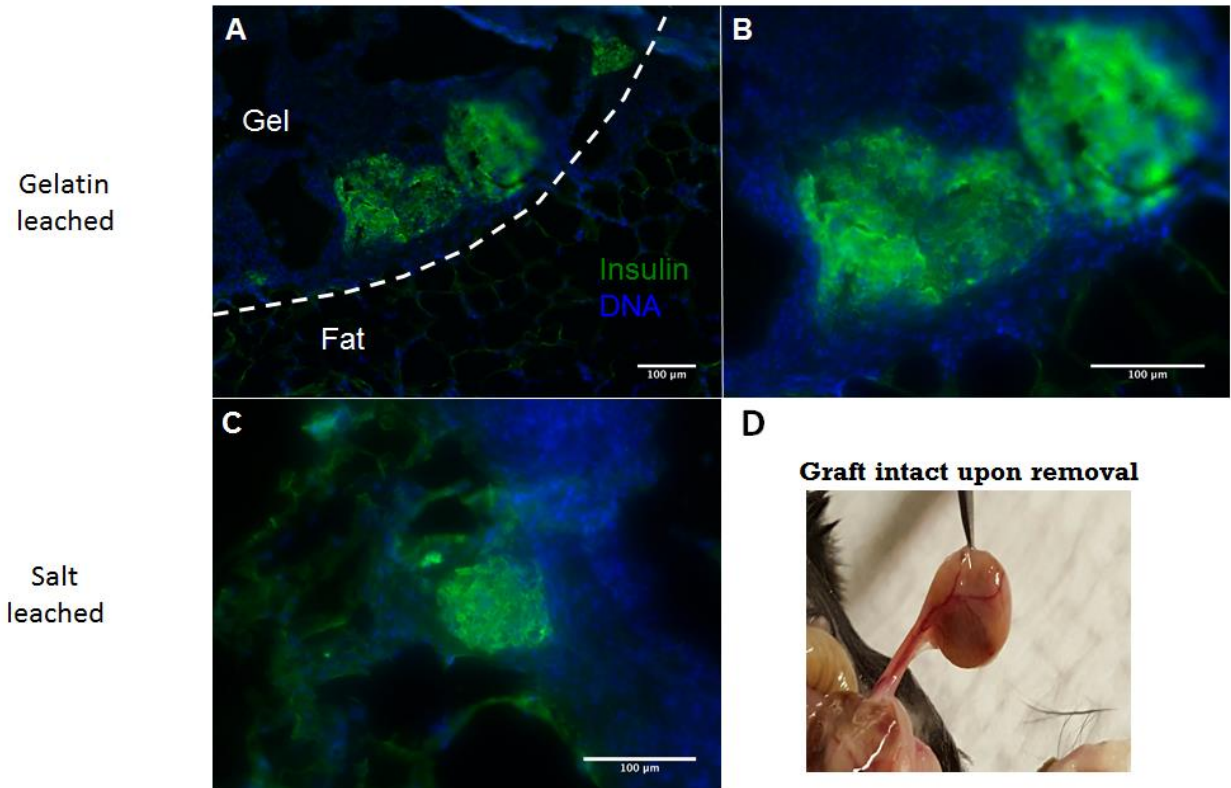


Figure 3-5. Insulin-positive islets confirmed in microporous hydrogels **(A-B)** Insulin-positive islets were identified in gelatin-leached, microporous scaffolds removed at Day 32 and **(C)** salt-leached, microporous scaffolds removed at Day 30 (Scale bar: 100 μm). **(D)** Explanted salt-leached microporous hydrogel 1 month post-transplant. Histology for encapsulated hydrogels will be completed in the near-future.

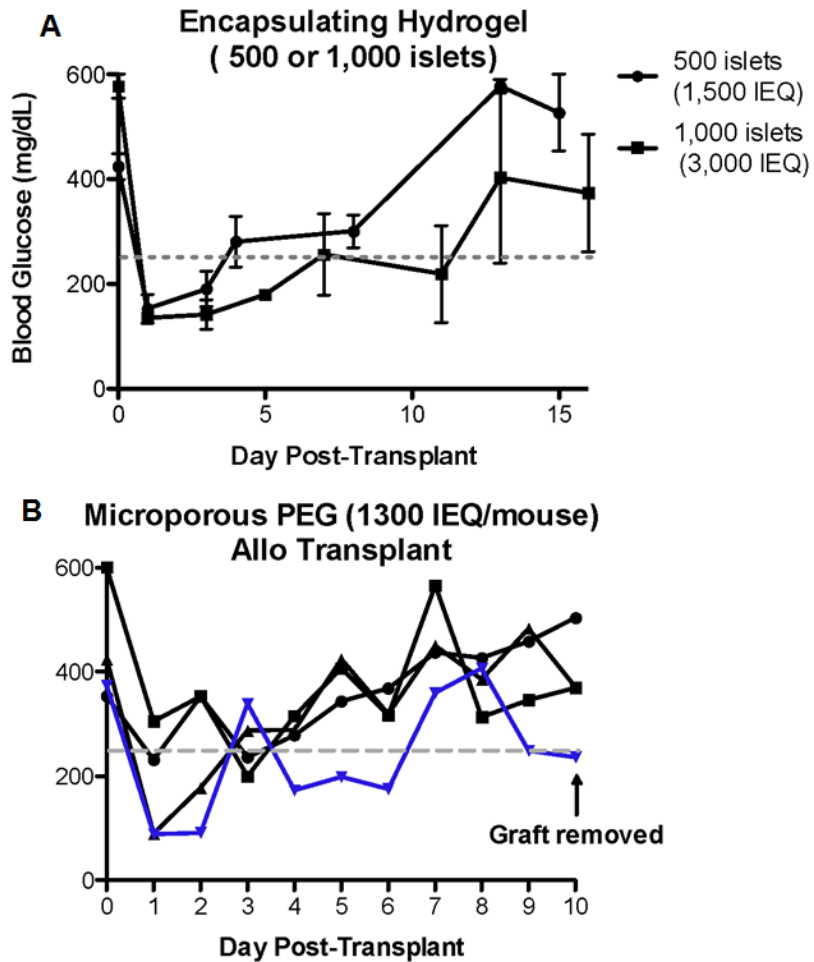


Figure 3-6. Allogeneic transplants failed to engraft before rejection. **(A)** Encapsulating hydrogels with 500 ($n=4, \pm$ SEM) or 1,000 islets ($n = 2, \pm$ SEM) are unable to maintain normal blood glucose levels more than 2 weeks post-transplant, indicating encapsulation alone is not sufficient to prevent graft rejection. **(B)** With the exception of one mouse (blue line), salt-leached microporous hydrogels with an IEQ of 1300 failed to achieve normoglycemia.

3.3.5 PEG hydrogels create a microenvironment conducive to islet survival

Localized release of soluble factors from the scaffold can enhance the microenvironment and combat nonspecific inflammation at early stages of the transplant. Previous reports have demonstrated efficacy of the relatively simple technique of delivering proteins from a small PLGA disc loaded with protein [117, 123]. TGF- β 1 was selected, as it is therapeutically relevant in nanogram quantities, thus making protein delivery easily detected. It inhibits inflammatory aspects of the immune system and stimulates regulatory T cell production, an important component of allogeneic tolerance [124, 125].

Non-porous PLGA inner layer scaffolds containing TGF- β were formed by pressing PLGA microparticles with lyophilized protein and mannitol into a disc then CO₂ foamed. The microporous hydrogel was formed around the inner layer by packing the PEG and salt mixture with the PLGA disc in a PDMS mold and cross linked. After leaching the salt, scaffolds were disinfected with ethanol and loaded with cells (Fig. 3-7D-F). Encapsulated hydrogels were simply implanted with the PLGA disc pressed between the adipose tissue and the scaffold (Fig. 3-7C). Prior to *in vivo* experiments, the release profile of protein from the scaffold was characterized by incubating the scaffolds in media for 30 days and the supernatant was periodically collected and replaced with fresh media. Eluted TGF- β 1 was quantified with an ELISA and demonstrated that 60% of the loaded protein is lost during the salt leaching step (Fig. 3-7A). Of the remaining protein, 60% was released by day 1 and 95% was released by day 7 (Fig 5-7B).

Next, studies were performed in an allogeneic model to directly compare islet engraftment in encapsulating and microporous hydrogels, with or without TGF- β 1 delivery, and to determine if rejection can be delayed. Rejection is denoted as two consecutive days of blood

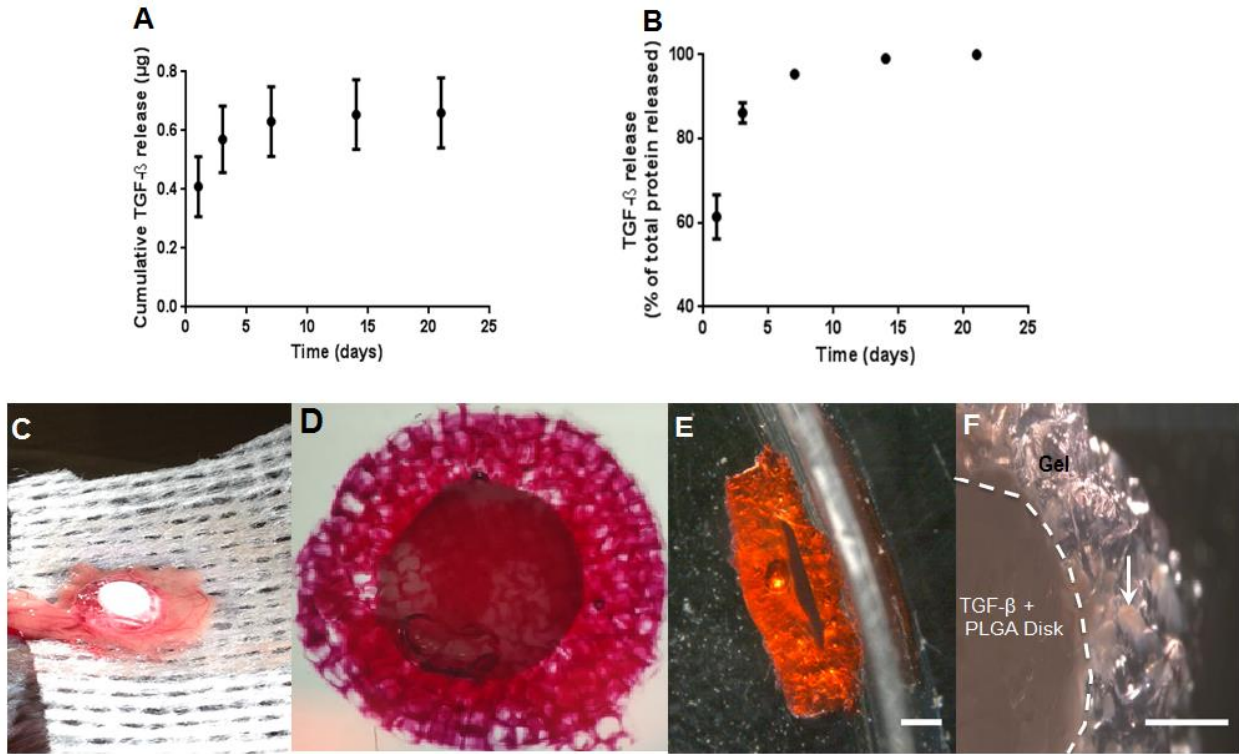


Figure 3-7. Transforming growth factor- β 1 (TGF- β 1) *in vitro* release from PLGA scaffolds and incorporation into hydrogel materials. **(A)** A cumulative release of 0.66 μ g was determined from PLGA disc loaded with 2 μ g of TGF- β 1. **(B)** More than 80 % of total protein was released by Day 3 ($n = 5$, \pm SEM). **(C)** For encapsulating hydrogel transplants, a PLGA disc containing 2 μ g of was placed on top of the hydrogel and wrapped in the fat pad. **(D)** For microporous hydrogels, the PLGA disc containing 2 μ g was incorporated into the middle of the hydrogel. **(E)** Cross-section view of PLGA scaffold in microporous hydrogel. **(F)** Islets seeded on a microporous scaffold. A representative islet is indicated with a white arrow.

glucose >250 mg/dL in this study. Mice receiving encapsulating hydrogels with 1300 islets without TGF- β 1 delivery were not able to maintain graft function and rejected after 2 weeks post-transplant (Fig. 3-8A). Encapsulation and TGF- β 1 delivery delayed rejection to day 24, compared to day 12 TGF- β 1, which is a similar rejection timeframe to a microporous PLGA scaffold loaded with TGF- β 1 [117]. A pilot study with microporous hydrogels loaded with TGF- β 1 and 1300 IEQ demonstrated potential efficacy in which mice with TGF- β 1 exhibited euglycemia by day 6 (Fig. 3-8B). Scaffolds were removed at day 7 for immune cell analysis via flow cytometry, but no significant difference between the innate or adaptive immune cell populations was detected (data not shown). This time point was selected due to graft rejection typically occurring around day 10, and thus populations at day 7 may provide insight into local immune cell populations dampened by TGF- β 1 delivery.

3.4 Discussion

In this study, we examined the utility of encapsulating and microporous PEG-based hydrogels for islet transplantation into the fat pad transplantation site in order to engineer an environment conducive to islet survival. Furthermore, this work offered the opportunity to study two unique scaffolds designs with the same material, allowing for a comparison to be made based on scaffold architecture. An important consideration in the development of biomaterial scaffolds is the ability to retrieve them for further studies without harming the host. Thus, non-degradable PEG scaffolds were developed for implantation into the epididymal fat pad to allow for straightforward recovery for further morphological analysis. Encapsulated islets are frequently microencapsulated in 400-800 μ m spheres and deposited in the peritoneal cavity,

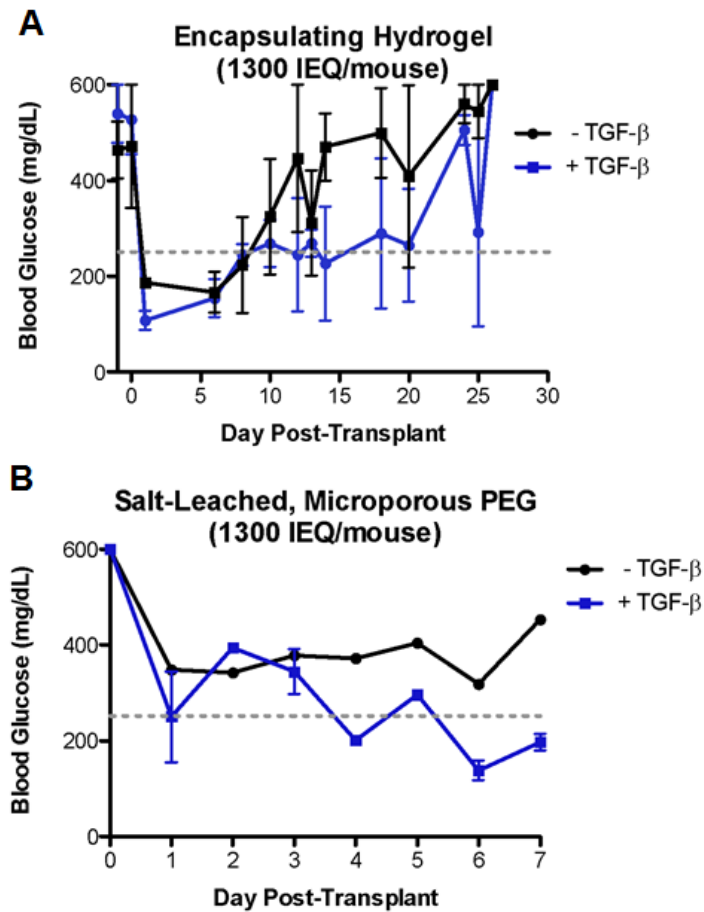


Figure 3-8. Allogeneic graft function of scaffolds with TGF- β 1 **(A)** Encapsulating hydrogels combined with TGF- β 1 delivery delays rejection until Day 24 compared to rejection at Day 12 without TGF- β 1 ($n = 2$ per group, \pm SEM). Rejection is denoted as two consecutive days of blood glucose >250 mg/dL. **(B)** Graft Function 7-days post-transplant in salt-leached microporous hydrogels. - TGF- β 1 condition ($n=2$, \pm SEM), + TGF- β 1 condition ($n=4$, \pm SEM). At day 7, the microporous hydrogels were removed for flow cytometry.

subcutaneously, or under the renal capsule, making recovery challenging [126]. By comparison, the macroencapsulated hydrogels and integrated host tissue was be easily removed from the epididymal fat pad for further analysis.

Microporous PEG hydrogels, comparable in design to PLGA scaffolds [104], allowed for rapid cellular infiltration and engraftment, a critical requirement for successful islet transplants. The average pore size of these microporous scaffolds was 107 μm and 274 μm for the gelatin- and salt-leached hydrogels, respectively. The minimum required pore size for vascularization has been determined to be 30 to 40 μm to facilitate endothelial cell entrance [127, 128], and 160 to 270 is suggested as ideal for hydrogels [129]. The difference in porogen not only affects pore size, but also the pore shape, as the gelatin microparticles are spherical whereas the salt grains are cuboidal. The gelatin contacts other spheres at points whereas the salt contacts at faces, which may affect pore interconnectivity. Despite these difference, both appear to be interconnected and tissue infiltrated throughout both of them by day 30. In regards to ease of fabrication, the gelatin-leached hydrogels were more straightforward, as the gelatin microparticles are not soluble in water at room temperature but can be dissolved at 37 °C, whereas the salt porogen requires a saturated salt/PEG solution which introduces solubility concerns. To fabricate clinically viable gelatin-leached hydrogels, the manufacturing process would need to be modified to meet Good Manufacturing Process (GMP) standards due to the use of mineral oil and porcine gelatin.

Normoglycemia in the syngeneic mouse model was achieved in both microporous hydrogels by day 15 and the encapsulated at day 21 post-transplant. Glucose responsiveness of islets seeded in microporous hydrogels was confirmed via an intraperitoneal glucose tolerance, with normoglycemic levels achieved by 60 minutes, identical to the nondiabetic control mice.

Restoration of normoglycemia post-transplant and in the glucose challenge was observed in a similar, if not earlier timeframe, than other rodent studies that have used natural or synthetic hydrogels for islet transplantation in vascularized sites [27, 130]. In contrast, the encapsulating hydrogels response to the glucose challenge was slower than the microporous and control mice and peaked at the later time point of 30 minutes. Similarly, the glucose readings at the 60 and 90 minute time points were significantly different from the control mice ($p \leq 0.05$), and appeared to lag behind the control's glucose response by approximately 30 minutes at these times. Whereas the microporous PEG and controls reached a maximum blood glucose of 300-350 mg/dL, the encapsulated reached a maximum of 450 mg/dL. This delayed responsiveness was expected due to the time needed for glucose and insulin to diffuse across the PEG barrier. It is also worth mentioning that the nondiabetic control mice for the microporous hydrogels were very similar whereas the encapsulated control was noticeably higher. This may be accounted by the fact that the microporous studies were completed at Northwestern University in Chicago, IL, while the encapsulated studies were done at the University of Michigan in Ann Arbor, MI.

In the allogeneic model, we hypothesized rejection may be delayed with the barrier provided by the non-degradable, encapsulating hydrogel design. Preventing direct contact with immune cells has been shown in some cases to improve allogeneic islet engraftment, with the goal of eliminating the need for immunosuppressive drugs. Precise control over mesh size and mesh size uniformity is critical to prevent entry of cytokines or exit of islet antigens that can exacerbate the host immune response [131]. However, smaller mesh sizes that are close to the hydrodynamic radius of insulin can hinder molecular transport through the hydrogel. Furthermore, many cytokines are similarly sized to insulin, making it challenging to identify an

ideal mesh size that selectively excludes harmful proteins and small molecules [132]. The mesh size of the hydrogels presented here is approximately 10 nm [41], similar to other reported mesh sizes for PEG hydrogels [133, 134]. Encapsulating hydrogels were unable to delay graft allogeneic rejection and were not different from microporous hydrogels which offer no inherent protection from the immune system. Rejection occurred within a two-week timeframe post-transplant, similar to the microporous PLGA hydrogel, thus indicating that a semipermeable PEG membrane was not sufficient to delay graft rejection. However, in this study, a physical barrier to immune cells was not sufficient to prevent graft rejection. Precise control over mesh size and mesh size uniformity is critical to prevent entry of cytokines or exit of islet antigen that can exacerbate the host immune response.

TGF- β 1 release from PEG scaffolds delayed rejection of allogeneic islets. *In vitro* release of TGF- β 1 from microporous hydrogels containing a protein loaded PLGA disc was similar to previously published porous PLGA systems in which 95% of the total delivered protein was detected by day 7 [117]. When encapsulating PEG scaffolds were implanted in the fat pad along with the TGF- β 1 loaded disc, rejection was delayed until day 24 compared to rejection at day 12 without TGF- β 1. This demonstrates the ability to locally deliver proteins from the hydrogels and allows for the delivery of other anti-inflammatory molecules like IL-2, IL-10, or TNF- α inhibitors that could be useful to manage short-term inflammation due to scaffold surgery and islet transplantation.

CHAPTER 4. Localized Lentivirus Delivery via Affinity Peptides

4.1 Introduction

Biomaterial scaffolds serve a central role in regenerative medicine by creating a space for tissue growth and a support for cell interactions serve as a vehicle for gene delivery vectors as a means to localize expression of tissue inductive factors. The delivery of soluble factors to the local environment of the transplanted islets can promote survival, vascularization, and growth [135-137]. Localized expression of tissue inductive factors enables some control over the local microenvironment that has been effective in multiple models such as spinal cord injury and bone regeneration [73, 138]. The delivery of viral vectors from scaffolds has been attempted through a variety of approaches, such as non-specific adsorption of the vector [86], modifying the vector to bind to a material [90], or modifying the material to interact with the vector. Material modifications have included modification of surfaces with hydroxyapatite [87, 88], or phosphatidylserine that is known to have specific interactions with the vector [89]. Proteins and peptides are regularly employed to functionalize biomaterials, and are emerging as a tool for providing binding sites for vectors on material surfaces. Poly-L-lysine (PLL) with a molecular weight of 70-150 kDa has been used for delivery of viral vectors [63]. Identifying the design requirements for peptides or proteins for promoting efficient gene delivery would be invaluable for developing biomaterials for use in regenerative medicine.

We investigated the design parameters for peptides and proteins to enhance delivery of lentiviral vectors from biomaterial scaffolds. Poly(ethylene glycol) based hydrogels were

employed as the biomaterial scaffold in these studies as they are widely used in vitro and in vivo for studies with cell culture, encapsulation, and transplantation and ultimately tissue formation, and provide a relatively low amount of non-specific binding for lentiviral vectors [107, 108]. 4-arm PEG-acrylate hydrogels were functionalized with peptides containing a cysteine to provide quick and straightforward functionalization via Michael-type addition. The design of proteins and peptides for gene delivery initially employed PLL at a range of molecular weights. These studies investigated the mechanism by which PLL enhances gene delivery through characterizing virus binding and stability. While PLL can produce efficient delivery, the relatively high molecular weight and polydispersity of PLL may be a challenge for translation. We thus sought to identify peptides using a phage display technology, which has had success with identifying ligands for multiple cell types [139-143], proteins [144-146], and small molecules [147-149]. The peptides can provide a high affinity and specific binding interactions with the viral vector, and we investigated multiple strategies for their presentation from the hydrogel. Modifying biomaterials with peptides offers great potential to enhance and modulate virus localization and promote transgene expression for numerous regenerative medicine applications.

4.2 Materials and methods

4.2.1 Virus production

Lentivirus was produced by co-transfecting HEK-293T cells with lentiviral packaging vectors (pMDL-GagPol, pRSV-Rev, pIVS-VSV-G), as previously described [150], and the gene of interest (pLenti-CMV-GFP and pLenti-CMV-GLuc) using jetPRIME (Polyplus Transfection, Illkirch, France). After 17 h, supernatant was replaced with fresh media containing 4 mM caffeine. After

an additional 31 hours, supernatant was collected and cell debris was spun down and removed. Virus particles were concentrated using PEG-it (Systems Biosciences, Mountain View, CA) and re-suspended in PBS. Lentivirus titers were determined by qRT-PCR lentivirus titration kit (ABM, Inc., Richmond, Canada). Virus was further purified for SDS-PAGE gel analysis via a Lenti-X Maxi Purification Kit (Clontech, Mountain View, CA) and desalted using a PD-10 column (GE Healthcare, Buckinghamshire, England). The SDS-PAGE gel used a NuPAGE 4-12% Bis-Tris pre-cast polyacrylamide gel and ran in MES SDS running buffer (Thermo Scientific) and stained with Coomassie Blue.

4.2.2 PLL functionalization with cysteine

A low molecular weight PLL (10 kDa, Alamanda Polymers, Huntsville, AL) and a high molecular weight PLL (30-70 kDa, Sigma Aldrich, St. Louis, MO) were functionalized with a cysteine using EDC/NHS chemistry to facilitate incorporation into the PEG-acrylate hydrogels. A solution of 2 mM EDC and 5 mM NHS was added to a 0.1 M MES buffer (pH 5.0) and the peptide was added to make a concentration of 1 mg/mL. After 15 minutes of incubation, the buffer was exchanged with centrifugal filtration (10 kDa, Amicon Ultra-0.5) to 0.1 M PBS (pH 8) containing 30 mg/mL of oxidized cysteine. After allowing the solution to react for 2 hours, excess cysteine was removed via dialysis and any oxidized thiol groups were reduced with 50 mg/mL of dithiothreitol. The PLL was quantified with a fluorescamine assay and the cysteines were quantified via Ellman's test.

4.2.3 Macrophage differentiation

Bone marrow derived macrophages (BMDM) were harvested and differentiated according to established protocol [151]. Briefly, femurs from male 8-12 week-old C57BL/6 mice (Charles River) were flushed to isolate bone marrow. Macrophages were cultured in RPMI 1640 (Life Technologies, Carlsbad, CA) supplemented with 10% FBS (Life Technologies), 1% penicillin/streptomycin (Life Technologies), and 20% L929 conditioned media in untreated cell culture plates. Media was replaced on days 3, 6, and 8. On day 10, cells were removed using 0.05 mM EDTA treatment. PEG hydrogels were formed and loaded with virus as described in materials and methods. Briefly, hydrogels were loaded with 10^7 viral particles encoding for GFP, washed to remove non-binding virus, then seeded with 10^4 macrophages per well in a 96-well plate. GFP expression was measured 72 hours later.

4.2.4 Peptide synthesis

Peptides were synthesized at Northwestern University's Peptide Synthesis Core Facility of the Institute for BioNanotechnology in Medicine. To facilitate peptide incorporation into the PEG-acrylate hydrogels via Michael-type addition, a cysteine was added to the C-terminus of the synthesized phage display peptide.

4.2.5 Biotinylated VSV-G

The VSV glycoprotein ectodomain (kindly gifted by Yves Gaudin, CNRS, Unité Mixte de Recherche) was biotinylated using sulfo-NHS-LC-biotin (Thermo Scientific, Rockford, IL) according to the manufacturer's recommended methods. Briefly, VSV-G was diluted in a 0.1 M NaHCO_3 buffer and the biotinylation reagent was added. The reaction was incubated on ice for two hours

then excess reagent was removed using centrifugal filtration (10 kDa, Amicon Ultra-0.5). The degree of biotinylation on the VSV-G proteins was assayed using a fluorescence biotin quantitation kit (Thermo Scientific).

4.2.6 Solution phase phage display

Peptides that bind to the biotinylated VSV-G protein were identified using a 12-mer phage display library (New England Biolabs, Ipswich, MA) using the suggested methods for solution phase panning. The phage library and biotinylated protein were combined in a TBS buffer with Tween-20 and allowed to interact. The mixture was then added to a streptavidin-coated 96-well plate blocked with BSA and incubated for 10 minutes. Biotin (0.5 μ L, 10 mM) was added to displace any phages bound to the streptavidin and the plates were washed 15 times with TBST to remove non-binding phages. Bound phages were eluted from the immobilized protein by incubating in an acidic glycine elution buffer (pH 2.2) for 30 minutes followed by neutralization with 1 M tris buffer (pH 9.1). Phages were then amplified in *E.coli* and purified using a PEG solution (20% w/v).

A total of three rounds of panning were completed, with each round introducing more rigorous conditions to select for stronger binding candidates. Tween-20 concentration was increased 0.1, 0.5, and 1%, and NaCl concentration was increased 150, 300, and 750 mM. Time the phages spent incubating with the target protein was reduced to 60, 45, and 30 minutes. After the third round of panning, individual phage clones were randomly sampled and their DNA was extracted then purified. DNA was sequenced at Northwestern University's Genomics Core Facility.

4.2.7 ELISA

VSV-G was incubated in 96-well plates overnight and phage solutions were allowed to bind at the listed concentrations. After 30 minutes of incubation, phages were washed with a buffered solution containing 1% Tween-20 and 750 mM NaCl. Phages were detected with an anti-M13 bacteriophage antibody conjugated with horseradish peroxidase (HRP) (GE Healthcare) and reacted with a 1-step 2,2'-Azinobis [3-ethylbenzothiazoline-6-sulfonic acid]-diammonium salt (ABTS) to produce a colorimetric reaction. The absorbance from the reaction was measured using a plate reader (Synergy 2, BioTek).

4.2.8 Hydrogel preparation

Hydrogels were formed by dissolving 4-arm polyethylene glycol acrylate (20 kDa) (Laysan Bio, Inc., Arab, AL) in 8.5 mM HEPES buffer (pH 8.0) at a concentration of 100 mg/mL. In hydrogels containing PLL, cysteine-functionalized PLL was added for a total concentration of 0.45 mg/mL, unless otherwise noted, in addition to 2.5 mM of the cell adhesion peptide, RGD (Ac-CGRGDS-NH₃) (Celtek Peptides). The RGD control gels contained 5 mM of the peptide. The PEG precursor solution was incubated at 37 °C for 30 minutes to facilitate the Michael-type addition between the acrylate and thiol. To initiate the free-radical polymerization of the acrylate groups, Irgacure 2959 dissolved in N-vinylpyrrolidinone (600 mg/mL) was added to the PEG for a final concentration of 1% (wt/vol). Gel precursor was added to non-adhesive silicon molds (diameter = 4.5 mm, height = 0.8 mm), cross linked with UV light for 90 seconds, then washed with PBS to remove unbound peptide and unreacted photoinitiator. To determine if virus binding to the walls of the polystyrene plate affected the results, wells of a tissue culture treated 96-well plate were

blocked with bovine serum albumin (5 mg/mL in 0.1 M NaHCO₃ buffer, pH = 8.6). No significant binding was observed.

Hydrogels functionalized with peptides from the phage display panning used a 5 kDa PEG linker (acrylate – PEG – maleimide) (Creative PEG Works, Winston Salem, NC). The PEG linker was added to the PEG precursor solution at a 2.5 mM concentration then photopolymerized using UV light. The peptides were incubated with the virus for 3 hours and then incubated with the hydrogels for 15 minutes, with hydrogels subsequently washed 2x with PBS.

4.2.9 Transgene expression

Lentivirus (1×10^7 particles) was added to the gels and allowed to incubate for 3 hours at room temperature (unless otherwise noted). Virus solution was then removed and gels were washed twice with 150 μ L of PBS to remove unbound virus. HT1080 cells were added (10^4 cells / well) and incubated with Dulbecco's modified Eagle's medium plus 10% fetal bovine serum at 37°C, and 5% CO₂. Cells expressing GFP were imaged 72 hours later, unless noted otherwise, using Leica X fluorescent microscope. The supernatant of cells expressing GLuc was gathered after 72 hours of incubation and measured using a Gaussia luciferase assay kit (New England BioLabs) with a luminometer (Turner Design, Sunnyvale, CA).

4.2.10 Statistics

One-way ANOVA followed by Tukey's posttest for multiple comparisons and two-tailed Student's t-test, where appropriate, was performed using GraphPad version 5.04 for Windows (La Jolla, CA). Statistical significance was set at $p \leq 0.05$ unless noted. Values shown represent the mean \pm SEM.

4.3. Results

4.3.1 PLL length

PEG hydrogels were functionalized with PLL of three molecular weights and subsequently investigated for their ability to localize lentiviral vectors to the substrate and promote gene transfer. PLL was modified with cysteine for attachment to the acrylate groups on the PEG hydrogel. Studies were performed with varying molecular weights of PLL, which were incorporated at equal masses (Table 4-1). Hydrogels functionalized with 1 kDa, 10 kDa, or 30-70 kDa PLL were incubated for three hours with lentivirus encoding for GFP. Fluorescence images demonstrated that the high molecular weight PLL (30-70 kDa) provided the greatest number of GFP positive cells (Fig. 4-1C), while the 1 kDa PLL had almost no cells expressing the transgene (Fig. 4-1A). The high molecular weight PLL resulted in transduction of 25% of the cells, whereas the lowest molecular weight PLL transduced less than 0.1% of the cells (Fig. 4-1D). Based on its ability to promote the greatest extent of transduction relative to the other PLL's, the 30-70 kDa was selected for further analysis. To demonstrate this system's broad potential to transduce other cell types, bone marrow derived macrophages were isolated from mice and incubated with hydrogels functionalized with 30-70 kDa PLL (Fig. 4-2). The extent of transgene expression for the virus immobilized to the hydrogel was subsequently characterized. The control condition for this study involved hydrogels without PLL, yet had the cell-adhesion peptide RGD, which is necessary for cell adhesion and provides minimal interactions with the virus. The assay displays effectively zero background signal in the absence of virus, indicating that any measured signal is produced via transgene expression (Fig. 4-3). Additionally, designated wells were blocked with bovine serum albumin (BSA) (5 mg/mL) for two hours prior to hydrogel formation and virus

PLL MW (kDa)	Lysine units
1	8
10	78
30-70	230-550

Table 4-1. Equal masses of the different poly-L-lysines were added to provide an identical net charge for each condition.

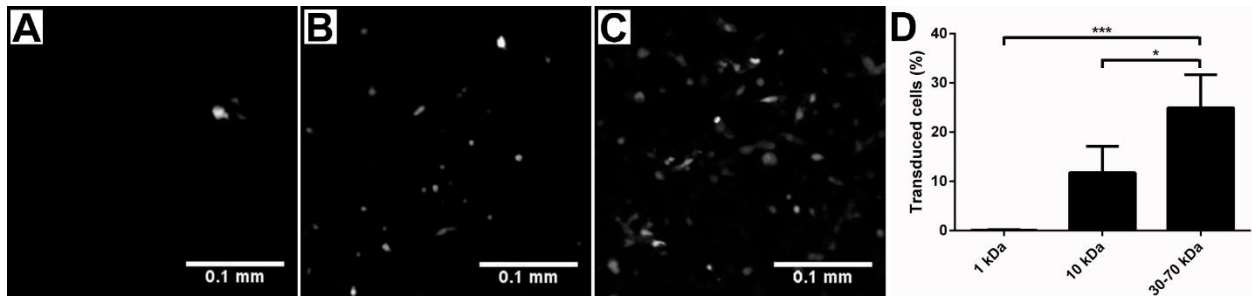


Figure 4-1. Influence of PLL molecular weight on virus localization. PEG hydrogels containing 2.5 mM RGD were functionalized with 0.45 mg/mL of 1 kDa (n=3) (A), 10 kDa (n=3) (B), and 30-70 kDa (n=5). (C) PLL and incubated with GFP-encoding lentivirus. Hydrogels were washed to remove non-binding virus then seeded with HT1080 cells for 72 hours. (D) Significantly more cells were transduced with 30-70 kDa PLL than the shorter PLL's. (*p<0.05; ***p<0.001)

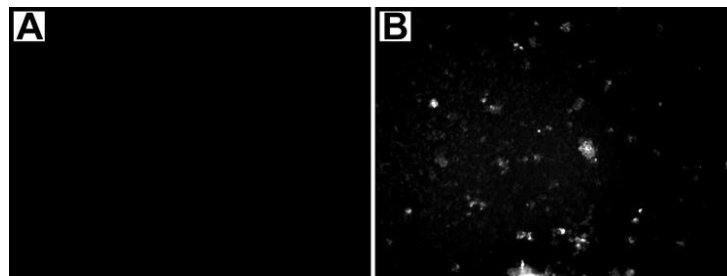


Figure 4-2. PLL functionalized hydrogels promote transduction of macrophages. PEG hydrogels were functionalized with 2.5 mM RGD (A) and 2.5 mM RGD + 1.35 mg/mL of 30-70 kDa PLL (B). Conditions without PLL (A) had no GFP expression while PLL functionalized hydrogels demonstrated significant GFP expression (B).

addition in order to determine the contribution of virus binding to the plastic walls of the plate. No significant difference was detected between blocked and unblocked plates. Luciferase activity was more than 10-fold greater on the PLL-containing gels relative to the control hydrogels, and the control gels were not statistically different from gels without virus.

4.3.2 Binding dynamics, release, and stability

We subsequently investigated the duration over which virus was incubated with hydrogels and the density of functionalization, as both have been previously reported to influence the binding of non-viral vectors and the extent of transgene expression. Hydrogels were functionalized with PLL and incubated with virus for times ranging from 15 to 270 minutes. A significant increase in luciferase activity was observed for virus incubated for 90 minutes with the hydrogels, with longer incubations of 270 minutes having no significant effect on transgene expression (Fig. 4-4A). The PLL concentration similarly influenced transgene expression, with increasing transgene expression observed between 0.15 and 1.35 mg/mL, and subsequent increases to 4.05 mg/mL not significantly affecting transgene expression (Fig. 4-4B). These observed trends in incubation time and PLL concentration are consistent with those reported for non-viral vectors, and are likely due to the quantities of the lentivirus associated with the substrate.

The release of lentivirus from PLL-functionalized PEG gels was investigated, as retention of the vector at the material can localize gene delivery. After virus incubation with the hydrogel and subsequent washing, released virus in the supernatant was collected and quantified with RT-qPCR (Fig. 4-5A,B). After washing, the PLL modified hydrogel did not have detectable levels of virus in the supernatant (Fig. 4-5A). In contrast, the RGD control had a steady release of virus for

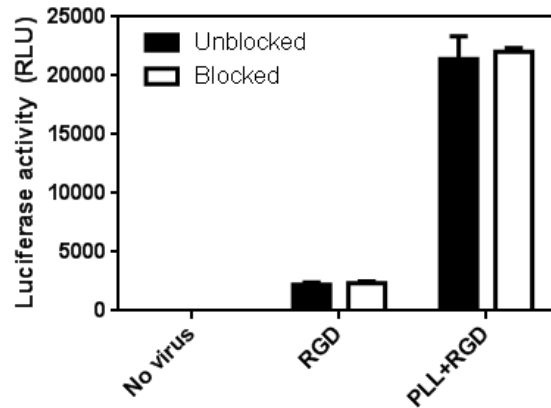


Figure 4-3. PLL enhances virus localization on PEG hydrogels. PEG hydrogels containing 2.5 mM RGD were functionalized with either 30-70 kDa PLL (0.45 mg/mL) or additional RGD (2.5 mM) (n=3). Designated wells were blocked with BSA (5 mg/mL) prior to forming the hydrogels. The “No virus” condition contains PLL but was incubated with PBS instead of lentivirus. Lentivirus encoding for GLuc was incubated with the hydrogels then washed with PBS to remove non-binding virus. HT1080 cells were incubated with the hydrogels for three days and then luciferase activity was assayed. Significant difference compared to No virus and RGD (****p≤0.0001).

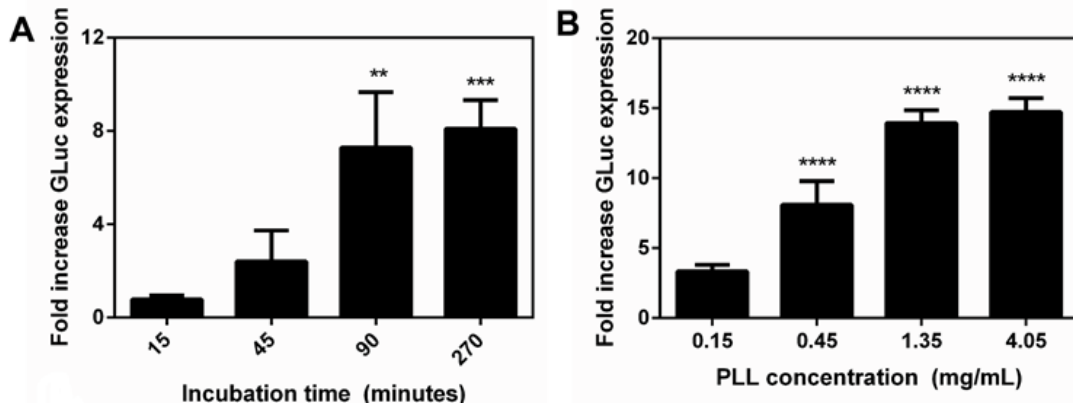


Figure 4-4. Transgene expression can be modulated via virus-hydrogel incubation time and PLL concentration. **(A)** PEG hydrogels functionalized with 2.5 mM RGD and 0.45 mg/mL of PLL were incubated with virus for varying times (n=3). Fold increase in GLuc expression relative to RGD control. Significant difference compared to RGD control (**p≤0.01; ***p≤0.001). **(B)** Hydrogels were functionalized with varied concentrations of PLL and incubated with virus for 3 hours (n=3). Significant difference compared to RGD control (****p≤0.0001).

the duration of the study (Fig. 4-5B). In a separate experiment, trypsin was added to PLL-conjugated hydrogels loaded with virus to elute bound lentivirus, but no detectable amounts of eluted virus could be detected. It is hypothesized that the trypsin may have damaged the lentivirus or inhibited the RT-qPCR reagents. The stability of the immobilized virus, another factor affecting transduction, was subsequently investigated by incubating hydrogels with immobilized virus at 37 °C for varying amounts of time. Following incubation, cells were seeded onto the hydrogels and luciferase expression was assayed at 72 hours. Increasing times of incubation led to decreased levels of transgene expression for both the PLL condition and the RGD control, and this decline in activity was used to determine a half-life of activity. The half-life of lentivirus on the control hydrogel was 8.3 hours, consistent with previous reports [152-154], whereas the PLL-functionalized hydrogels demonstrated a half-life of 10. hours, a 20% increase in half-life relative to control ($p \leq 0.05$) (Fig. 4-6).

4.3.3 VSV-G protein solution-phase panning

We subsequently sought to replace the high molecular weight PLL with a peptide, which are routinely used to functionalize biomaterials. The low molecular weight PLL has an insufficient affinity for lentivirus binding, and subsequently applied phage display to identify peptides with a high affinity for the lentivirus. Phage display requires a highly pure target to prevent undesired sequence selection, so two lentivirus purification techniques were explored and their purity was tested with an SDS-PAGE protein gel (Fig. 4-7). The PEG precipitation technique (lanes 7,8) resulted in a relatively large quantity of protein coprecipitated with the virus. The affinity column (lanes 5, 6) removed the majority of protein detected in the PEG precipitation, but a faint band at 60 kDa was detected. As a result, it was determined that the production of lentivirus resulted

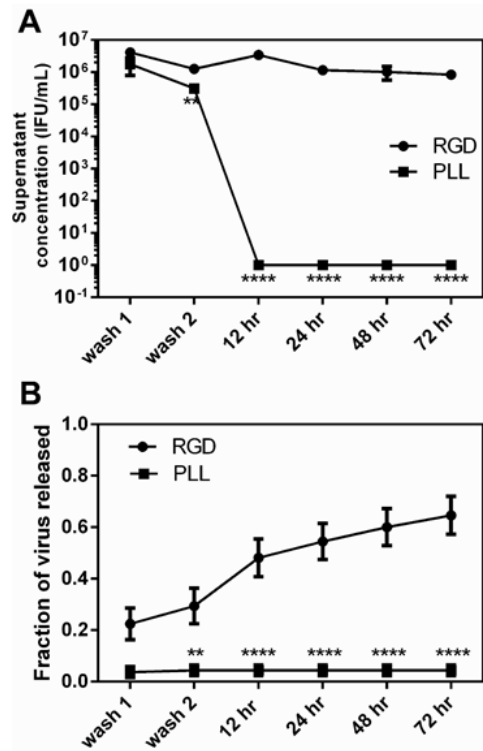


Figure 4-5. Retention of lentivirus on PLL-functionalized PEG hydrogels. **(A)** PEG hydrogels containing 2.5 mM RGD were functionalized with either 30-70 kDa PLL or additional RGD (0.45 mg/mL) (n=4). Virus was incubated with the hydrogels for three hours at 37 °C then washed with PBS to remove non-binding virus. Unbound virus in the supernatant was collected and assayed via qPCR at different time points. Following the two washes, no detectable level of virus was found in the PLL-functionalized hydrogels. **(B)** The fraction of lentivirus released from the hydrogel was calculated by dividing the eluted virus particles by the initial virus loading. Significant differences between corresponding RGD and PLL conditions are denoted by an asterisk (**p≤0.01; ****p≤0.0001).

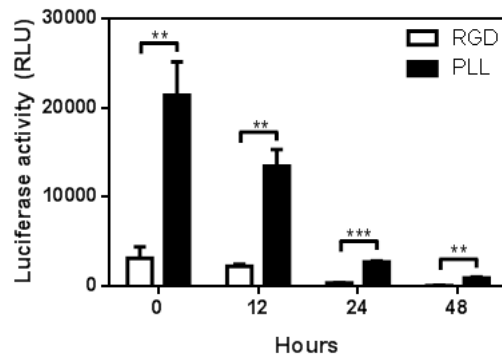


Figure 4-6. Increased viral stability in PLL-functionalized hydrogels at 37°C. PEG hydrogels with 2.5 mM RGD and either 30-70 kDa PLL or additional RGD (0.45 mg/mL) were incubated with virus at 37 °C for three hours (n=3). All hydrogels were washed and incubated with PBS. At each time point, the PBS was replaced with HT1080 cells and subsequent luciferase expression was assayed 72 hours later. (**p≤0.01; ***p≤0.001)

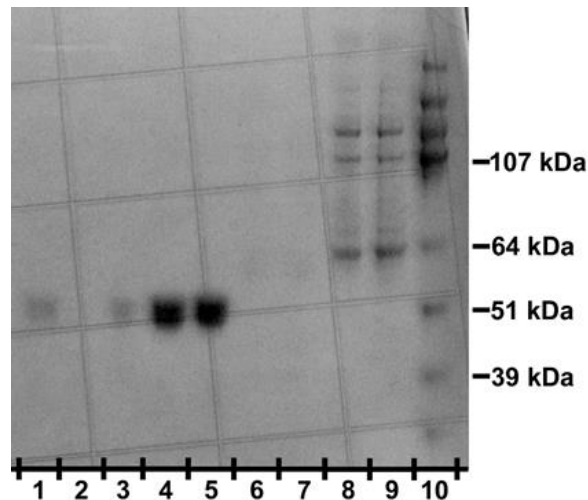


Figure 4-7. Analysis of lentivirus purification methods using SDS-PAGE protein gel. (Lane 1, 3 = VSV-G, 0.5 µg; lane 4, 5 = VSV-G, 2.0 µg; lane 6, 7 = Lentivirus, Lenti-X purification; lane 8, 9 = Lentivirus, PEG-it purification; lane 10 = ladder; Lane 2 intentionally left blank). The Lenti-X affinity column removed almost all detectable amounts of contaminating protein, except for a faintly detectable band at approximated 65 kDa whereas the PEG-it precipitation failed to remove significant amounts of undesired protein.

in the presence of contaminating proteins at sufficient quantities that prohibited solution-phase phage display.

Phage display was thus applied to the envelope protein of the lentivirus, VSV-G (Fig. 4-8). VSV-G was biotinylated at a ratio of 0.8 mol of biotin per 1 mol of VSV-G protein. The protein was biotinylated at slightly less than a 1:1 ratio of biotin to protein in order to minimize the risk of phage display targeting excessive biotin groups on the protein. Initial panning experiments utilized a 7-mer sequence and resulted in strong selection of double insert phages. Phage display libraries contain a small percentage of phages containing multiple inserts of the randomized peptide sequence and these clones are strongly selected for when the ligand specificity spans a distance greater than the seven amino acid sequence. Consequently, panning experiments utilized phages with a longer 12-mer randomized sequence.

Three rounds of panning with the VSV-G protein were performed to enrich the phage pool for VSV-G binding sequences. The binding specificity of these sequences was assessed using a fourth round of panning with and without the VSV-G protein, with 10^5 pfu/ μ L phages bound in the presence of the VSV-G protein, and 10^1 pfu/ μ L in the absence of the protein (Fig. 4-9), confirming the eluted phages are enriched in VSV-G specific phage clones. From solutions with the target protein, 108 phage clones were sequenced. The relative variance of these sequences (repeated sequences were removed) was analyzed using the following equation:

$$D = \frac{N_{max}}{N_{Total}}$$

$$V = N_{seq}/D$$

$$Relative\ Variance = V - 1$$

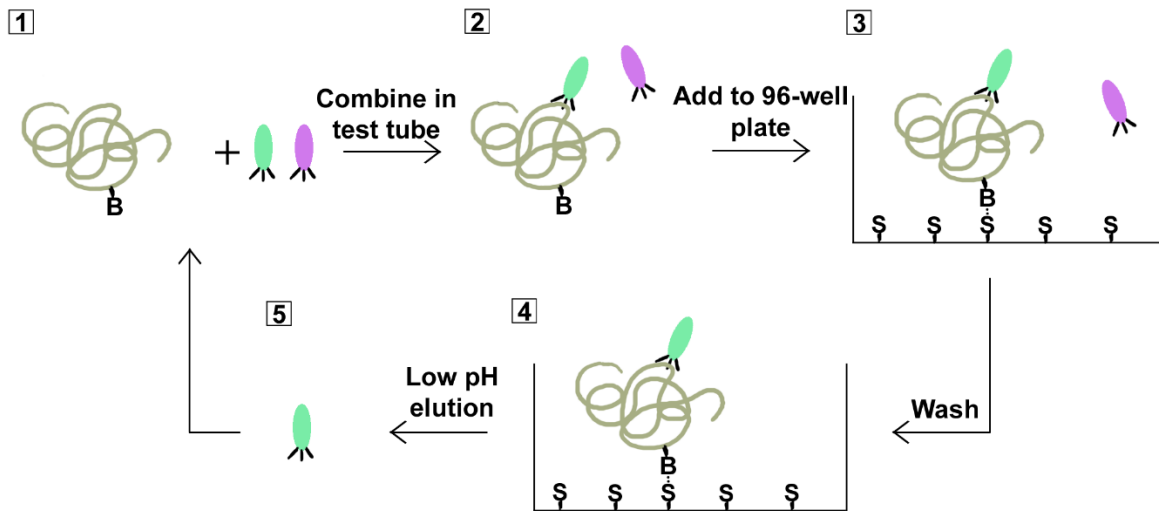


Figure 4-8. Solution phase phage display. Biotinylated VSV-G and the phage library are mixed (1) and allowed to incubate (2). (3) Phage/VSV-G complexes are captured on a streptavidin-coated plate and non-binding phages are washed away (4). VSV-G bound phages are eluted from the plate using a low pH buffer (5) and the phages are collected for additional rounds of panning.

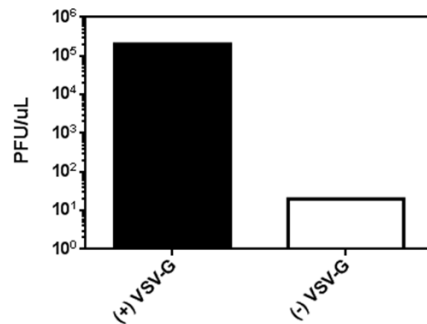


Figure 4-9. After three rounds of panning, phages demonstrate binding affinity to VSV-G. A fourth round of panning was completed with (+) and without (-) VSV-G immobilized on the plate surface. After washing to remove non-binding phages, 10⁵ PFU/μL were eluted from the plate surface coated with VSV-G whereas only 10 PFU/μL.

Where N_{\max} is the number of times the highest occurring amino acid appeared at a given position, N_{Total} is the total number of peptides sequences considered, and N_{seq} is the number of unique amino acids at a given position. The peptide sequence is listed N to C terminus, where the peptide is attached on the N-terminus of the phage's pIII coat protein. Thus, amino acids at position 1 are farthest from the phage body and position 12 are closest. In between the randomized 12-mer sequence and the phage body is a GGGS spacer that is not included in the relative variance analysis. The results shows a high degree of relative variability at amino acids proximal to the phage (positions 9, 10, 11, 12) and an area of low variability in the center (positions 4, 5, 6, 7) and distal from the phage (position 1) (Fig. 4-10). This area of low variability in the center corresponds to a high frequency of the amino acid histidine. Next, the sequence STQHHSKQSR (STQ) was selected for binding analysis in an ELISA. Wells were coated with VSV-G and phages from either the naïve 12-mer library or phages displaying the STQ sequence were incubated with the target protein. After washing, bound phages were quantified with an anti-M13 bacteriophage antibody conjugated with HRP and reacted ABTS. Due to the high concentration of VSV-G bound on the plate which allows for multivalent binding to the phage, this technique cannot produce a dissociation constant (K_D). However, it provides information on the relative binding affinities and can distinguish target binding from background binding to the plastic plate. ELISA results confirmed affinity binding for the STQ sequence compared to the non-specific binding of the naïve phage library (Fig. 4-11).

After confirming with ELISA that the STQ sequence demonstrated an affinity for VSV-G, it was synthesized along with three other peptides that appeared multiple times for further analysis (Table 4-2). The potential of these sequences to bind lentivirus and enhance gene delivery was

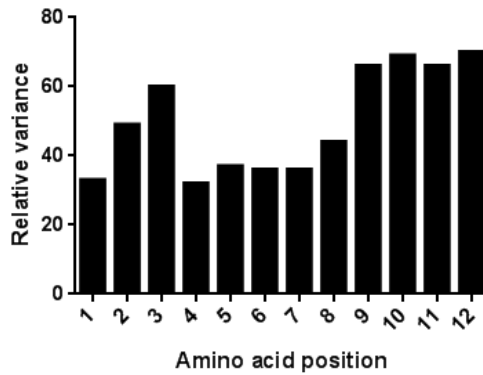


Figure 4-10. Relative variability analysis of the sequences derived from phage display shows a decreased variability at position 1 and 4-7. Position 12 is closest to the phage body and position 1 has the most freedom of movement. This analysis removed any repeat sequences.

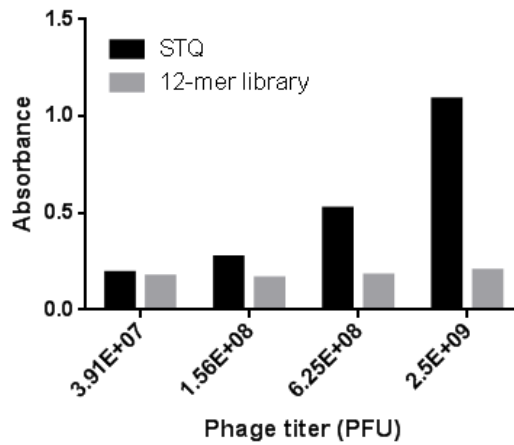


Figure 4-11. ELISA results of the STQ phage shows increased binding compared to the naïve phage library. As the titer of phages added to VSV-G coated plates was increased, phages displaying the STQ sequence demonstrated increased binding whereas the non-specific naïve library did not demonstrate a noticeable change in binding.

subsequently investigated. Peptides were synthesized with a terminal thiol group, and initial studies incorporated these peptides through Michael type addition, consistent with the mechanism of attachment for PLL and RGD peptides. The peptide density and incubation time of the peptide with virus were those identified to maximize expression with PLL (Fig. 4-4). Peptides that were directly incorporated into the PEG hydrogel failed to promote transgene expression. Subsequent studies involved attaching a 5 kDa PEG linker to the peptide, which was hypothesized to provide greater flexibility for lentivirus binding. PEG hydrogels functionalized with linker-modified peptides promoted substantial transgene expression (Fig. 4-12). The four peptides identified by phage display provided a 6- to 20-fold increase in luciferase activity relative to RGD modified hydrogels (with RGD presented on a linker), and had expression levels that were comparable to the 30-70 kDa PLL. The use of the linker to connect the peptide to the hydrogel enhanced expression by the 30-70 kDa PLL relative to the absence of the linker (Fig. 4-2). Interestingly, a 1 kDa PLL peptide immobilized on a linker did not promote significant gene transfer above that produced with RGD. Taken together, these results indicate that peptides can promote substantial transgene expression by immobilization to hydrogels, though their presentation on a linker is necessary.

4.4 Discussion

This chapter investigated the design of peptides for immobilization of lentivirus to hydrogels and subsequently promote transgene expression. PLL is a cationic polypeptide that has been previously employed in non-viral gene delivery and has also been used to modify biomaterials to promote virus association. PLL has been proposed to associate with the lentiviral

Peptide	Occurrence
HLKHTHNTHYKT	4
HWKPHSNLHLSR	8
STQHSHHSKQSR	32
WPGHHNHSMKHK	6

Table 4-2. Phage display clones that appeared multiple times were selected for further analysis.

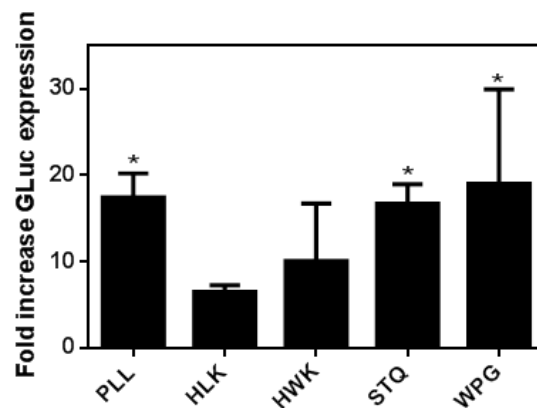


Figure 4-12. Phage display identified peptides specific to the VSV-G protein on the lentivirus. Specific binding of lentivirus to phage display peptides. PEG hydrogels were functionalized with 2.5 mM RGD and 2.5 mM of the synthesized phage display peptides conjugated with a 5 kDa PEG linker (n=4). HLKHTHNTHYKT (‘‘HLK’’), HWKPHSNLHLSR (‘‘HWK’’), STQHSHHSKQSR (‘‘STQ’’), and WPGHHNHSMKHK (‘‘WPG’’). RGD and 30-70 kDa PLL (0.45 mg/mL) were also functionalized to the PEG linker to serve as negative and positive controls, respectively. Lentivirus was incubated with the hydrogels for 3 hours followed by washing to remove non-binding virus. HT1080 cells were seeded on the hydrogels and luciferase activity was assayed 72 hours later. Fold increase in GLuc expression relative to RGD control. Significant differences between RGD and PLL are denoted by an asterisk (p<0.05).

vector through non-specific interactions. Our studies, consistent with previous reports [155], demonstrated that relatively high molecular weight PLL led to greater transgene expression. The enhanced transgene expression likely results from the retention of virus at the surface, which would overcome mass transport limitations by localizing the virus to the substrate to which cells were adhered [156, 157]. Immobilization also served to increase the stability by approximately 20%, and the extent of immobilization increased through concentrations of 1.35 mg/mL and subsequently reached a plateau. Hydrogels functionalized with PLL concentrations higher than 4.05 mg/mL were generally associated with decreased cell viability. Gene expression could theoretically be further manipulated by modifying PEG concentration, the molecular weight of PEG, and the amount of loaded virus. The collection of positive charges presented by the PLL provide sufficient avidity to effectively act to bind, yet the interaction between the virion and cell is sufficient to disrupt the PLL-lentivirus binding.

PEG hydrogels were functionalized with PLL at multiple molecular weights (1 kDa, 10 kDa, and 30-70 kDa). These studies were performed for a similar extent of surface modification to isolate the effect of chain length. These studies demonstrated a significant effect of the chain length, with the shortest not supporting binding, the intermediate providing low level transduction, and the longest providing the greatest levels of expression. The peptide RGD served as a control for these studies and small quantities of virus was associated with this condition; however, this low association may be influenced by non-specific interaction with the hydrogel.

We sought to identify shorter peptides for virus immobilization, as large peptides can be difficult to work with, relatively expensive, and have potential for cytotoxicity. The results with 1 kDa PLL indicated that the peptide would need greater affinity, and thus phage display was used.

Phage display requires a highly pure target, which was not achievable with the existing lentivirus purification kits (LentiX). The crystal structure for the pre-fusion form of the VSV-G protein had recently been determined [158], and the purified VSV-G ectodomain was generously provided by the Gaudin group. Using the 12-mer library, we identified 108 clones, and the sequences that were most commonly observed were investigated for lentivirus binding. The STQ sequence was obtained with the greatest frequency after sequencing the phage clones. Several of the non-STQ sequences displayed a preference for four histidines at amino acid positions 4, 5, 6, and 7. A high abundance of aromatic amino acids could signify that the phages are interacting with the plastic instead of the target protein [159, 160]. In a fourth round of panning, the phages showed a 10,000-fold higher binding affinity for wells coated with VSV-G, suggesting that our experiments did not identify proteins based on non-specific binding to the plastic. The precise nature of how this histidine motif interacts with VSV-G will need to be explored in future studies.

Peptides identified through phage display were able to support transduction if a linker was employed for peptide immobilization. Initial studies with direct peptide attachment to the PEG hydrogel had minimal levels of transgene expression. Linkers have been used by others to conjugate antibodies to epidermal growth factor (EGF), which were hypothesized to reduce steric hindrance and thereby improve interactions between the target [161]. Peptide immobilization with a 5 kDa PEG linker led to significant transgene expression, with the STQ and WPG peptides providing the greatest levels of expression. Interestingly, the transgene expression levels obtained with the immobilized peptide were comparable to the levels obtained with the relatively high molecular weight PLL. A linker applied to the 30-70 kDa PLL increased transgene expression by approximately 80%, yet was required for the peptides. Finally, we note that the

affinity provided by the peptides identified by phage display was necessary for transduction, as a 1 kDa PLL did not support gene transfer.

Viral gene delivery represents a versatile tool to modify the microenvironment of damaged or diseased tissue and promote regeneration by converting the transduced cells into bioreactors to produce therapeutic proteins or downregulate undesired genes. Hydrogels are employed as a substrate that creates a space to promote regeneration, possess mechanical properties similar to native extracellular matrices, and can be readily functionalized. Hydrogels functionalized with proteins or peptides capable of binding lentivirus retained the virus at the material, enhanced the virus stability, and ultimately promoted gene transfer. High molecular weight proteins that non-specifically bind the lentivirus were directly attached to support binding and gene transfer. Alternatively, short peptides that specifically bind the lentivirus had to be immobilized onto biomaterials through linkers in order to promote binding and gene transfer, yet offered comparable gene expression levels. Taken together, affinity peptides or proteins can be attached to biomaterials to promote the binding of gene therapy vectors and subsequent gene transfer, with the efficiency a function of the peptide length and binding affinity.

CHAPTER 5. Localized Immune Tolerance from FasL-Functionalized PLGA Scaffolds

5.1 Introduction

Graft rejection is a central limitation in current clinical islet transplants. Although improvements in immunosuppressants have improved graft survival, chronic administration of these drugs leads to additional complications [18, 162]. In contrast, localized modulation of the immune system provides tolerance in allogeneic hosts without body-wide negative side effects associated with systemic immunosuppressants. Encapsulating hydrogels are a widely explored alternative that create a semipermeable membrane designed to block immune cells and exclude inflammatory cytokines while allowing insulin, nutrients, and waste to diffuse across the barrier [163-166]. Consequently, this approach excludes blood vessel infiltration and, in the absence of adequate blood supply, islets face acute hypoxic stress and poor insulin exchange [167]. As demonstrated in Chapter 3, microporous scaffolds are an attractive option due to their rapid engraftment and response to changes in blood glucose levels, but they do not offer any inherent protection from the immune system. Therefore, the purpose of this chapter is to demonstrate the feasibility of functionalizing microporous scaffolds with immunoregulatory proteins to locally induce islet tolerance.

Destruction of β cells in T1D is caused by autoreactive T cells responding to β cell-specific antigens [91]. Experimental evidence suggest that the direct recognition of class I MHC molecules on the surface of islet cells by CD8⁺ T cells plays a critical role in islet allograft rejection [168-171].

Controlling the auto- and allogeneic T cell response would allow for long term survival of transplanted islets. Fas ligand (FasL), a well-studied regulatory protein, binds to cells expressing the FasR and plays an important role in tolerance to self-antigens [172-175]. Previous attempts to utilize the regulatory capability of FasL were met with some success by transplanting a composite graft consisting of islets and syngeneic myoblasts transfected to express FasL [176], but it was later demonstrated that this approach was prone to neutrophil-mediated inflammation [177]. Similarly, other groups have utilized islets that directly expressed FasL, but also encountered rapid islet death from host neutrophils [178, 179]. As an alternative to ectopic gene expression, islets were biotinylated and functionalized with a streptavidin-FasL (SA-FasL) chimera protein that has shown indefinite cell survival when combined with a short course of rapamycin [180].

It is clear that FasL is a potent immunoregulatory molecule and localized delivery of FasL represents an attractive option, but proper presentation of the protein remains a challenge. Although surface decoration of FasL on biotinylated islets has demonstrated robust tolerance, manipulating a biomaterial scaffold to present SA-FasL would eliminate the steps needed for direct islet engineering, and as such save time and overcome potential undesired effects associated with engineering process, such as cell fragmentation. The studies in this chapter describe the attachment of SA-FasL to microporous scaffolds to achieve chronic immunosuppression-free, long-term survival of allogeneic pancreatic islets transplanted into an extrahepatic site. Initial studies employed the established model in which islets are modified with SA-FasL, with subsequent transplantation onto a microporous scaffold. Subsequently, we developed the procedures for modifying microporous PLGA scaffolds with biotin for subsequent

immobilization of SA-FasL, and characterized the binding and functionality of the immobilized protein. Although it would be desirable to utilize PEG hydrogels due to their tissue-like mechanical properties and ease of functionalization, PLGA scaffolds were used in these studies as allogeneic transplants in this material is already well-characterized. These studies employed islets isolated from BALB/c mouse and transplanted into the epididymal fat pad of C57/BL6 mouse, a fully mismatched transplantation model. The omentum has emerged as a leading candidate in human clinical trials due to its thin and highly vascularized membrane, and portal draining that recreates the physiological effects of insulin in the liver [34, 181]. In mice, the epididymal fat pad has many similar features to the omentum, and we have developed scaffolds to support engraftment of transplanted islets at this site. The function of the transplanted islets was monitored by blood glucose levels as well as an intraperitoneal glucose tolerance test. Collectively, these studies address two major issues with clinical islet transplantation; development of an extrahepatic site for islet engraftment, and overcoming immune rejection without of the use of chronic immunosuppression.

5.2 Materials and methods

5.2.1 Materials:

Poly(lactide-co-glycolide) (75:25) (PLGA) (approx. 80,000 g/mol) with a single carboxylic acid end-group and an inherent viscosity of 0.76 dL/g was purchased from Lakeshore Biomaterials (Birmingham, AL). Poly(ethylene-alt-maleic anhydride) (PEMA) was purchased from Polyscience, Inc. (Warrington, PA). EZ link Amine-PEG2-Biotin was purchased from Fisher Scientific. 1-ethyl-3-(3-dimethylaminopropyl)carbodiimide hydrochloride (EDC) and N-

hydroxysuccinimide (NHS). Dichloromethane (DCM), dimethyl sulfoxide (DMSO). All other reagents were purchased from Sigma Aldrich (St. Louis, MO) unless noted otherwise.

5.2.1 Biotinylation of PLGA and characterization

PLGA (890 mg, 0.011 mmol) was added to a 20 mL glass scintillation vial and dissolved in 10 mL DMSO. The carboxyl end group of PLGA was activated by first adding EDC (10.6 mg, 0.056 mmol) dissolved in 1 mL DMSO followed by NHS (6.4 mg, 0.056 mmol) dissolved in 1 mL DMSO and the reaction was allowed to stir for 15 min. Amine-PEG2-Biotin (5 mg, 0.056 mmol) was dissolved in 1 mL DMSO and added dropwise to the stirring solution of PLGA-NHS and the reaction was allowed to stir overnight. Excess biotin was removed by extraction. The reaction mixture was diluted into 200 mL of DCM and washed 4 times with 150 mL of brine. The organic layer was dried over anhydrous sodium sulfate, filtered, concentrated by rotary evaporation, precipitated into ice cold methanol, and stored in vacuum overnight to remove residual solvents. Functionalization was confirmed with $^1\text{H-NMR}$ (DMSO- d_6).

5.2.2 Particle and scaffold fabrication

PLGA microparticles were formed for scaffold fabrication as previously described [182]. Briefly, PLGA was dissolved in DCM at a concentration of 6 wt% and sonicated in a 1% solution of PEMA at 100% amplitude (Cole-Parmer, 130 W, 3 mm stepped tip). The emulsion was poured into 200 mL of 0.5% PEMA and the organic solvent were evaporated by stirring the emulsion overnight. The particles were recovered by washing four times with deionized water by centrifugation at 7000 x g for 15 min at 4 °C. Particles were lyophilized for 48 hours and stored under vacuum. Biotin-PLGA microparticles were similarly fabricated, however biotin-PLGA

conjugates were combined with unmodified PLGA at a mass ratio of 3:1 (biotin-PLGA:PLGA) for a final concentration of 6 wt% in DCM.

Porous scaffolds were formed by mixing PLGA particles with NaCl ($250 \mu\text{m} < d < 425 \mu\text{m}$) at a 1:30 ratio (PLGA:NaCl). The mixture was pressed in a 5 mm KBr die using a Carver press at 1500 psi and foamed in CO₂ at 750 psi for 16 hours. Scaffolds were leached in water for 1 hour followed by a second wash for 30 minutes. Scaffolds were disinfected by soaking them in 70% ethanol and washed with deionized water.

5.2.3 Particle characterization

The size and zeta potential of the particles was determined by dynamic light scattering (DLS) by mixing 10 μL of a 25 mg/mL particle solution into 990 μL of MilliQ water using a Malvern Zetasizer ZSP (Westborough, MA) as previously described [Citation].

5.2.4 Scanning electron microscopy

SEM images were taken using a scanning electron microscope (FEI Quanta 3D) instrument. A gold sputter coating was applied and the microscope was operated at 10 kV.

5.2.5 Protein loading and quantification

Particles were incubated with various concentrations of fluorophore-labeled streptavidin at 1 mg particles/mL for 20 minutes at various concentrations. Unbound streptavidin was removed by washing the particles with PBS by centrifugation (7000 x g, 5 min, 4 deg. C). To quantify the amount of fluorophore binding to the particles, particles were dissolved in DMSO and fluorescence was quantified using a plate reader, (Synergy 2 (BioTek)) at 578 nm excitation and 605 nm emission.

Scaffolds were incubated with fluorescent streptavidin by applying 10 μL of the SA solution (0-40 $\text{ng}/\mu\text{L}$) to both sides of the disc (a total of 20 μL) for 20 minutes. Unbound streptavidin was removed by washing the scaffold three times with 1.5 mL of PBS in a microcentrifuge tube. Scaffolds were dissolved in DMSO and fluorescence was quantified as described above.

5.2.6 Apoptosis assay

Particles (1 mg) and scaffolds were incubated with SA-FasL (supplied by the Shirwan lab, University of Louisville, KY) (Particles: 1 mL, 400 $\text{ng}/\mu\text{L}$; scaffold: 20 μL , 0-50 $\text{ng}/\mu\text{L}$) and washed as described above. To assess the ability for FasL particles or scaffolds to induce apoptosis in vitro, 1 mg/mL particles or a single scaffold was added to a 96 well plate containing A20 cells (mouse B lymphoma) at a concentration of 1.5×10^6 cells/mL and incubated for 18 hours. Cells were removed from the plate, stained with annexin V and propidium iodide (Life Technologies), and analyzed via flow cytometry.

5.2.7 Mice and recombinant proteins

Animal studies were completed at the University of Louisville in collaboration with the Haval Shirwan lab. C57BL/6 (*H-2^b*) and BALB/c (*H-2^d*) mice were purchased from Jackson Laboratory and bred according to protocol as approved by the Institutional Animal Care and Use Committee in our specific pathogen-free animal facility at the University of Louisville. Recombinant SA and SA-FasL proteins were made with the *Drosophila* DES expression system (Invitrogen)[183].

5.2.8 Islet isolation and engineering with SA-FasL protein

BALB/c islets were harvested from 8 to 12-week-old donors under anesthesia. Donor pancreases were perfused with 3 mL of cold Liberase TL (Roche Diagnostics) then removed and incubated for 20 minutes at 37°C. Islets were isolated using a Ficoll gradient (Sigma-Aldrich). Islets were kept overnight in RPMI-1640 medium supplemented with penicillin/streptomycin (100 U/ml and 100 µg/ml) and 10% fetal bovine serum in an incubator at 37°C with 5% CO₂. Islets were transferred to a 14-mL round bottom tube and washed in PBS. Islets were then incubated in 5 µM EZ-Link™ Sulfo-NHS-LC-Biotin solution (Thermo Scientific) at 20°C for 30 minutes. After incubation, islets were washed twice in PBS to remove any unbound biotin. Then, islets were incubated in PBS containing SA-FasL protein (~200 ng SA-Fas/500-550 islets/200 µl PBS) at 20°C for 30 minutes. Islets were washed twice in PBS to remove any unbound protein before transplantation. Biotin-PLGA scaffolds were engineered by placing scaffolds to a round bottom tube and adding SA-FasL (0.5 or 2.5 µg /scaffold) diluted in PBS and incubating at 20°C for 30 minutes while rotating and shaking the tube every 10 minutes. Scaffolds were washed twice before being loaded with islets.

5.2.9 Islet transplantation

C57BL/6 mice were chemically induced with diabetes by intraperitoneal (i.p.) injection of streptozotocin (200 mg/kg). Mice were monitored by reading blood glucose where ≥ 250 mg/dL for two consecutive days was considered diabetic. Islets were loaded onto PLGA scaffolds (2 scaffolds/mouse). Diabetic mice were given anesthesia and a small incision was made on the abdomen to allow scaffolds to be placed on epididymal fat pads. Adipose tissue was wrapped around scaffolds before being returned to the abdomen. Mice were then sutured. Select mice

were administered with rapamycin through i.p. injection of 0.2 mg/kg daily for 15 days starting the day of transplant. Mice were monitored for diabetes and those with ≥ 250 mg/dL blood glucose level for two consecutive days considered rejecting the islet graft.

5.2.10 Intraperitoneal Glucose Tolerance Test

Mice were put in clean cages without food and allowed to fast for 6 hours. After fasting, mice were injected with 25% glucose solution (2 gm/kg body weight). Mice were monitored for blood glucose levels before injection and at 10, 20, 30, 60, 90, and 120 minutes post glucose injection.

5.2.11 Immune monitoring

Spleen and draining lymph nodes were harvested from mice after rejection of graft or at experimental end point (> 200 days) if mice remained euglycemic up to that point. Organs were dissociated into single cell suspensions by shearing between two frosted slides. ACK lysis buffer (ThermoFisher Scientific) was added to spleen to lyse red blood cells. For T cell phenotyping, after washing and counting, cells were stained with antibodies for surface markers (Alexa 700-CD4 Ab, APC-Cy7-CD8 Ab, PE-Cy7-CD25 Ab from Pharmingen, BD, and eFlour 450-CD44 Ab and PerCP-Cy5.5-CD62L Ab from eBioscience). Cells were then fixed and permeabilized, and FoxP3 staining was done using FoxP3 Transcription Factor Staining Buffer set (eBioscience).

For mixed lymphocyte reaction, splenocytes were panned and labelled with CFSE. Stimulator cells were prepared from either naïve BALB/c (donor) or C3H (3rd party) mice, irradiated with 200 cGy, and cocultured with equal numbers of responder cells in 96-well plates (0.1×10^6 cells/well). Cells were cultured in 200 μ L DMEM supplemented with HEPES buffer,

sodium pyruvate, penicillin/streptomycin, L-Glutamine (ThermoFisher Scientific), FBS, L-Arginine HCL, folic acid, L-Asparagine, 2-Mercaptoethanol (Sigma), and responder serum. Cells were harvested after four days of culture at 37°C and stained with Alexa 700-CD4 Ab, APC-Cy7-CD8 Ab, and 7AAD to separate dead cells (BD Pharmingen). Cells were analyzed using BD LSR II and analyzed using Diva software.

5.2.12 Statistical analysis

Flow data was tested for significance using a two tailed Welch's t-test. Graft survival was tested for significance using the log-rank test. P values of <0.05 were considered significant. Survival curves, IPGTT, and flow graphs were created and analyzed using GraphPad Prism software.

5.3 Results

5.3.1 Transplantation of SA-FasL modified islets onto microporous scaffolds

We investigated the transplantation of SA-FasL on microporous scaffolds implanted into the epididymal fat pad (Fig. 5-1A). Initial studies employed the transplantation of syngeneic islets into streptozotocin-induced diabetic mice to determine the impact of the scaffolds and short term rapamycin on the engraftment and function of the transplanted islets. Transplantation of the syngeneic islets led to the establishment of euglycemia within 10 days for all animals, and the animals maintained euglycemia for the duration of the study (200 days) (Fig. 5-1B). Subsequently, allogeneic islets modified with SA-FasL were transplanted on microporous scaffolds. Unmodified islets transplanted on scaffolds with transient rapamycin had rejection of the grafts, as indicated by increased blood glucose levels, by day 40 (Fig. 5-1B). Mice transplanted with allogeneic islets

modified with SA-FasL and receiving the transient rapamycin had normalized blood glucose levels that were sustained for 200 days (Fig. 5-1B), similar to the results with syngeneic islets. Rapamycin has been previously reported to synergize with FasL presentation to prolong graft survival [180], as either factor alone results in only short-term graft function. An IPGTT study demonstrated that the normalization of blood glucose levels by the transplanted islets was similar to that observed with naïve mice (i.e., non-diabetic) (Fig. 5-1C), which is consistent with previous reports of islets transplanted on scaffolds [122, 123].

T cell proliferative responses were analyzed from the spleens and draining lymph nodes of the grafts. The collected cells were labeled with CFSE and used against BALB/c donor and third party C3H stimulators in a standard ex vivo mixed lymphocyte reaction. After 4 days of culture, the responses from CD8 T cells indicated similar proliferative responses for the SA-FasL islets, the unmodified islets, and an age-matched C57Bl6 control, with responses similar to both the donor and third party stimulators (Fig. 5-1D). Interestingly, CD4 T cell responses were greater for the SA-FasL modified islets relative to either the unmodified islets or age-matched control. This response was similar for both the donor and third party stimulators. These results demonstrate that CD4 and CD8 responsiveness is maintained outside the graft. Collectively, these studies demonstrate that the microporous scaffolds for transplantation of FasL modified islets to an extrahepatic, extra-renal site provides for engraftment of the islets and protection from the immune response similar to previous reports performed with transplantation into the kidney capsule or liver ([180, 184]).

5.3.2 Synthesis and characterization of biotin-poly(lactide-co-glycolide) conjugates and particle formation

While multiple strategies for functionalizing PLGA particles with ligands are available, evidence suggests that directly conjugating the polymer prior to particle fabrication enhances target binding [185]. To produce biotin-PLGA conjugates, the carboxyl-terminal group of PLGA

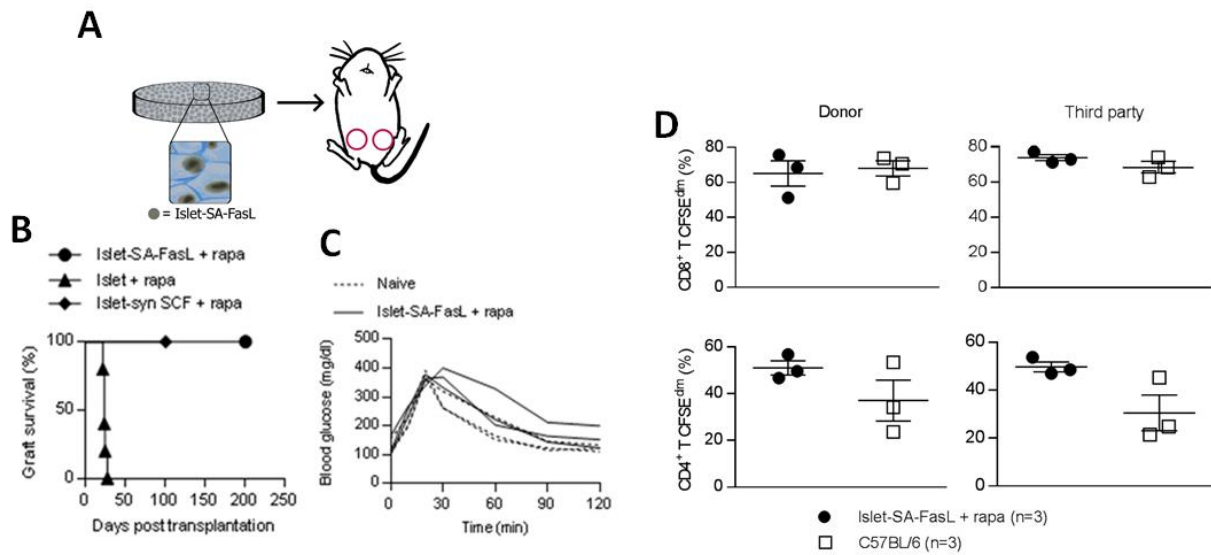


Figure 5-1. SA-FasL engineered islets establish allogeneic tolerance when transplanted on PLGA scaffolds. **(A)** Schematic showing biotinylated allogeneic islets functionalized with SA-FasL are loaded on microporous PLGA scaffolds and planted in the epididymal fat pad of mice. **(B)** Kaplan Meier analysis of allogeneic BALB/c islets transplanted under the short cover of rapamycin on unmodified PLGA scaffolds in C57BL/6 recipients. Conditions include SA-FasL-engineered islets (n = 5, MST >200 days, P=0.0018 vs. rapamycin alone, P=0.0308), naïve islets (n = 5, MST = 23 ±2.19 days), and unmodified syngeneic islets (n = 3, MST > 100 days). **(C)** Intra-peritoneal glucose tolerance test of long-term islet grafts compared to naïve C57BL/6 mice after fasting for 6 hours, followed by i.p. glucose injection. Blood glucose of mice was taken starting just before injection and at the indicated time points. **(D)** T cell proliferative response from recipients of long-term (> 200 days) BALB/c SA-FasL-engineered islets mounted on unmodified PLGA scaffolds plus rapamycin (n = 3) and naïve C57BL/6 as controls (n = 3). Responders were labeled with CFSE and used against BALB/c donor and third party C3H stimulators in a standard ex vivo mixed lymphocyte reaction. After 4 days of culture, cells were stained with antibodies against CD4 and

CD8 molecules and incubated with 7AAD to gate out dead cells before flow cytometry analysis. Bars represent mean and SEM. Asterisks represent level of significance (* $p < 0.05$, ** $p < 0.01$) found by using a two-tailed Welch's t-test.

was conjugated to the heterobifunctional linker NH₂-PEG₂-Biotin using carbodiimide chemistry and confirmed using ¹H-NMR (Fig. 5-2A and 5-2B). Biotin-PLGA particles were prepared by employing a single emulsion-solvent evaporation procedure using the biotin-PLGA conjugates. The formed particles displayed an average size of 860 ± 40 nm and a zeta potential of -16 ± 5.0 mV (Fig. 5-2C). SEM images confirmed the size and demonstrated the spherical morphology of the biotin-PLGA particles (Fig. 5-2D). When only biotin-PLGA was used in microparticle fabrication, particles did not form stable spheres (Fig. 5-3A). Thus, a 3:1 mix of biotin-PLGA to unmodified PLGA was used. When additional unmodified PLGA was blended in for a ratio of 1:1, there was no significant difference in the amount of protein absorbed at the concentrations tested (Fig. 5-3B).

To demonstrate the ability of biotin-PLGA particles to load streptavidin-functionalized protein on their surface, we first quantified the maximum loading and efficiency of biotin-PLGA particle to load fluorescently-tagged streptavidin (AF568-SA) (Fig. 5-4A). AF568-SA was incubated with biotin-PLGA particles at concentrations between 100 – 40,000 ng SA per mg of particles for 15 minutes. After incubation, the particles were with PBS to remove non-binding protein, dissolved in DMSO, and the fluorescence was measured (Fig. 5-4B). As expected, the loading of AF568-SA on the particles increased with increasing amounts of AF568-SA added but the loading did not increase linearly. The corresponding loading concentrations were 75 – 280 ng SA per mg of particles, and the loading efficiency (defined as the amount of protein bound divided by the amount incubated) decreased from 75% to 35% over this range as the particles became saturated with protein (Fig. 5-4C). A significant increase in the loading was observed between 200 ng/mg and 400 ng/mg, which potentially indicated that threshold for binding was reached at

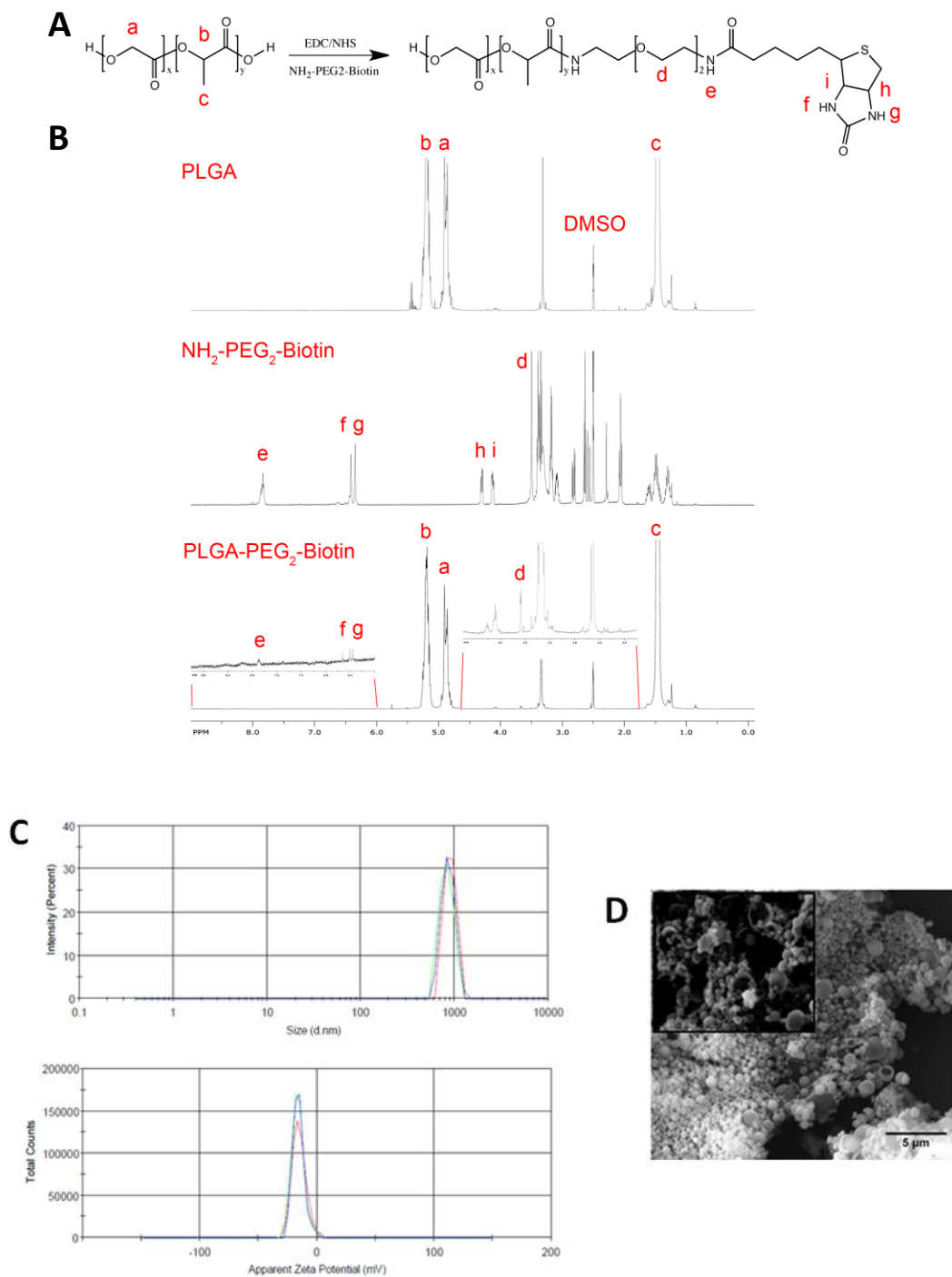


Figure 5-2. Characterization of biotin-PLGA microparticles. **(A)** Conjugation of $\text{NH}_2\text{-PEG}_2\text{-biotin}$ to PLGA resulting in biotin-PLGA. **(B)** $^1\text{H-NMR}$ of PLGA (top), biotin linker (middle), and biotin-PLGA (bottom). **(C)** Size (860 ± 40 nm) and charge (-15.8 ± 4.98 eV) of biotin-PLGA particles was measured using dynamic light scattering (DLS). **(D)** Scanning electron microscope (SEM) image of biotin-PLGA particles.

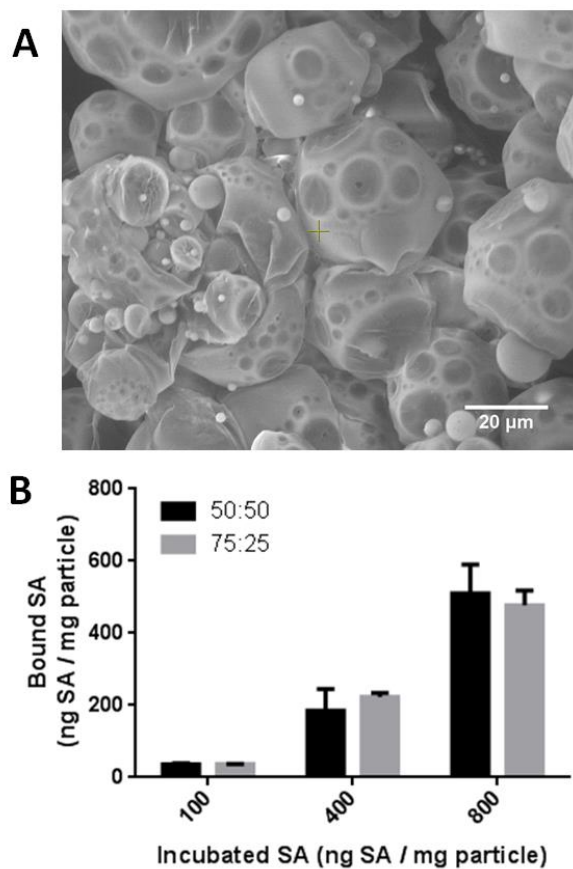


Figure 5-3. Blending unmodified PLGA with biotin-PLGA is necessary to consistently form spherical particles. **(A)** SEM image of particles formed only with biotin-PLGA formed unstable particles. **(B)** Two ratios of biotin-PLGA : PLGA (50:50 and 75:25) were analyzed. There was no significant difference in SA binding between the two blends.

400 ng/mg. This result was further supported by the measured loading efficiencies, where, as the amount of AF568-SA was increased, the loading efficiency decreased. Saturation of the particles was achieved by incubating the particles in a 40,000 ng SA per mg particles solution, which bound 8600 ng SA per mg particles. To demonstrate that the protein binding is due to biotin-SA interaction and not passive adsorption of protein to the particle surface, unmodified PLGA particles were used as a control and demonstrated significantly lower binding and lower binding efficiency.

Utilizing the information from the binding curves, it was determined that one milligram of particles incubated with 400 ng SA-FasL was optimal and this concentration was used for subsequent apoptosis assays. Particles were loaded with SA-FasL, washed three times with PBS, and incubated with 1.5×10^5 A20 cells (mouse B lymphoma cells) for 18 hours. Following incubation, cell death was quantified via propidium iodide (PI) live/dead stain and flow cytometry (Fig. 5-4D). As a positive control, soluble SA-FasL at concentrations known to induce apoptosis were included. While biotin-PLGA particles without FasL did not induce cell death, cells incubated with FasL-PLGA particles induced cell death in 50% of the population.

5.3.3 FasL loading on biotin-PLGA scaffolds

Biotin-functionalized PLGA scaffolds were prepared by pressing biotin-PLGA and salt to form discs then gas foamed to fuse the particles (Fig. 5-5A). Following salt leach, porous scaffolds were left. In a similar manner to biotin-PLGA particles, the binding of SA-AF568 was evaluated by incubating the scaffolds with 100 to 800 ng SA-AF568 per mg of scaffold (one scaffold weighs 2.5 mg) and quantifying the fluorescence (Fig. 5-5B). The amount of bound protein ranged from 70

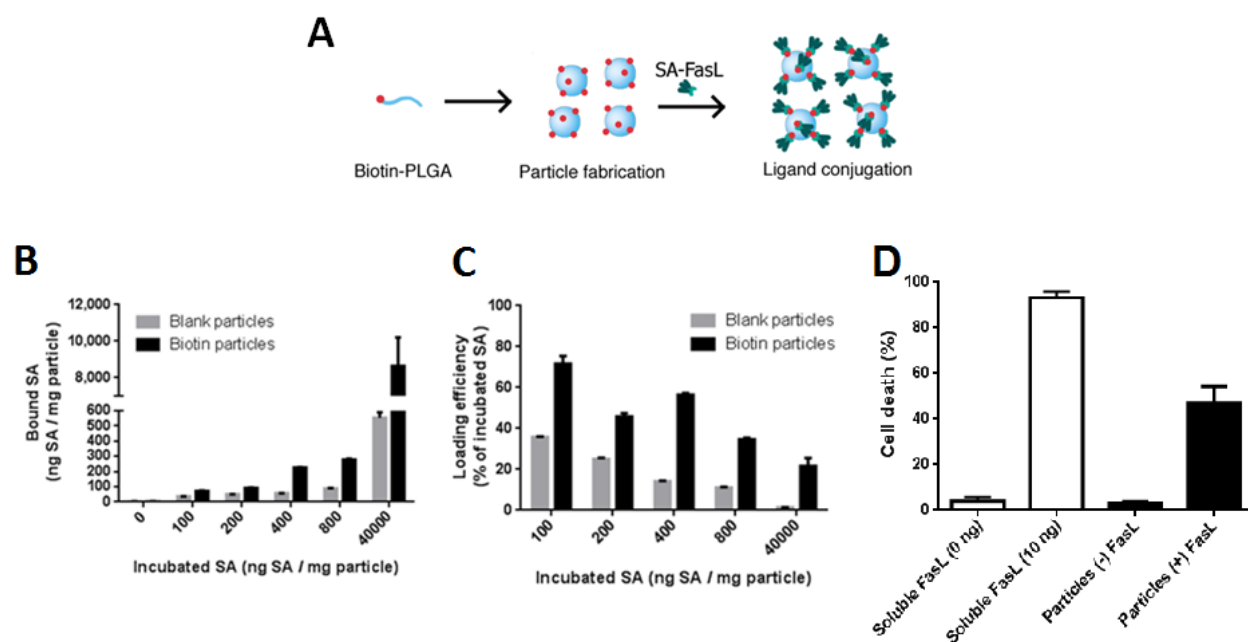


Figure 5-4. Biotin-PLGA particles can be efficiently conjugated with SA-FasL and induce apoptosis in mouse B lymphoma cell line. **(A)** Schematic of biotin-PLGA particles being functionalized with SA-FasL. **(B)** The amount of fluorescently tagged SA bound to the particles was investigated by varying the protein concentration (0, 100, 200, 400, 800, and 40,000 ng SA/mL in 1 mL) incubated with 1 mg of biotin-PLGA particles (“biotin particles”). As a control, 1 mg of unmodified PLGA particles was incubated with the same SA concentrations (“blank particles”). After two spins and washes, particles were dissolved in DMSO and fluorescence was measured, $n=3$. **(C)** The loading efficiency was calculated by dividing the bound SA by the incubated SA, $n=3$. **(D)** Biotin-PLGA particles functionalized with SA-FasL induce cell death in A20 cells. Particles were incubated with 400 ng / mL of SA-FasL in 1 mL with 1 mg of particles. After washing to remove unbound SA-FasL, particles were incubated with 1.5×10^5 A20 cells for 18 hours and cell death was analyzed via propidium iodide stain and flow cytometry ($n=3$). For comparison, soluble FasL was added to cells (0 and 10 ng) and demonstrated the ability to induce cell death at low concentrations ($n=3$).

to 620 ng SA per mg of scaffold, which was similar to particles at low concentrations, but more than twice as much at higher concentrations. This difference may be due to increased surface area of the porous scaffold compared to the spherical particles. Additionally, the loading efficiency for all conditions tested was near 70% with no decline in efficiency at higher protein concentrations, indicating that the scaffolds are capable of binding protein at considerably higher concentrations than what was tested (Fig. 5-5C). Unmodified scaffolds were used as a control, and showed similar concentrations of non-specific binding to unmodified particles at higher protein concentrations.

The effectiveness of FasL-loaded scaffolds to induce apoptosis in immune cells was subsequently investigated by incubating the biotinylated scaffolds with SA-FasL, washing three times to remove unbound SA-FasL, and incubated with 1.5×10^5 A20 cells for 18 hours. Apoptosis induction was evaluated using PI/annexin V staining and quantified using flow cytometry (Fig. 5-6A). The induction of apoptosis was concentration-dependent as 40 ng FasL/mg scaffold was not significantly different than the control but 200 ng/mg and 400 ng/mg increased apoptosis (Fig. 5-6B). These results demonstrate that FasL could be functionalized to the surface of PLGA scaffolds and induce apoptosis in immune cells.

5.3.4 FasL scaffolds support allogeneic graft function without sustained immunosuppression

We examined whether FasL modified scaffolds could prevent allogeneic islet rejection and support long-term engraftment and function of allogeneic islets to maintain normoglycemia. Scaffolds decorated with SA-FasL were loaded with 500-550 islets from BALB/c donors and transplanted into the IP fat pad of diabetic C57BL/6 mice (two scaffolds per animal). Naïve islets

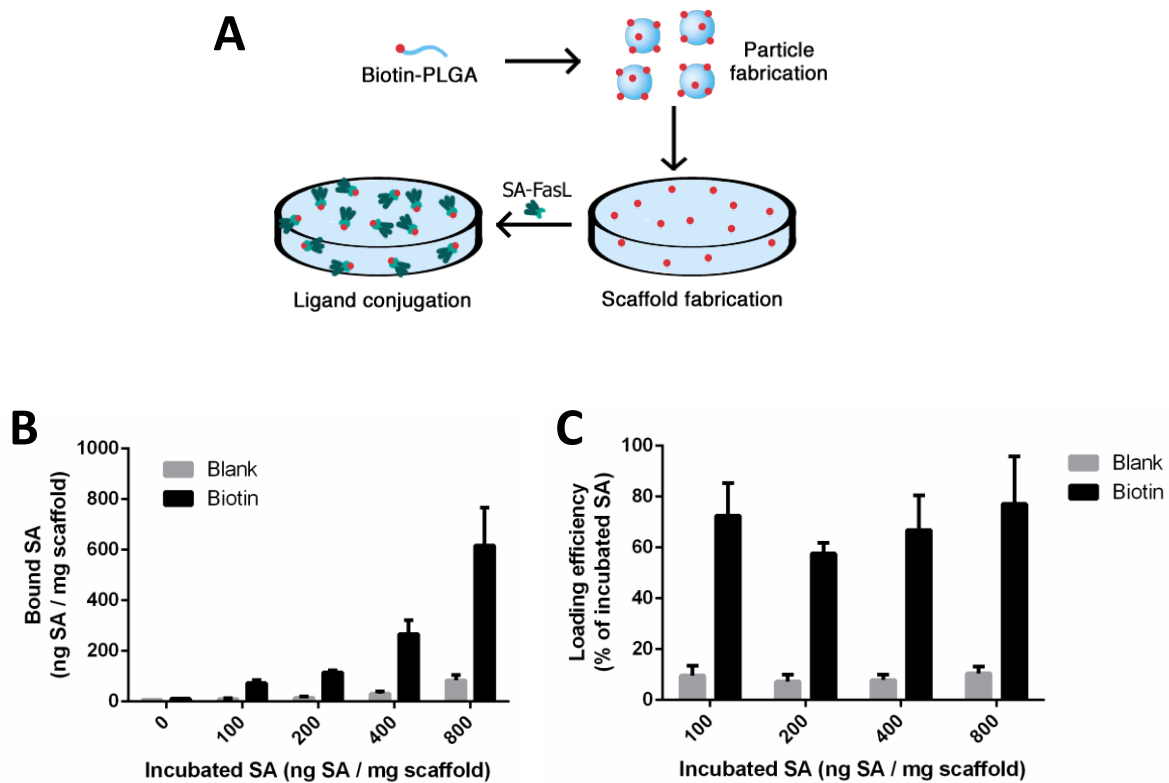


Figure 5-5. Biotin-PLGA scaffolds can be efficiently conjugated with SA-FasL. **(A)** Schematic of biotin-PLGA particles functionalization with SA-FasL. **(B)** The amount of fluorescently tagged SA bound to scaffolds was investigated by varying the protein concentration (0, 100, 200, 400, and 800 ng SA/20 μ L) incubated with 2.5 mg biotin-PLGA scaffolds (“biotin”). As a control, unmodified PLGA scaffolds were incubated with the same SA concentrations (“blank”). After two washes, scaffolds were dissolved in DMSO and fluorescence was measured, n=3. **(C)** The loading efficiency was calculated by dividing the bound SA by the incubated SA, n=3.

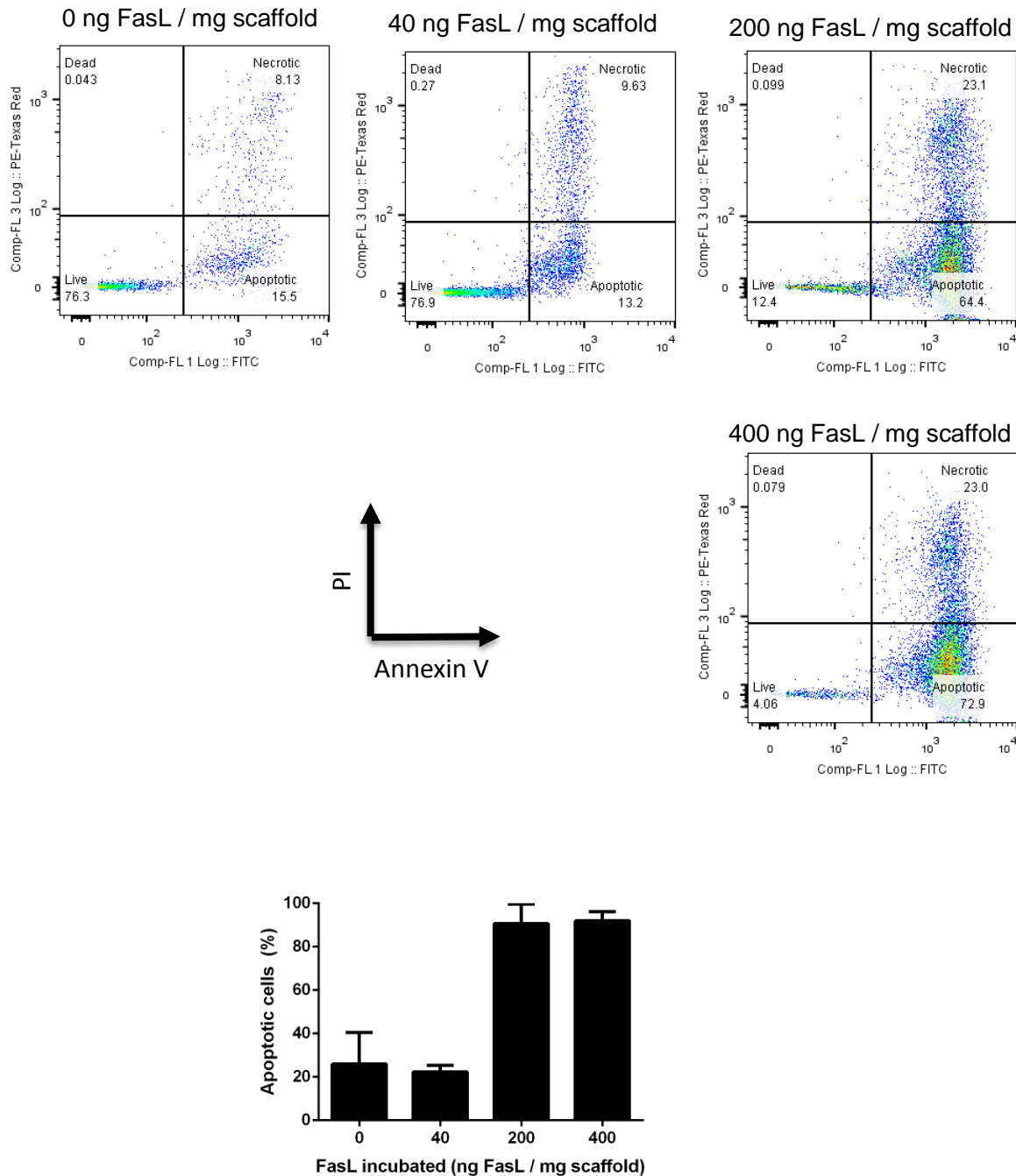


Figure 5-6. FasL-decorated scaffolds induce apoptosis in mouse lymphoma cell line. **(A)** Scaffolds were incubated with SA-FasL (0, 40, 200, and 400 ng / 20 μ L). After washing to remove unbound SA-FasL, scaffolds were incubated with 1.5×10^5 A20 cells for 18 hours. Apoptotic and dead cells were analyzed via propidium iodide and annexin V staining and flow cytometry (n=3). **(B)** Scaffolds required a minimum loading of 200 ng FasL / mg scaffold to induce apoptosis in the majority of A20 cells.

mounted on SA-FasL-engineered PLGA scaffolds along with transient rapamycin demonstrated graft survival for more than 200 days in more than 80% of the animals (Fig. 5-7A), with one animal rejecting at day 30. Normoglycemia was established within days of transplantation (Fig. 5-7B), and an IPGTT performed at day 200 demonstrated restoration of normoglycemia on similar times as naïve animals (Fig. 5-7C). Rapamycin without FasL had a mean graft survival time of 23 ± 2 days (Fig. 5-7A, B). The combination of SA-FasL-engineered islets mounted on SA-FasL-engineered PLGA scaffolds did extend graft function beyond that provided by rapamycin alone (Fig. 5-6A), yet unexpectedly was substantially shorter in duration (mean survival time = 46 days) than the SA-FasL engineered scaffolds. Prior to rejection, an IPGTT performed at day 200 demonstrated a restoration of euglycemia on the same time scales as naïve mice (Fig. 5-7C).

5.4 Discussion

This chapter investigated the combination of FasL and biomaterial scaffolds as a means to create a site that supports the engraftment and long term function of allogeneic islets at an extrahepatic and extrarenal site. Immunoprivileged sites, such as the testes, anterior chamber of the eye, brain, and tumors, have the ability to suppress destructive immune responses by various mechanisms [186-188]. Importantly, FasL was initially discovered as one of the molecules that plays a critical role in immunoprivileged sites [172, 173]. Indeed, we have recently reported that SA-FasL-engineered allogeneic islets induced localized immune privilege when transplanted under the kidney capsule [180]. Therefore, FasL not only contributes to the regulatory mechanisms in naturally occurring immunoprivileged sites in the body, but can also be used to create “induced” immunoprivileged sites [180]. While inducing tolerance in the subrenal model

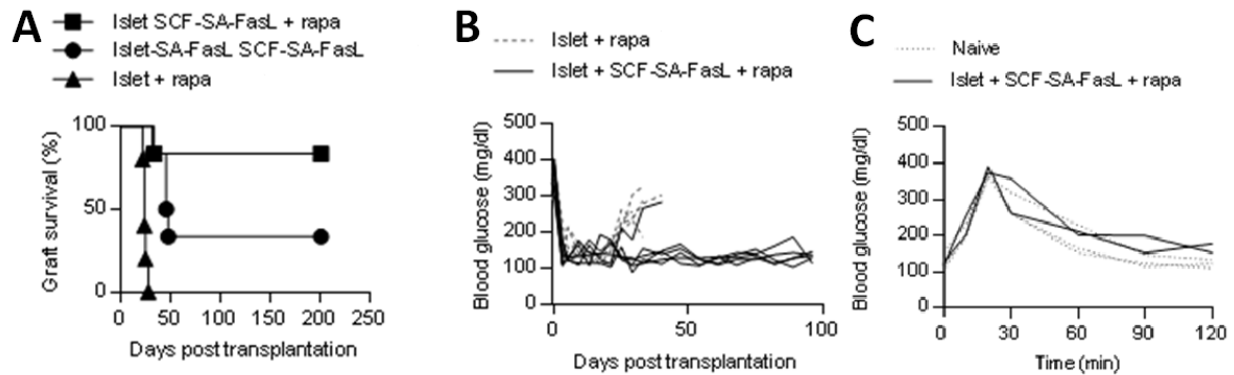


Figure 5-7: Islets on scaffolds conjugated with SA-FasL demonstrate robust long-term tolerance. **(A)** Survival of allogeneic BALB/c islets mounted on PLGA scaffolds and transplanted in the epididymal fat pad of chemically diabetic C57BL/6 recipients. Groups included naïve islets mounted on SA-FasL-engineered PLGA scaffolds plus rapamycin ($n = 6$, MST > 200 days, $P=0.0007$ vs rapamycin alone), SA-FasL-engineered islets mounted on SA-FasL-engineered PLGA scaffolds ($n = 6$, MST = 46 days, $P = 0.0007$ vs rapamycin alone), and naïve islets transplanted under a short cover of rapamycin ($n = 5$, MST = 23 ± 2.19 days). All mice received islets loaded on 2 PLGA scaffolds. PLGA scaffolds were engineered with $2.5 \mu\text{g/scaffold}$, except 3 mice in the islet-FasL+PLGA-SA-FasL that were transplanted with PLGA scaffolds engineered with $0.5 \mu\text{g/scaffold}$ and all 3 animals rejected their grafts. Rapamycin was given to the indicated groups through i.p. injection at 0.2 mg/kg daily for 15 days starting on the day of transplantation. Mice were monitored twice weekly for blood glucose levels. Those with $> 250 \text{ mg/dL}$ for two consecutive readings 24 hours apart were considered diabetic and rejecting the graft. Analysis done using log-rank test, $**P<0.01$, $***P<0.001$. **(B)** Blood glucose readings of two groups of mice from (A). **(C)** Intraperitoneal glucose tolerance test (IPGTT) of long-term islet grafts compared to naïve C57BL/6 mice after fasting for 6 hours, followed by i.p. glucose injection. Blood glucose of mice was taken starting just before injection and at the indicated time points.

was 100% effective, the SA-FasL immunomodulatory protocol had moderate efficacy in inducing tolerance to allogeneic islets transplanted intraportally as practiced in the clinic [184]. This finding provided rationale for the development of an extrahepatic site for islet transplantation. Herein, we demonstrated that allogeneic SA-FasL-engineered islets engrafted and normalized blood glucose levels for more than 200 days under a transient cover of rapamycin (0.2 mg/kg daily starting the day of transplantation for a total of 15 doses) with transplantation on PLGA scaffold into an extrahepatic site, one that has translational potential [38].

Given that localized presentation of SA-FasL on islets supported long-term function, we subsequently investigated the immobilization of SA-FasL to the scaffold as a means to minimize the cellular manipulation prior to transplantation. Manipulating the scaffold to present SA-FasL would eliminate the steps needed for direct islet engineering, and as such save time and overcome potential undesired effects associated with engineering process, such as cell fragmentation. Importantly, the presentation of SA-FasL from surfaces has previously been reported not to interfere with its apoptotic function [180, 189]. To create scaffolds modified with SA-FasL, we initially modified the polymer in solution [190, 191], which was subsequently formed in to particles and then into scaffolds. Initial attempts to functionalize scaffolds involved conjugation of biotin to the surface of a pre-formed scaffold, which produced inconsistent modification with SA-FasL and thus the direct modification of the polymer was pursued based on prior reports indicating enhanced target binding [185]. Stable spherical particles could only be formed from mixtures of the biotinylated and non-biotinylated polymer, as particles formed from only biotinylated polymer were unstable. The microspheres were employed to construct the scaffold using a gas foaming and particulate leaching process [39, 118, 192]. As a potential off-

the-shelf product, further studies will be needed to test long-term storage of SA-FasL pre-engineered scaffolds for downstream applications.

The microporous structure of the scaffold enhanced protein loading and bioactivity relative to the particles. This observation likely results from the higher surface area of the scaffolds. Protein loading and efficiency were similar to other techniques like carbodiimide coupling to PLGA particles [193, 194]. The presentation of SA-FasL from particles or scaffolds maintained the ability to induce apoptosis, although it was not as efficient as delivering soluble SA-FasL which induced apoptosis with 10 ng, which may reflect the availability of FasL for binding to receptors. Interestingly, for concentrations between 40 and 400 ng/mg, the extent of binding was highly consistent within experiments (i.e., low standard deviation), yet considerable variation in apoptosis was observed between experiments, suggesting a sensitivity to the protein loading or presentation within this range. Previous reports of surface modified apoptosis systems utilized surface anchored polymer chains with covalently linked anti-Fas antibodies but were only able to achieve up to 34% apoptosis in cells expressing FasR, whereas the method presented here achieved 92% apoptosis and *in vivo* protection of allogeneic islets [195]. This may be due to the far greater surface density of protein (up to 150 ng/cm² vs 1.6 ng/cm²) and the choice FasR binding protein.

Importantly, microporous scaffolds functionalized with SA-FasL supported engraftment and function of the transplanted allogeneic islets that maintained normoglycemia for more than 200 days. Islets transplanted on unmodified PLGA scaffolds promptly rejected 6-12 days after the rapamycin treatment ended, consistent with our previous results [180]. This long-term function without immunosuppression has a likely contribution from rapamycin allowing for the expansion

of regulatory T cells, an important cell population in establishing alloimmunity [180]. SA-FasL alone without rapamycin was able to delay rejection, consistent with previous reports suggesting that tolerance is dependent on the presence of SA-FasL yet a short course of rapamycin may accentuate the effect. In conclusion, our approach of functionalizing SA-FasL onto the surface of biotin-PLGA scaffolds is an effective method to induce long-term function without immunosuppression.

CHAPTER 6. Conclusions and Future Directions

6.1 Conclusions

Type 1 Diabetes can be successfully treated with islet transplants to restore the body's ability to endogenously produce insulin and rapidly respond to changes in blood glucose levels. However, current clinical practice requires an unsustainable number of donors and long-term success is limited. This may change if we are able to engineer an alternative transplant site that does not suffer from immediate islet loss and provides long-term protection from the immune system.

Herein, we present the utility of encapsulating and microporous PEG hydrogels for islet transplantation and subsequent engraftment *in vivo* in a syngeneic mouse model of diabetes. Hydrogels are employed as a substrate that creates a space to promote regeneration, possess mechanical properties similar to native extracellular matrices, and can be readily functionalized. In an allogeneic model, encapsulating hydrogels and microporous hydrogels containing islets rejected in a similar timeframe, demonstrating that unmodified PEG hydrogels do not offer sufficient allogeneic protection. This result underscores the need for sustained release strategies and incorporation of cytokine antagonists to further protect islets, in either encapsulating or microporous materials, from apoptosis. These findings provide a basis for continued studies with allogeneic islets and demonstrate the need for improvements in delivery of immune-modulating agents to extend graft function.

Viral gene delivery represents a versatile tool to modify the microenvironment of damaged or diseased tissue and promote regeneration by converting the transduced cells into bioreactors to produce therapeutic proteins or downregulate undesired genes. Hydrogels functionalized with proteins or peptides capable of binding lentivirus retained the virus at the material, enhanced the virus stability, and ultimately promoted gene transfer. High molecular weight proteins that non-specifically bind the lentivirus were directly attached to support binding and gene transfer. Alternatively, short peptides that specifically bind the lentivirus had to be immobilized onto biomaterials through linkers in order to promote binding and gene transfer, yet offered comparable gene expression levels. Taken together, affinity peptides or proteins can be attached to biomaterials to promote the binding of gene therapy vectors and subsequent gene transfer, with the efficiency a function of the peptide length and binding affinity.

The surface of biomaterial scaffolds were modified with SA-FasL to create a localized immunoprivileged site and provide long-term protection and function. Initial studies utilized allogeneic islets modified with SA-FasL seeded on PLGA microporous scaffolds to establish long-term tolerance. As an alternative to modifying islets, PLGA was conjugated with biotin that created a fast and efficient method to present SA-FasL on the polymer surface at concentrations that induced apoptosis in cells expressing FasR. Scaffolds functionalized with FasL demonstrated robust engraftment and tolerance similar to the FasL functionalized islets. In summary, this study introduces a new method to surface functionalize PLGA particles and scaffolds with immunoregulatory proteins and offers an alternative to systemic immunosuppression for allogeneic islet transplants.

6.2 Future directions

6.2.1 Scaffold improvement

Future work should focus on the PEG microporous scaffolds as they provided better glucose response and faster tissue infiltration compared to the encapsulating hydrogels. Without significant modification to address inflammatory cytokine infiltration, the encapsulating hydrogels do not offer significant protection in the allogeneic transplant model. Additionally, scale up of the current macroencapsulating design poses serious challenges. In contrast, the microporous hydrogels are easily scalable and have already been modified for non-human primate studies in a collaboration with the Oberholzer lab at the University of Illinois at Chicago. Future improvements to the hydrogel can optimize the pore size. Based on simulations, the ideal pore size in PEG hydrogels is 160 to 270 μm , whereas the pore sizes presented here were just above and below the suggested range. Micropore size is readily adjusted by adding different grain size salt, which is sorted by a series of simple mechanical sieves. To improve ease of transplant, we recommend future hydrogels utilize a smaller mold than the current 5 mm diameter PDMS mold. After swelling, the hydrogels are approximately 6.5 mm in diameter, making implantation into a diabetic mouse's epididymal fat pad challenging. Based on preliminary experiments, a 3 mm mold produced hydrogels too small to properly load desired volumes of islets. Thus, a 4 mm diameter mold is predicted to balance scaffold size and loading capacity.

Although encapsulating hydrogels inherently limit vascularization, a hybrid design that incorporates microporous aspects into an encapsulated hydrogel may improve glucose

response. Efforts to increase surface area of macroencapsulated islets has seen early success in PEG hydrogels and has been translated into the clinic in devices like the TheraCyte System and Nanogland device [41, 196, 197]. If scaffold degradation for the microporous or encapsulating hydrogel is required, plasmin-degradable peptides (e.g. YKNR) can be incorporated into the design, thus allowing the hydrogel to degrade as cells infiltrate and establish native ECM. Although not the focus of this dissertation, stem cells have the capacity for infinite expansion and are a renewable source, but require a microenvironment that promotes stem cell maturation. Degradable microporous hydrogels might be useful for β -progenitor stem cells as they provide a three-dimensional environment for cell-material signaling during stem cell maturation.

6.2.2 Localized protein delivery from biomaterial scaffolds

In the context of islet transplantation, a sophisticated release system may be needed to promote long-term engraftment. Such a delivery system would deliver a combination of agents in phases, designed to coincide with host immune response to transplanted islets. The short-term release of anti-inflammatory molecules like TGF- β 1 coupled with long-term tolerance provided by FasL may provide synergy and enhance graft function beyond their individual components. To further modify the microenvironment, lentiviral vectors can transduce infiltrating cells to produce a variety of growth factors and inhibitors.

The release profile of soluble factors from PLGA discs implanted with PEG scaffolds can be modified by adjusting the ratio of lactic acid to glycolic acid monomers or modifying the carboxylic acid end group to control the rate of polymer hydrolysis [198]. However, based on the

rate of protein release from the disc, the release kinetics are likely primarily determined by the dissolution of the mannitol cryoprotectant. Replacing the mannitol with a slower dissolving sugar may not only extend the release profile, but reduce protein lost during the salt leaching step. In an effort to address this protein loss during the leaching step, we have developed a PDMS insert that is placed in the mold with the PEG and salt instead of the PLGA disc. After polymerization and porogen leaching, the insert is pulled out and the protein loaded disc is slid in. However, this process has not been tested and it is unknown if the PLGA disc can slip out when transplanted in an animal.

Localized lentiviral delivery from hydrogels is a versatile tool that allows for the delivery and long-term expression of a wide range of therapeutic proteins and small molecules in scaffold microenvironment. VEGF is a particularly attraction option, as it has been extensively utilized in bioengineering to stimulate angiogenesis, a critical requirement for the survival of insulin producing cells [199, 200]. Additionally, sustained expression of exendin-4 (Ex4), an insulin-like growth factor-1 (IGF-1) has demonstrated useful applications in enhancing islet function [123, 201]. Long-term tolerance from these hydrogel scaffolds may be achieved by functionalizing SA-FasL to their surface. PEG-maleimide is easily functionalized with a biotin-PEG-thiol linker in a single step reaction that that requires no purification. Taken together, the tools presented in this dissertation can be applied to treat T1D and may someday be used to develop minimally invasive techniques that do not require chronic immune suppression to achieve routine islet transplantations.

BIBLIOGRAPHY

1. JDRF, P.G.f., *Type 1 Diabetes, 2010*. 2011.
2. Woodrow, G., A.M. Brownjohn, and J.J. Turney, *Acute renal failure in patients with type 1 diabetes mellitus*. *Postgrad Med J*, 1994. **70**: p. 192-194.
3. Roy, M.S., et al., *The prevalence of diabetic retinopathy among adult type 1 diabetic person in the United States*. *Arch Ophthalmol*, 2004. **122**(4): p. 546-551.
4. Steer, S.A., et al., *Interleukin-1 stimulates beta-cell necrosis and release of the immunological adjuvant HMGB1*. *PLoS Med*, 2006. **3**(2): p. e17.
5. Sarwar, N., et al., *Diabetes mellitus, fasting blood glucose concentration, and risk of vascular disease: a collaborative meta-analysis of 102 prospective studies*. *Lancet*, 2010. **375**: p. 2215-2222.
6. Szuts, E.Z., et al., *Blood glucose concentrations of arm and finger during dynamic glucose conditions*. *Diabetes Technol Ther*, 2002. **4**(1): p. 3-11.
7. Thompson, D.M., et al., *Reduced progression of diabetic microvascular complications with islet cell transplantation compared with intensive medical therapy*. *Transplantation*, 2011. **91**(3): p. 373-8.
8. Erlich, H., et al., *HLA DR-DQ haplotypes and genotypes and type 1 diabetes risk: analysis of the type 1 diabetes genetics consortium families*. *Diabetes*, 2008. **57**(4): p. 1084-92.
9. Farney, A.C., D.E. Sutherland, and E.C. Opara, *Evolution of islet transplantation for the last 30 years*. *Pancreas*, 2016. **45**(1): p. 8-20.
10. Fowler, M.J., *Microvascular and macrovascular complications of diabetes*. *Clinical Diabetes*, 2008. **26**(2): p. 77-82.
11. Pickup, J.C., *Insulin-pump therapy for type 1 diabetes mellitus*. *N Engl J Med*, 2012. **366**(17): p. 1616-24.
12. Samnegard, B., et al., *Effects of C-peptide on glomerular and renal size and renal function in diabetic rats*. *Kidney Int*, 2001. **60**(4): p. 1258-65.

13. Barton, F.B., et al., *Improvement in outcomes of clinical islet transplantation: 1999-2010*. Diabetes Care, 2012. **35**(7): p. 1436-45.
14. Carlsson, P.O., et al., *Markedly decreased oxygen tension in transplanted rat pancreatic islets irrespective of the implantation site*. Diabetes, 2001. **50**(3): p. 489-95.
15. Shapiro, A.M., *State of the art of clinical islet transplantation and novel protocols of immunosuppression*. Curr Diab Rep, 2011. **11**(5): p. 345-54.
16. Gibly, R.F., et al., *Advancing islet transplantation: from engraftment to the immune response*. Diabetologia, 2011. **54**(10): p. 2494-505.
17. Starzl, T.E., et al., *Iatrogenic alterations of immunologic surveillance in man and their influence on malignancy*. Transplant Rev., 1971. **7**: p. 112-145.
18. Ryan, E.A., et al., *Five-year follow-up after clinical islet transplantation*. Diabetes, 2005. **54**: p. 2060-2069.
19. Brennan, D.C., et al., *Long-Term Follow-Up of the Edmonton Protocol of Islet Transplantation in the United States*. Am J Transplant, 2016. **16**(2): p. 509-17.
20. McCall, M. and A.M. Shapiro, *Update on islet transplantation*. Cold Spring Harb Perspect Med, 2012. **2**(7): p. a007823.
21. Ryan, E.A., et al., *Clinical outcomes and insulin secretion after islet transplantation with the Edmonton protocol*. Diabetes, 2001. **50**(4): p. 710-9.
22. Ryan, E.A., et al., *Successful islet transplantation: continued insulin reserve provides long-term glycemc control*. Diabetes, 2002. **51**(7): p. 2148-57.
23. Barshes, N.R., et al., *Transaminitis after pancreatic islet transplantation*. J Am Coll Surg, 2005. **200**(3): p. 353-61.
24. Ballian, N. and F.C. Brunicardi, *Islet vasculature as a regulator of endocrine pancreas function*. World J Surg, 2007. **31**(4): p. 705-14.
25. Lau, J., et al., *Implantation site-dependent dysfunction of transplanted pancreatic islets*. Diabetes, 2007. **56**(6): p. 1544-50.
26. Hayek, A. and G.M. Beattie, *Intrapancreatic islet transplantation in experimental diabetes in the rat*. Metabolism, 1992. **41**(12): p. 1367-9.

27. Berman, D.M., et al., *Long-term survival of nonhuman primate islets implanted in an omental pouch on a biodegradable scaffold*. Am J Transplant, 2009. **9**(1): p. 91-104.
28. Szot, G.L., P. Koudria, and J.A. Bluestone, *Transplantation of pancreatic islets into the kidney capsule of diabetic mice*. J Vis Exp, 2007(9): p. 404.
29. Echeverri, G.J., et al., *Endoscopic gastric submucosal transplantation of islets (ENDO-STI): technique and initial results in diabetic pigs*. Am J Transplant, 2009. **9**(11): p. 2485-96.
30. Perez, V.L., et al., *The anterior chamber of the eye as a clinical transplantation site for the treatment of diabetes: a study in a baboon model of diabetes*. Diabetologia, 2011. **54**(5): p. 1121-6.
31. Nasr, I.W., et al., *Testicular immune privilege promotes transplantation tolerance by altering the balance between memory and regulatory T cells*. J Immunol, 2005. **174**(10): p. 6161-8.
32. Stagner, J.I., S.P. Mokshagundam, and E. Samols, *Induction of mild hypoglycemia by islet transplantation to the pancreas*. Transplant Proc, 1998. **30**(2): p. 635-6.
33. Stagner, J.I., H.L. Rilo, and K.K. White, *The pancreas as an islet transplantation site. Confirmation in a syngeneic rodent and canine autotransplant model*. JOP, 2007. **8**(5): p. 628-36.
34. Cantarelli, E. and L. Piemonti, *Alternative transplantation sites for pancreatic islet grafts*. Curr Diab Rep, 2011. **11**(5): p. 364-74.
35. al-Abdullah, I.H., et al., *Site for unpurified islet transplantation is an important parameter for determination of the outcome of graft survival and function*. Cell Transplant, 1995. **4**(3): p. 297-305.
36. Yasunami, Y., P.E. Lacy, and E.H. Finke, *A new site for islet transplantation--a peritoneal-omental pouch*. Transplantation, 1983. **36**(2): p. 181-2.
37. Ao, Z., et al., *Survival and function of purified islets in the omental pouch site of outbred dogs*. Transplantation, 1993. **56**(3): p. 524-9.
38. Chen, X., et al., *The epididymal fat pad as a transplant site for minimal islet mass*. Transplantation, 2007. **84**(1): p. 122-5.

39. Gibly, R.F., et al., *Extrahepatic islet transplantation with microporous polymer scaffolds in syngeneic mouse and allogeneic porcine models*. *Biomaterials*, 2011. **32**(36): p. 9677-84.
40. Dufour, J.M., et al., *Development of an ectopic site for islet transplantation, using biodegradable scaffolds*. *Tissue Eng*, 2005. **11**(9-10): p. 1323-31.
41. Rios, P.D., et al., *Mold-casted non-degradable, islet macro-encapsulating hydrogel devices for restoration of normoglycemia in diabetic mice*. *Biotechnol Bioeng*, 2016. **113**(11): p. 2485-95.
42. Litbarg, N.O., et al., *Activated omentum becomes rich in factors that promote healing and tissue regeneration*. *Cell Tissue Res*, 2007. **328**(3): p. 487-97.
43. Pepper, A.R., et al., *Revascularization of transplanted pancreatic islets and role of the transplantation site*. *Clin Dev Immunol*, 2013. **2013**: p. 352315.
44. Shultz, L.D., et al., *Subcapsular transplantation of tissue in the kidney*. *Cold Spring Harb Protoc*, 2014. **2014**(7): p. 737-40.
45. Lacy, P.E., C. Ricordi, and E.H. Finke, *Effect of transplantation site and alpha L3T4 treatment on survival of rat, hamster, and rabbit islet xenografts in mice*. *Transplantation*, 1989. **47**(5): p. 761-6.
46. Mellgren, A., et al., *The renal subcapsular site offers better growth conditions for transplanted mouse pancreatic islet cells than the liver or spleen*. *Diabetologia*, 1986. **29**(9): p. 670-2.
47. van Suylichem, P.T., et al., *Rat islet isograft function. Effect of graft volume and transplantation site*. *Transplantation*, 1994. **57**(7): p. 1010-7.
48. Wszola, M., et al., *TransEndoscopic Gastric SubMucosa Islet Transplantation (eGSM-ITx) in pigs with streptozotocine induced diabetes - technical aspects of the procedure - preliminary report*. *Ann Transplant*, 2009. **14**(2): p. 45-50.
49. Sageshima, J., et al., *Small bowel subserosal space as a site for islet transplantation and local drug delivery*. *Transplant Proc*, 2001. **33**(1-2): p. 1710.
50. Tchervenivanov, N., et al., *Morphological and functional studies on submucosal islet transplants in normal and diabetic hamsters*. *Cell Transplant*, 2002. **11**(6): p. 529-37.

51. Taylor, A.W., *Ocular immune privilege*. Eye (Lond), 2009. **23**(10): p. 1885-9.
52. Speier, S., et al., *Noninvasive in vivo imaging of pancreatic islet cell biology*. Nat Med, 2008. **14**(5): p. 574-8.
53. Adeghate, E. and T. Donath, *Morphological findings in long-term pancreatic tissue transplants in the anterior eye chamber of rats*. Pancreas, 1990. **5**(3): p. 298-305.
54. Ferguson, J. and R.J. Scothorne, *Extended survival of pancreatic islet allografts in the testis of guinea-pigs*. J Anat, 1977. **124**(Pt 1): p. 1-8.
55. Ar'Rajab, A., et al., *Immune privilege of the testis for islet xenotransplantation (rat to mouse)*. Cell Transplant, 1994. **3**(6): p. 493-8.
56. Nasr, I.W., et al., *Testicular Immune Privilege Promotes Transplantation Tolerance by Altering the Balance between Memory and Regulatory T Cells*. The Journal of Immunology, 2005. **174**(10): p. 6161-6168.
57. Kin, T., et al., *Development of an immunoprivileged site to prolong islet allograft survival*. Cell Transplantation, 2002. **11**(6): p. 547-552.
58. Geiger, B., et al., *Transmembrane extracellular matrix - cytoskeleton crosstalk*. Nature Reviews, 2001. **2**: p. 793-805.
59. Sidney, L.E., et al., *Investigation of localized delivery of diclofenac sodium from poly(D,L-lactic acid-co-glycolic acid)/poly(ethylene glycol) scaffolds using an in vitro osteoblast inflammation model*. Tissue Eng Part A, 2015. **21**(1-2): p. 362-73.
60. Suarez-Gonzalez, D., et al., *Controlled multiple growth factor delivery from bone tissue engineering scaffolds via designed affinity*. Tissue Eng Part A, 2014. **20**(15-16): p. 2077-87.
61. Kim, S.E., et al., *Local delivery of alendronate eluting chitosan scaffold can effectively increase osteoblast functions and inhibit osteoclast differentiation*. J Mater Sci Mater Med, 2012. **23**(11): p. 2739-49.
62. Teng, S.H., et al., *Functionally gradient chitosan/hydroxyapatite composite scaffolds for controlled drug release*. J Biomed Mater Res B Appl Biomater, 2009. **90**(1): p. 275-82.
63. Phillips, J.E., et al., *Engineering graded tissue interfaces*. Proc Natl Acad Sci U S A, 2008. **105**(34): p. 12170-5.

64. Liang, W.H., et al., *Concentrated collagen-chondroitin sulfate scaffolds for tissue engineering applications*. J Biomed Mater Res A, 2010. **94**(4): p. 1050-60.
65. Odrliin, T.M., et al., *Heparin-binding domain of fibrin mediates its binding to endothelial cells*. Arteriosclerosis, Thrombosis, and Vascular Biology, 1996. **16**: p. 1544-1551.
66. Tabata, Y., et al., *Controlled release of vascular endothelial growth factor by use of collagen hydrogels*. J Biomater Sci Polym Ed, 2000. **11**(9): p. 915-930.
67. Zhu, J. and R.E. Marchant, *Design properties of hydrogel tissue-engineering scaffolds*. Expert Rev Med Devices, 2011. **8**(5): p. 607-26.
68. Shepard, J.A., et al., *Balancing cell migration with matrix degradation enhances gene delivery to cells cultured three-dimensionally within hydrogels*. J Control Release, 2010. **146**(1): p. 128-35.
69. McMahan, S.S., et al., *Thermosensitive hydrogel for prolonged delivery of lentiviral vector expressing neurotrophin-3 in vitro*. J Gene Med, 2011. **13**(11): p. 591-601.
70. Akala, E.O., P. Kopeckova, and J. Kopecek, *Novel pH-sensitive hydrogels with adjustable swelling kinetics*. Biomaterials, 1998. **19**: p. 1037-1047.
71. Peppas, N.A., et al., *Poly(ethylene glycol)-containing hydrogels in drug delivery*. Journal of Controlled Release, 1999. **62**: p. 81-87.
72. Janeway, C.A., et al., *Immunobiology: The Immune System in Health and Disease*. 5th ed. 2001, New York: Garland Science.
73. Thomas, A.M., et al., *Sonic hedgehog and neurotrophin-3 increase oligodendrocyte numbers and myelination after spinal cord injury*. Integr Biol (Camb), 2014. **6**(7): p. 694-705.
74. Shen, Y., et al., *Triple transduction with adeno-associated virus vectors expressing tyrosine hydroxylase, aromatic-L-amino-acid decarboxylase, and GTP cyclohydrolase I for gene therapy of Parkinson's disease*. Human Gene Therapy, 2000. **11**: p. 1509-1519.
75. Lentz, T.B., S.J. Gray, and R.J. Samulski, *Viral vectors for gene delivery to the central nervous system*. Neurobiol Dis, 2012. **48**(2): p. 179-88.
76. BluebirdBio, *A phase 2/3 study of the efficacy and safety of hematopoietic stem cells transduced with Lenti-D lentiviral vector for the treatment of Childhood Cerebral*

Adrenoleukodystrophy (CCALD). ClinicalTrials.gov, 2013-2018: p. NLM Identifier: NCT01896102.

77. Lewis, P., M. Hensel, and M. Emerman, *Human immunodeficiency virus infection of cells arrested in the cell cycle*. EMBO Journal, 1992. **11**(8): p. 3053-3058.
78. Bukrinsky, M.I., et al., *A nuclear localization signal within HIV-1 matrix protein that governs infection of non-dividing cells*. Nature, 1993. **365**(14): p. 666-669.
79. Lewis, P.F. and M. Emerman, *Passage through mitosis is required for oncoretroviruses but not for the human immunodeficiency virus*. Journal of Virology, 1993. **68**(1): p. 510-516.
80. Naldini, L., et al., *Efficient transfer, integration, and sustained long-term expression of the transgene in adult rat brains injected with a lentiviral vector*. Proc Natl Acad Sci U S A, 1996. **93**: p. 11382-11388.
81. Abordo-Adesida, E., et al., *Stability of lentiviral vector-mediated transgene expression in the brain in the presence of systemic antivector immune responses*. Hum Gene Ther, 2005. **16**(6): p. 741-51.
82. Aiuti, A., et al., *Gene therapy for immunodeficiency due to adenosine deaminase deficiency*. N. Engl. J. Med. , 2009. **360**(5): p. 447-458.
83. Cartier, N., et al., *Hematopoietic stem cell gene therapy with a lentiviral vector in X-linked adrenoleukodystrophy*. Science, 2009. **326**(5954): p. 818-23.
84. Bainbridge, J.W., et al., *Effect of gene therapy on visual function in Leber's congenital amaurosis*. N. Engl. J. Med., 2008. **358**(21): p. 2231-2239.
85. Buch, P.K., J.W. Bainbridge, and R.R. Ali, *AAV-mediated gene therapy for retinal disorders: from mouse to man*. Gene Ther, 2008. **15**(11): p. 849-57.
86. Jen, M.C., et al., *Sustained, localized transgene expression mediated from lentivirus-loaded biodegradable polyester elastomers*. J Biomed Mater Res A, 2013. **101**(5): p. 1328-35.
87. Boehler, R.M., et al., *A PLG/HAp composite scaffold for lentivirus delivery*. Biomaterials, 2013. **34**(21): p. 5431-8.

88. Shin, S. and L.D. Shea, *Lentivirus immobilization to nanoparticles for enhanced and localized delivery from hydrogels*. Mol Ther, 2010. **18**(4): p. 700-6.
89. Shin, S., et al., *Phosphatidylserine immobilization of lentivirus for localized gene transfer*. Biomaterials, 2010. **31**(15): p. 4353-9.
90. Padmashali, R.M. and S.T. Andreadis, *Engineering fibrinogen-binding VSV-G envelope for spatially- and cell-controlled lentivirus delivery through fibrin hydrogels*. Biomaterials, 2011. **32**(12): p. 3330-9.
91. Nakayama, M., et al., *Priming and effector dependence on insulin B:9-23 peptide in NOD islet autoimmunity*. J Clin Invest, 2007. **117**(7): p. 1835-43.
92. Van Belle, T. and M. von Herrath, *Immunosuppression in islet transplantation*. J Clin Invest, 2008. **118**(5): p. 1625-8.
93. Vegas, A.J., et al., *Long-term glycemic control using polymer-encapsulated human stem cell-derived beta cells in immune-competent mice*. Nat Med, 2016. **22**(3): p. 306-11.
94. Sakata, N., et al., *Encapsulated islets transplantation: Past, present and future*. World J Gastrointest Pathophysiol, 2012. **3**(1): p. 19-26.
95. Suzuki, K., et al., *Function and survival of macroencapsulated syngeneic islets transplanted into streptozocin-diabetic mice*. Transplantation, 1998. **66**(1): p. 21-28.
96. Jang, J.Y., et al., *Immune reactions of lymphocytes and macrophages against PEG-grafted pancreatic islets*. Biomaterials, 2004. **25**(17): p. 3663-9.
97. de Groot, M., T.A. Schuur, and R. van Schilfgaarde, *Causes of limited survival of microencapsulated pancreatic islet grafts*. J Surg Res, 2004. **121**(1): p. 141-50.
98. Bouillet, P. and L.A. O'Reilly, *CD95, BIM and T cell homeostasis*. Nat Rev Immunol, 2009. **9**(7): p. 514-9.
99. Elkin, G., T.B. Prigozhina, and S. Slavin, *Prevention of diabetes in nonobese diabetic mice by nonmyeloablative allogeneic bone marrow transplantation*. Exp Hematol, 2004. **32**(6): p. 579-84.
100. Li, H., et al., *Mixed allogeneic chimerism induced by a sublethal approach prevents autoimmune diabetes and reverses insulinitis in nonobese diabetic (NOD) mice*. Journal of Immunology, 1996. **156**: p. 380-388.

101. Beilhack, G.F., et al., *Purified allogeneic hematopoietic stem cell transplantation blocks diabetes pathogenesis in NOD mice*. *Diabetes*, 2003. **52**: p. 59-68.
102. Kheradmand, T., et al., *Permanent protection of PLG scaffold transplanted allogeneic islet grafts in diabetic mice treated with ECDI-fixed donor splenocyte infusions*. *Biomaterials*, 2011. **32**(20): p. 4517-24.
103. Opara, E.C., et al., *Design of a bioartificial pancreas(+)*. *J Investig Med*, 2010. **58**(7): p. 831-7.
104. Salvay, D.M., et al., *Extracellular matrix protein-coated scaffolds promote the reversal of diabetes after extrahepatic islet transplantation*. *Transplantation*, 2008. **85**(10): p. 1456-64.
105. Alejandro, R., et al., *Long-term function (6 years) of islet allografts in type 1 diabetes*. *Diabetes*, 1997. **46**: p. 1983-1989.
106. Leach, J.B., A.K. Achyuta, and S.K. Murthy, *Bridging the Divide between Neuroprosthetic Design, Tissue Engineering and Neurobiology*. *Front Neuroeng*, 2010. **2**: p. 18.
107. Raeber, G.P., M.P. Lutolf, and J.A. Hubbell, *Molecularly engineered PEG hydrogels: a novel model system for proteolytically mediated cell migration*. *Biophys J*, 2005. **89**(2): p. 1374-88.
108. Shepard, J.A., et al., *Hydrogel macroporosity and the prolongation of transgene expression and the enhancement of angiogenesis*. *Biomaterials*, 2012. **33**(30): p. 7412-21.
109. Phelps, E.A., et al., *Maleimide cross-linked bioactive PEG hydrogel exhibits improved reaction kinetics and cross-linking for cell encapsulation and in situ delivery*. *Adv Mater*, 2012. **24**(1): p. 64-70, 2.
110. Elbert, D.L. and J.A. Hubbell, *Conjugate addition reactions combined with free-radical cross-linking for the design of materials for tissue engineering*. *Biomacromolecules*, 2001. **2**: p. 430-441.
111. Fontaine, S.D., et al., *Long-term stabilization of maleimide-thiol conjugates*. *Bioconjug Chem*, 2015. **26**(1): p. 145-52.

112. Hou, Y., et al., *Photo-cross-linked PDMSstar-PEG hydrogels: synthesis, characterization, and potential application for tissue engineering scaffolds*. *Biomacromolecules*, 2010. **11**(3): p. 648-56.
113. Annabi, N., et al., *Controlling the porosity and microarchitecture of hydrogels for tissue engineering*. *Tissue Engineering*, 2010. **16**(4): p. 371-383.
114. Tong, X., et al., *Long-term controlled protein release from poly(ethylene glycol) hydrogels by modulating mesh size and degradation*. *Macromolecular Bioscience*, 2015. **15**: p. 1679-1686.
115. McCall, J.D., C.C. Lin, and K.S. Anseth, *Affinity peptides protect transforming growth factor beta during encapsulation in poly(ethylene glycol) hydrogels*. *Biomacromolecules*, 2011. **12**(4): p. 1051-7.
116. Skoumal, M., et al., *Localized lentivirus delivery via peptide interactions*. *Biotechnol Bioeng*, 2016.
117. Liu, J.M., et al., *Transforming growth factor-beta 1 delivery from microporous scaffolds decreases inflammation post-implant and enhances function of transplanted islets*. *Biomaterials*, 2016. **80**: p. 11-9.
118. Mooney, D.J., et al., *Novel approach to fabricate porous sponges of poly(D,L-lactic-co-glycolic acid) without the use of organic solvents*. *Biomaterials*, 1996. **17**: p. 1417-1422.
119. Chiu, Y.C., et al., *Generation of porous poly(ethylene glycol) hydrogels by salt leaching*. *Tissue Engineering*, 2010. **16**(5): p. 905-912.
120. Ghasemi-Mobarakeh, L., et al., *Electrospun poly(epsilon-caprolactone)/gelatin nanofibrous scaffolds for nerve tissue engineering*. *Biomaterials*, 2008. **29**(34): p. 4532-9.
121. Williams, C.G., et al., *Variable cytocompatibility of six cell lines with photoinitiators used for polymerizing hydrogels and cell encapsulation*. *Biomaterials*, 2005. **26**(11): p. 1211-8.
122. Blomeier, H., et al., *Polymer scaffolds as synthetic microenvironments for extrahepatic islet transplantation*. *Transplantation*, 2006. **82**(4): p. 452-9.
123. Hlavaty, K.A., et al., *Enhancing human islet transplantation by localized release of trophic factors from PLG scaffolds*. *Am J Transplant*, 2014. **14**(7): p. 1523-32.

124. Yang, L., Y. Pang, and H.L. Moses, *TGF-beta and immune cells: an important regulatory axis in the tumor microenvironment and progression*. Trends Immunol, 2010. **31**(6): p. 220-7.
125. Fu, S., et al., *TGF-beta induces Foxp3 + T-regulatory cells from CD4 + CD25 - precursors*. Am J Transplant, 2004. **4**(10): p. 1614-27.
126. Song, S. and S. Roy, *Progress and challenges in macroencapsulation approaches for type 1 diabetes (T1D) treatment: Cells, biomaterials, and devices*. Biotechnol Bioeng, 2016. **113**(7): p. 1381-402.
127. Oliviero, O., M. Ventre, and P.A. Netti, *Functional porous hydrogels to study angiogenesis under the effect of controlled release of vascular endothelial growth factor*. Acta Biomater, 2012. **8**(9): p. 3294-301.
128. Madden, L.R., et al., *Proangiogenic scaffolds as functional templates for cardiac tissue engineering*. Proc Natl Acad Sci U S A, 2010. **107**(34): p. 15211-6.
129. Artel, A., et al., *An agent-based model for the investigation of neovascularization within porous scaffolds*. Tissue Eng Part A, 2011. **17**(17-18): p. 2133-41.
130. Phelps, E.A., et al., *Vasculogenic bio-synthetic hydrogel for enhancement of pancreatic islet engraftment and function in type 1 diabetes*. Biomaterials, 2013. **34**(19): p. 4602-11.
131. Nafea, E.H., et al., *Immunoisolating semi-permeable membranes for cell encapsulation: focus on hydrogels*. J Control Release, 2011. **154**(2): p. 110-22.
132. Zhang, X., et al., *A biodegradable, immunoprotective, dual nanoporous capsule for cell-based therapies*. Biomaterials, 2008. **29**(31): p. 4253-9.
133. Zustiak, S.P. and J.B. Leach, *Characterization of protein release from hydrolytically degradable poly(ethylene glycol) hydrogels*. Biotechnol Bioeng, 2011. **108**(1): p. 197-206.
134. Zustiak, S.P. and J.B. Leach, *Hydrolytically degradable poly(ethylene glycol) hydrogel scaffolds with tunable degradation and mechanical properties*. Biomacromolecules, 2010. **11**(5): p. 1348-57.
135. Kim, S.W., *Polymeric gene delivery for diabetic treatment*. Diabetes Metab J, 2011. **35**(4): p. 317-26.

136. Brissova, M., et al., *Pancreatic islet production of vascular endothelial growth factor--a is essential for islet vascularization, revascularization, and function*. *Diabetes*, 2006. **55**(11): p. 2974-85.
137. Xu, R., et al., *Diabetes gene therapy: potential and challenges*. *Curr Gene Ther*, 2003. **3**(1): p. 65-82.
138. Luk, K.D.K., et al., *Adeno-associated virus-mediated bone morphogenetic protein-4 gene therapy for in vivo bone formation*. *Biochemical and Biophysical Research Communications*, 2003. **308**(3): p. 636-645.
139. Samoylova, T.I. and B.F. Smith, *Elucidation of muscle-binding peptides by phage display screening*. *Muscle Nerve*, 1999. **22**(4): p. 460-466.
140. Chamrathy, S.P., et al., *Gene delivery to dendritic cells facilitated by a tumor necrosis factor alpha-competing peptide*. *Mol Immunol*, 2004. **41**(8): p. 741-9.
141. Mummert, M.E., et al., *Development of a peptide inhibitor of hyaluronan-mediated leukocyte trafficking*. *Journal of Experimental Medicine*, 2000. **192**(6): p. 769-779.
142. Romanczuk, H., et al., *Modification of an adenoviral vector with biologically selected peptides: a novel strategy for gene delivery to cells of choice*. *Human Gene Therapy*, 1999. **10**: p. 2615-2626.
143. Hardy, B., et al., *Angiogenesis induced by novel peptides selected from a phage display library by screening human vascular endothelial cells under different physiological conditions*. *Peptides*, 2007. **28**(3): p. 691-701.
144. Binetruy-Tournaire, R., et al., *Identification of a peptide blocking vascular endothelial growth factor (VEGF)-mediated angiogenesis*. *EMBO Journal*, 2000. **19**(7): p. 1525-1533.
145. Birkenmeier, G., et al., *Epitope mapping by screening of phage display libraries of a monoclonal antibody directed against the receptor binding domain of human α 2-macroglobulin*. *FEBS Letters*, 1997. **416**(2): p. 193-196.
146. Dore, J.M., et al., *Identification and location on syndecan-1 core protein of the epitopes of B-B2 and B-B4 monoclonal antibodies*. *FEBS Letters*, 1998. **426**: p. 67-70.
147. Rodi, D.J., et al., *Screening of a library of phage-displayed peptides identifies human Bcl-2 as a taxol-binding protein*. *J. Mol. Biol.*, 1999. **285**(197-203).

148. Rozinov, M.N. and G.P. Nolan, *Evolution of peptides that modulate the spectral qualities of bound, small-molecule fluorophores*. Chem. Biol., 1998. **5**: p. 713-728.
149. Miura, Y., et al., *Peptides binding to a Gb3 mimic selected from a phage library*. Biochim Biophys Acta, 2004. **1673**(3): p. 131-8.
150. Dull, T., et al., *A third-generation lentivirus vector with a conditional packaging system*. Journal of Virology, 1998. **72**(11): p. 8463-8471.
151. Zhang, X., R. Goncalves, and D.M. Mosser, *The isolation and characterization of murine macrophages*. Curr Protoc Immunol, 2008. **Chapter 14**: p. 1-18.
152. Tolmachov, O.E., T. Tolmachova, and F.A. Al-Allaf, *Designing Lentiviral Gene Vectors*. Viral Gene Therapy, ed. K. Xu. 2011: InTech.
153. Higashikawa, F. and L. Chang, *Kinetic analyses of stability of simple and complex retroviral vectors*. Virology, 2001. **280**(1): p. 124-31.
154. Zhang, B., et al., *The significance of controlled conditions in lentiviral vector titration and in the use of multiplicity of infection (MOI) for predicting gene transfer events*. Genet Vaccines Ther, 2004. **2**(1): p. 6.
155. Davis, H.E., et al., *Charged polymers modulate retrovirus transduction via membrane charge neutralization and virus aggregation*. Biophysical Journal, 2004. **86**: p. 1234-1242.
156. Bengali, Z., et al., *Efficacy of immobilized polyplexes and lipoplexes for substrate-mediated gene delivery*. Biotechnol Bioeng, 2009. **102**(6): p. 1679-91.
157. Luo, D. and M.W. Saltzman, *Enhancement of transfection by physical concentration of DNA at the cell surface*. Nature Biotechnology, 2000. **18**: p. 893-895.
158. Roche, S., et al., *Structure of the prefusion form of the vesicular stomatitis virus glycoprotein G*. Science, 2007. **315**(5813): p. 843-8.
159. Adey, N.B., et al., *Characterization of phage that bind plastic from phage-displayed random peptide libraries*. Gene, 1995. **156**: p. 27-31.
160. Menendez, A. and J.K. Scott, *The nature of target-unrelated peptides recovered in the screening of phage-displayed random peptide libraries with antibodies*. Anal Biochem, 2005. **336**(2): p. 145-57.

161. Deguchi, Y., A. Kurihara, and W.M. Pardridge, *Retention of biologic activity of human epidermal growth factor following conjugation to a blood-brain barrier drug delivery vector via an extended poly(ethylene glycol) linker*. *Bioconjug Chem*, 1998. **10**: p. 32-37.
162. Wilson, J.T. and E.L. Chaikof, *Challenges and emerging technologies in the immunoisolation of cells and tissues*. *Adv Drug Deliv Rev*, 2008. **60**(2): p. 124-45.
163. Lim, F. and A.M. Sun, *Microencapsulated islets as bioartificial endocrine pancreas*. *Science*, 1980. **210**(4472): p. 908-10.
164. Chandy, T., D.L. Mooradian, and G.H. Rao, *Evaluation of modified alginate-chitosan-polyethylene glycol microcapsules for cell encapsulation*. *Artif Organs*, 1999. **23**(10): p. 894-903.
165. Strand, B.L., et al., *Alginate-polylysine-alginate microcapsules: effect of size reduction on capsule properties*. *J Microencapsul*, 2002. **19**(5): p. 615-30.
166. Aung, T., et al., *Insulin release from a bioartificial pancreas using a mesh reinforced polyvinyl alcohol hydrogel tube. An in vitro study*. *ASAIO J*, 1993. **39**(2): p. 93-6.
167. Krishnan, R., et al., *Strategies to combat hypoxia in encapsulated islet transplantation*. *Surgery: Current Research*, 2016. **6**(2): p. 1-10.
168. Markmann, J.F., et al., *Indefinite survival of MHC class I-deficient murine pancreatic islet allografts*. *Transplantation*, 1992. **54**: p. 1085-9.
169. Osorio, R.W., et al., *Major histocompatibility complex class I deficiency prolongs islet allograft survival*. *Diabetes*, 1993. **42**: p. 1520-7.
170. Osorio, R.W., N.L. Ascher, and P.G. Stock, *Prolongation of in vivo mouse islet allograft survival by modulation of MHC class I antigen*. *Transplantation*, 1994. **57**: p. 783-8.
171. Simeonovic, C.J., et al., *Differences in the contribution of CD4+ T cells to proislet and islet allograft rejection correlate with constitutive class II MHC alloantigen expression*. *Transplantation*, 1996. **5**: p. 525-41.
172. Griffith, T.S., et al., *FasL ligand-induced apoptosis as a mechanism of immune privilege*. *Science*, 1995. **270**(5239): p. 1189-92.
173. Bellgrau, D., et al., *A role for CD95 ligand in preventing graft rejection*. *Nature*, 1995. **377**: p. 630-2.

174. Wu, J., et al., *Correction of accelerated autoimmune disease by early replacement of the mutated *lpr* gene with the normal *Fas* apoptosis gene in the T cells of transgenic MRL-*lpr/lpr* mice*. Proc Natl Acad Sci U S A, 1994. **91**: p. 2344-8.
175. Ju, S.-T., et al., *Fas(CD95)/FasL interactions required for programmed cell death after T-cell activation*. Nature, 1996. **373**: p. 444-8.
176. Lau, H.T., et al., *Prevention of islet allograft rejection with engineered myoblasts expressing FasL in mice*. Science, 1996. **273**: p. 109-112.
177. Turvey, S.E., et al., *FasL Ligand-transfected myoblasts and islet cell transplantation*. Transplantation, 2000. **69**(9): p. 1972-1976.
178. Kang, S., et al., *Fas ligand expression in islets of Langerhans does not confer immune privilege and instead targets them for rapid destruction*. Nature Medicine, 1997. **3**(7): p. 738-743.
179. Allison, J., et al., *Transgenic expression of CD95 ligand on islet beta cells induces a granulocytic infiltration but does not confer immune privilege upon islet allografts*. Proc Natl Acad Sci U S A, 1997. **94**: p. 3943-3947.
180. Yolcu, E.S., et al., *Pancreatic islets engineered with SA-FasL protein establish robust localized tolerance by inducing regulatory T cells in mice*. J Immunol, 2011. **187**(11): p. 5901-9.
181. van der Windt, D.J., et al., *The choice of anatomical site for islet transplantation*. Cell Transplantation, 2008. **17**: p. 1005-14.
182. Tuinstra, H.M., et al., *Bridges delivering neurotrophin encoding lentivirus enhance regeneration following spinal cord injury*. Biomaterials, 2012. **33**(5): p. 1618-26.
183. Yolcu, E.S., et al., *Cell membrane modification for rapid display of proteins as a novel means of immunomodulation: FasL-decorated cells prevent islet graft rejection*. Immunity, 2002. **17**: p. 795-808.
184. Zhao, H., et al., *Porcine islets engineered to display SA-FasL protein on their surface induce tolerance in mice following transplantation into the liver or under the kidney capsule [abstract]*. Am J Transplant, 2016. **16**.
185. Valetti, S., et al., *Peptide conjugation: before or after nanoparticle formation?* Bioconjug Chem, 2014. **25**(11): p. 1971-83.

186. Zhao, S., et al., *Testicular defense systems: immune privilege and innate immunity*. Cell Mol Immunol, 2014. **11**(5): p. 428-37.
187. Benhar, I., A. London, and M. Schwartz, *The privileged immunity of immune privileged organs: the case of the eye*. Front Immunol, 2012. **3**: p. 296.
188. Carson, M.J., et al., *CNS immune privilege: hiding in plain sight*. Immunol Rev, 2006. **213**: p. 48-65.
189. Yolcu, E.S., H. Zhao, and H. Shirwan, *Immunomodulation with SA-FasL protein as an effective means of preventing islet allograft rejection in chemically diabetic NOD mice*. Transplant Proc, 2013. **45**(5): p. 1889-91.
190. Donaldson, O., Z.J. Huang, and N. Comolli, *An integrated experimental and modeling approach to propose biotinylated PLGA microparticles as versatile targeting vehicles for drug delivery*. Biomaterials, 2013. **2**(3): p. 1-10.
191. Mehdizadeh, M., et al., *Biotin decorated PLGA nanoparticles containing SN-38 designed for cancer therapy*. Artif Cells Nanomed Biotechnol, 2017. **45**(3): p. 495-504.
192. Shea, L.D., et al., *DNA delivery from polymer matrices for tissue engineering*. Nature Biotechnology, 1999. **17**: p. 551-4.
193. Yap, W.T., et al., *Quantification of particle-conjugated or particle-encapsulated peptides on interfering reagent backgrounds*. Biotechniques, 2014. **57**(1): p. 39-44.
194. Hunter, Z.N., et al., *A biodegradable nanoparticle platform for the induction of antigen-specific immune tolerance for treatment of autoimmune disease*. ACS Nano, 2014. **8**(3): p. 2148-60.
195. Hume, P.S. and K.S. Anseth, *Inducing local T cell apoptosis with anti-Fas-functionalized polymeric coatings fabricated via surface-initiated photopolymerizations*. Biomaterials, 2010. **31**(12): p. 3166-74.
196. Kumagai-Braesch, M., et al., *The TheraCyte device protects against islet allograft rejection in immunized hosts*. Cell Transplant, 2013. **22**(7): p. 1137-46.
197. Sabek, O.M., et al., *Characterization of a nanogland for the autotransplantation of human pancreatic islets*. Lab Chip, 2013. **13**(18): p. 3675-88.

198. Samadi, N., et al., *The effect of lauryl capping group on protein release and degradation of poly(D,L-lactic-co-glycolic acid) particles*. J Control Release, 2013. **172**(2): p. 436-43.
199. Golub, J.S., et al., *Sustained VEGF delivery via PLGA nanoparticles promotes vascular growth*. Am J Physiol Heart Circ Physiol, 2010. **298**(6): p. H1959-65.
200. Narang, A.S., et al., *Vascular endothelial growth factor gene delivery for revascularization in transplanted human islets*. Pharmaceutical Research, 2004. **21**(1): p. 15-25.
201. Sharma, A., et al., *Exendin-4 treatment improves metabolic control after rat islet transplantation to athymic mice with streptozotocin-induced diabetes*. Diabetologia, 2006. **49**(6): p. 1247-53.